Effects of diabaticity on fusion of heavy nuclei in the dinuclear model

Inaugural-Dissertation
zur
Erlangung des Doktorgrades
der naturwissenschaftlichen Fakultät
der Justus-Liebig-Universität Gießen
Fachbereich 07
Fachrichtung Physik

vorgelegt von

Alexis Diaz Torres

aus Gießen

Institut für Theoretische Physik
der Justus-Liebig-Universität Gießen
Januar 2000

Effects of diabaticity on fusion of heavy nuclei in the dinuclear model

by

Alexis Diaz Torres

Submitted to the Naturwissenschaftiche Fakultät der Justus-Liebig-Universität Gießen
on 21 January 2000, in partial fulfillment of the
requirements for the degree of
Doctor

Abstract

Der Fusionsprozeß schwerer Kerne wird unter Verwendung des Zweizentren-Schalenmodells (TCSM für Two-Center Shell Model) untersucht. Zuerst werden diabatische Potentiale als Funktion geometrischer Parameter und des sogenannten Neckparameters im Rahmen des TCSM für verschiedene symmetrische und asymmetrische Systeme berechnet. Zur Berechnung der Energieniveaus wird die Methode der maximalen Symmetrie angewandt. Die diabatischen Potentiale behinden die Bewegung der Kerne zu geringeren relativen Abständen und das Anwachsen des Necks. Sie ähneln den im dinuklearen Fusionsmodell verwendeten Kern-Kern- Potentialen. Die Abhängigkeit des diabatischen Potentials von Temperatur und Massenasymmetrie wird diskutiert. Die Isotopen-Abhängigkeit des im TCSM berechneten Potentials wird für verschiedene schwere dinukleare Systeme (DNS für Dinuclear System) untersucht. Ein DNS wird aus zwei sich berührenden Kernen im Minimum des Kern-Kern-Potentials gebildet, wobei die individuellen Eigenschaften der beteiligten Kerne erhalten bleiben. Des weiteren wird das Potential des DNS als Funktion der Massenasymmetrie mit anderen mikroskopischen und phänomenologischen Potentialen verglichen.

Massenparameter für die Variablen eines DNS und eines stark deformierten vereinigten Kerns werden mikroskopisch unter Verwendung der Breite der Einteilchen-Zustände bestimmt. Für die Beschreibung der Relativbewegung der Kerne und die Ausbildung des Necks zwischen den Kernen werden die Massenparameter mit Basis-Zuständen des adiabatischen und diabatischen TCSM berechnet. Die mikroskopischen Massenparameter erweisen sich größer als die nach dem hydrodynamischen Modell erhaltenen Parameter und verursachen eine starke Behinderung für das Verschmelzen des DNS entlang der Kernverbindungsachse. Das bedeutet, daß das DNS eine lange Zeit lebt, die mit der Reaktionszeit für eine Fusion durch Nukleonen-Transfer vergleichbar ist. Konsequenzen dieses Effekts für den gesamten Fusionsprozeß werden diskutiert.

Der zeitabhängige Übergang zwischen einem diabatischen Wechselwirkungspotential im Eingangskanal und einem adiabatischen Potential während des Fusionsprozesses wird im Rahmen des TCSM untersucht. Es wird eine große Behinderung für die Bewegung zu geringeren Kernabständen von fast symmetrischen DNS gefunden. Der Vergleich der berechneten Energieschwellen für die vollständige Fusion in verschiedenen relevanten kollektiven Koordinaten zeigt, daß das DNS vorzugsweise in der Massenasymmetrie-Koordinate durch Nukleonen-Transfer zum vereinigten Kern verschmilzt.

Der Prozeß der Quasi-Spaltung des DNS wird durch die Lösung einer Transport-Mastergleichung für den Austausch von Nukleonen zwischen den Teilen des DNS behandelt, die auch den Zer-

fallsprozeß des DNS entlang der Kernverbindungsachse berücksichtigt. Die Quasi-Spaltung-Produkte von Fusionsreaktionen werden korrekt beschrieben und stimmen mit den experimentellen Daten überein. Es wird gezeigt, daß der Prozeß der Quasi-Spaltung einer der entscheidenden Faktoren ist, der die vollständige Fusion schwerer Kerne behindert.

Chapter 1

The elements existing in nature are ordered according to their atomic (chemical) properties in the periodic system which was developed by Mendeleev and Lothar Meyer. The heaviest element of natural origin is uranium. The transuranium elements range from neptunium (Z=93) via californium (Z=98) and fermium (Z=100) up to lawrencium (Z=103). For the heaviest systems the Coulomb repulsion between the increasing number of protons grows faster than the attractive nuclear forces. The heavy nuclear systems are macroscopically instable, their existence is determined by shell effects. Theoretical nuclear physicists ([1], [2]) predicted that so-called closed proton and neutron shells should counteract the repelling Coulomb forces. Atomic nuclei with these special "magic" proton and neutron numbers and their neighbours could again be rather stable. These magic proton (Z) and neutron (N) numbers were thought to be Z=114, N=184 or 196. Studies of the shell structure of superheavy elements in the framework of the meson field theory and the Skyrme-Hartree-Fock approach have recently shown that the magic shells in the superheavy region are very dependent on isotopes [3]. According to these investigations, the region of maximum stability may be near Z=120 or Z=126.

The synthesis of new nuclear species relies on the constituents of the premordial nuclei available in nature. The available nuclei are limited in their neutron-to-proton ratio by the beta decay and in size by charged-particle decay and fission due to the increasing electrostatic repulsion between the constituent protons. The first method used to produce transuranium elements, which is still used to synthesize larger quantities of specific isotopes of elements from neptunium to einsteinium, was the consecutive capture of neutrons by uranium isotopes and

the subsequent β^- decay of the capture products in nuclear reactors or in nuclear explosions. However, the number of nuclei attainable by this method is very limited. Isotopes of elements beyond Mendelevium were synthesized by fusion of heavy nuclei. This nuclear reaction was most successful in heavy-element production. The synthesis of elements Z=102-106 started from the heaviest possible actinide targets fused with light projectiles ranging from ^{10}B to ^{26}Mg. This technique depends on the availability of heavy actinides in microgram quantities, and was widely used with the accelerators of LBL and ORNL in the US and of JINR in Russia. The Berkeley and Dubna groups developed the pioneering techniques of using heavy-ion accelerators to fuse nuclei and detection systems to identify the new species [4].

For the synthesis of heavy nuclei, the cold fusion reaction with lead targets introduced by Oganessian et al [5] successfully replaced the method of the hot fusion reaction using actinide targets. Based on the fragmentation theory, Gupta, Sandulescu and Greiner [6] theoretically understood and substantiated the concept of bombarding of double magic lead nuclei with suitable projectiles. Cold fusion necessitated the development of more powerful ion sources and accelerators for the heavier ions needed in the reactions with lead. Chemical separation techniques and mechanical transport systems were replaced by electromagnetic recoil separators, which reduced the separation time to a few microseconds. The resolving power of detectors was increased and the introduction of position sensitive detectors allowed for the observation of generic parent-daughter decays to the known isotopes over a wide range of half-lives. The electronic data acquisition systems were miniaturized allowing the use of multiple parameter detector systems. The resulting large volume of data was analysed by fast computers. In cold fusion reactions at the GSI, the isotopes were unambiguously identified by means of $\alpha - \alpha$ correlations.

During the last years the region of heavy elements was extended by the production of elements up to Z=112. Here the group at the GSI was very successful utilizing cold fusion reactions of ^{208}Pb and ^{209}Bi targets with medium heavy projectiles like ^{40}Ar or ^{50}Ti [7]. The advantage of these reactions is that only slightly excited ($E^* \approx 10 - 20MeV$) compound nuclei at bombarding energies close to the Bass barrier are produced. Low-excitation energies were considered to be one of the reasons for the survival of fragile heavy nuclei against prompt fission. Producing the elements from Z=104 to Z= 112 in the cold fusion reactions, the experimentalists

observed the rapid fall-off of the evaporation residue cross section (about four orders of magnitude) with increasing Z of the compound nucleus ([4], [7], [8]). The measured cross section of the production of the element with Z=112 was $1^{+1.3}_{-0.6}$ pb.

The usual extrapolations of existing data on the synthesis of elements 110-112 indicate that to reach still heavier elements will require orders of magnitude increases in accelerator beam currents and new target technologies. It has proven difficult to proceed beyond element 112 using cold fusion reactions [9]. However, the synthesis of the element $^{293}118$ by cold fusion reaction of ^{86}Kr with ^{208}Pb in the LBL [10] has recently been reported. The production cross section was $2.2^{+2.6}_{-0.8}$ pb. This experiment has been repeated at the GSI, but unfortunately without positive results. Moreover, new experiments [11] on fission and quasi-fission of the superheavy element $^{293}118$ produced by the same reaction deny the production cross section obtained in Berkeley.

At the JINR, further isotopes were produced using hot fusion reactions induced by ^{48}Ca ions on heavy actinide targets, such as ^{232}Th, ^{238}U and ^{244}Pu, with the evaporation of 3 or 4 neutrons [12]. These reactions allow us the study of decay properties of more neutron rich isotopes of transfermium elements, which are impossible to synthesize directly by cold fusion reactions, e.g. long lived isotopes with neutron numbers close to N=162 and Z$\geq$106. Very asymmetric systems fuse with a higher probability at the Coulomb barrier. Simultaneously however, the excitation energies of the compound nuclei change from typically 10-20 MeV in the case of cold fusion reactions to 30-50 MeV. This increase of the excitation energy reduces the survival probability of heavy compound nuclei. At the same time the fusion probability is much larger in these reactions than in the Pb-based reactions.

The presently produced heavy elements are rather neutron deficient and close to the border of proton instability. Especially with stable targets and stable beams it is not possible to reach the interesting region of magic spherical nuclei with $Z = 110 - 114$ and $N = 180 - 184$. Here new possibilities can be opened up with neutron-rich beams and targets [13]. One might expect that a neutron skin and larger radii of neutron-rich projectiles may lead to enhanced fusion cross sections. On the other hand, the fast dissipative heating, when transfering loosely bound neutrons from the projectile to the target, may lead to a reduction of the cross sections.

Here improved models for the reaction mechanisms are required, which in comparison with

experiment have to be developed to describe the extremely small fraction of the total cross section leading to fusion. Predictions based on these models are useful in the preparation of the next generation of experiments. The macroscopic models ([14], [15], [16]) do not reproduce the excitation function of the reactions used for the synthesis of superheavy elements. Compensating the dissipative losses in the relative motion, the macroscopical dynamical model (MDM) of Swiatecki [16] and the surface friction model by Fröbrich [15] have to take an extra-extra-push energy into account leading to an excitation energy of the compound nucleus which results too large compared to the experimental data for superheavy elements [17]. In addition, the MDM concept yields too large evaporation residue cross sections as demonstrated for example for the $^{100}Mo + ^{100}Mo$ and $^{110}Pd + ^{110}Pd$ reactions [18] since the MDM does not take into account the competition between complete fusion and quasi-fission processes. In the MDM, the following qualitative picture was considered: i) after the capture, the neck between the nuclei grows quite quickly and a deformed united system is formed; (ii) the united system either overcomes the saddle point and moves to the equilibrium state of the compound nucleus or goes to the quasi-fission channel. The choice of the channel of complete fusion or quasi-fission depends on the initial kinetic energy of the projectile.

Another method to calculate fusion cross sections is based on the dinuclear system (DNS) concept [19]. Within this concept, calculations of the complete fusion probability and optimal excitation energy for the production of compound nuclei between Z=102 and Z=114 are in agreement with the experimental data ([20], [21] and [22]). The model based on the DNS-concept gives an explanation of the reduction of the fusion cross sections by quasi-fission and can be used for the prediction of evaporation residue cross sections in the production of heavy and superheavy elements by cold and hot fusion reactions [22]. The main idea of the DNS-concept is the assumption that complete fusion and deep inelastic transfer reactions are similar nuclear processes. Both of them are realized according to similar scenarios. The scenario of the complete fusion process is as follows. At the capture stage, after full dissipation of the collision kinetic energy, the DNS is formed. The complete fusion process is the DNS evolution that proceeds via nucleon transfer, shell by shell from one nucleus to the other. The DNS nuclei retain their individuality throughout their way to the compound nucleus. This peculiarity of the DNS evolution is the consequence of the shell structure of the nuclei.

Figure 1-1 illustrates the compound nucleus formation process in the framework of the MDM and the DNS-concept. Reviews on the theoretical basis of the DNS-concept and on the model treating the competition between fusion and quasi-fission are given in Refs. [17], [21] and [23].

Newer calculations based on the MDM model are the following: In Japan an approach is being developed on the basis of the MDM model with the fluctuation-dissipation effects [24], for the description of hot fusion of heavy symmetric systems leading to the formation of superheavy elements. Estimation of the formation cross sections of superheavy elements in the standard statistical model taking into account the limitations on fusion from empirical systematics were made in Ref. [25]. In [26], a simple model for description of cold fusion reactions based on the doubly magic lead target nucleus was proposed. This model assumes that the compound nucleus is formed by quantal tunneling through the fusion barrier. The model predicts that the most promising reaction for the production of superheavy nuclei is $^{208}Pb(^{86}Kr, 1n)^{293}118$, but the predicted cross section for this reaction is considerably larger (670 pb) than the production cross section obtained in Berkeley [10]. The model of fusion based on the DNS-concept predicts a production cross section of the order of 10^{-2} pb [27] for this reaction.

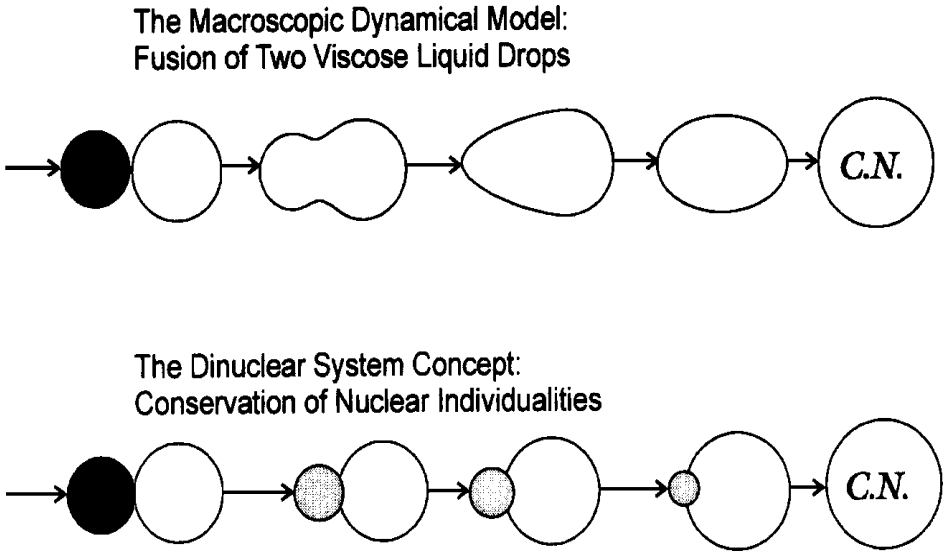

Figure 1-1: Illustration of the compound nucleus formation in the framework of the MDM and DNS-concept.

1.1 The DNS-concept of fusion

A special feature of deep-inelastic collisions is that they lead to the formation of a DNS [28]. During the entire formation and evolution of the DNS there is a continuous redistribution of nucleons, excitation energy and angular momentum between the nuclei. An unstable formation like a dinuclear system "lives" for the order of a few 10^{-21}s and decays before it achieves complete statistical equilibrium with respect to all degrees of freedom. The establishment of equilibrium between the proton and neutron numbers [29] occurs practically instantaneously in light systems and is a monotonic continuous process in heavy systems [30]. Nucleons are exchanged slowly between the parts of the DNS. As it evolves, a DNS can in principle pass with some definite probability through many macroscopic configurations allowed by the conservation laws for the particle number, charge and total energy. A DNS decays either by the dominance of forces of repulsion between the interacting nuclei or by the coupling of modes of motion. Experimental data on the widths of the charge (mass) distributions of the reaction products [29], the dependence of the yields of nuclei on their nucleon composition [31], and data on the yields of light particles in collisions that lead to the formation of compound nuclei [32] indicate that as dinuclear systems evolve, individual features of the nuclei are preserved, and shell effects play an important part. A review on these experimental evidences is given in Ref. [33]. The considered experimental data confirm the idea that the individuality of the interacting nuclei is preserved even for a relatively high excitation energy of the DNS and indicate that shell effects play a fundamental role in the evolution of the DNS. The study of the influence of shell effects is topical in connection with planned experiments with radioactive beams, which will significantly extend the possibilities for investigating the mechanism of nuclear reactions [13].

In the model of fusion based on the DNS-concept, the fusion process is considered as the evolution of a DNS caused by the transfer of nucleons from the light nucleus to the heavy one. The dynamics of the DNS is considered as a combined diffusion in the degrees of freedom of the mass asymmetry $\eta = (A_1 - A_2)/(A_1 + A_2)$ (A_1 and A_2 are the mass numbers the DNS nuclei) and of the relative distance between the centers of nuclei R describing the quasi-fission process (decay of the DNS), respectively (Fig.1-2). The potential barrier B^*_{fus} in η supplies a hindrance for the fusion. The energy required to overcome the fusion barrier B^*_{fus} is contained in the DNS excitation energy. As was found in [34], the value of B^*_{fus} can be much

smaller than the extra-extra push energy predicted in the MDM. The DNS concept is based on the assumption that the nuclei keep their individuality near their touching distance. This assumption is justified by diabatic shell model effects [35] and the structural forbiddennes for fusion [36], which hinder the nuclei to melt together along the relative coordinate R. These aspects are phenomenologically described with a double folding potential in frozen density approximation which shows a minimum near the touching distance of the nuclei. The nuclei of the DNS are in the touching configuration during the evolution of system in the mass asymmetry degree of freedom and the decay of the system can only occur in the relative coordinate. There is experimental evidence that the mass asymmetry degree of freedom equilibrates more rapidly than the elongation of the system which allows to treat the evolution of the DNS by statistical models. In order to calculate the probability for fusion P_{CN}, the Fokker-Planck equation for the complete set of collective coordinates and conjugate momenta (η, p_η, R, p_R) was solved [34] within the global momentum approach. The data obtained with this method are in agreement with the ones calculated in the approach based on the Kramers-type expression for the fusion rate through the inner fusion barrier of the DNS [34]. The main advantage of the Kramers-type expression for the fusion rate in contrast to the statistical method [18] is the possibility to include nuclear viscosity in the fusion process. In these calculations the neck degree of freedom that is important in the MDM is not considered. As follows from Ref. [37], the extension of the relevant collective variable set by the neck variable may be questionable for the values of R considered in the DNS. For a small overlap of the nuclei (that takes place in the DNS), the neck size is close to the one obtained by a simple superposition of the frozen density tails.

The values of the fusion probabilities obtained in the DNS-model are in agreement with the values extracted from the experimental data for most of the reactions of heavy nuclei. Thus, the competition between the complete fusion and quasi-fission processes is extremely important in the DNS evolution.

The new model suggested in [18] and [34], yields a good agreement between the theoretical predictions and experimental data on the fusion of heavy nuclei.

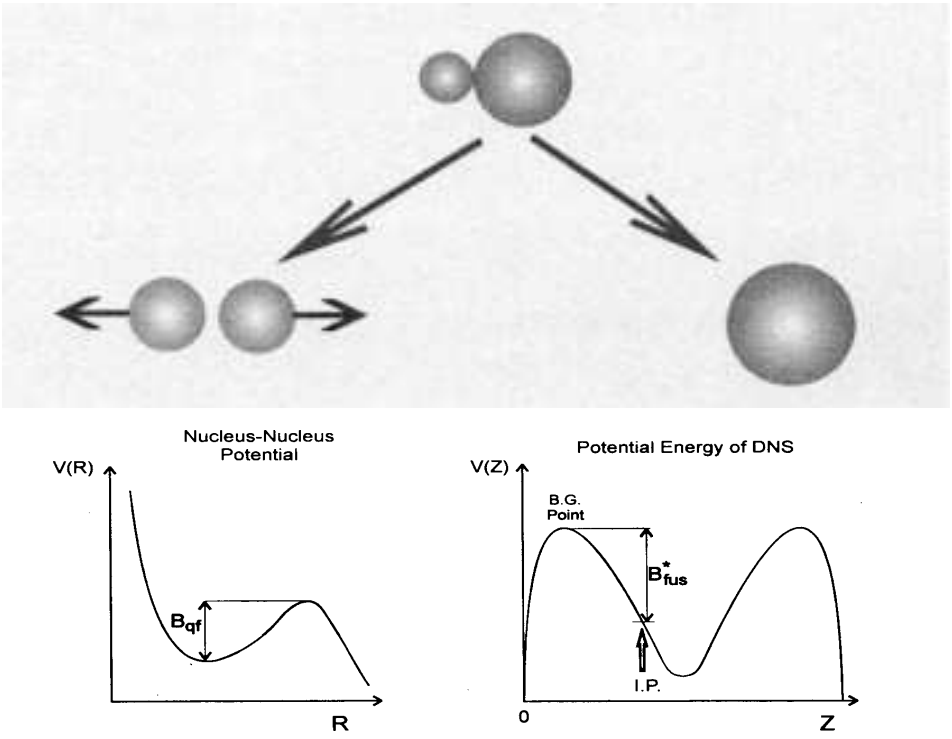

Figure 1-2: Two ways of evolution of the DNS to quasi-fission and fusion.

Within this model the evaporation residue cross-section can be written as

$$\sigma_{ER}(E_{c.m.}) = \sum_{J=0}^{J_{\max}} \sigma_c(E_{c.m.}, J) \cdot P_{CN}(E_{c.m.}, J) \cdot W_{sur}(E_{c.m.}, J). \tag{1.1}$$

The capture cross-section σ_c describes the transition of the colliding nuclei over the Coulomb barrier and the formation of the DNS when the kinetic energy is transformed into the excitation energy of the DNS. This initial stage of a collision was recently studied with a dynamical model [38]. Calculations were performed for $^{48}Ca + ^{244}Pu$ and $^{74,76}Ge + ^{208}Pb$ reactions which could lead to the formation of the superheavy element Z=114. It was shown that for the considered reactions, there is an energy window for the bombarding energy $E_{c.m.}$ at which the capture cross-section σ_c is large enough to have a physical interest. The value of $J_{\max}$ corresponds to $E_{c.m.}$ and is larger than the limit of the value of J for the compound nucleus formation. The probability of complete fusion P_{CN} depends on the competition between the complete

fusion and quasi-fission processes after the capture stage in the DNS. In these reactions the quasi-fission channel dominates and leads to a strong reduction of the magnitude of the fusion cross-section. The surviving probability W_{sur} estimates the competition between fission and neutron evaporation in the excited compound nucleus and may be calculated according to the statistical model [39] on the basis of the Monte Carlo method.

1.2 Goals of the present work

The basic microscopical model for the dinuclear system is the two-center shell model (TCSM) [40] (see Appendix). The usual parametrisation of the two-center potential consists of the relative distance between the centers (or elongation), the mass (charge) asymmetry $\eta = (A_1 - A_2)/(A_1 + A_2)$, the deformations of the fragments β_i and the neck coordinate ε. The elongation $\lambda = l/(2R_0)$ measures the length l of the system in units of the diameter $2R_0$ of the spherical compound nucleus. This variable can be used to describe the relative motion. The mass ratio between the fragments and the transition of the nucleons through the neck are described by the mass asymmetry η. The neck parameter $\varepsilon = E_0/E'$ is defined by the ratio of the actual barrier height E_0 to the barrier height E' of the two-center oscillator. The deformations $\beta_i = a_i/b_i$ of axial symmetric fragments are defined by the ratio of their semiaxes. The neck grows with decreasing ε (Fig.1-3). The potential energy surface (PES) in these coordinates is generally calculated with the Strutinsky method [41]. This is an adiabatic approach since the nucleons occupy the single particle states up to the Fermi level in calculating the shell corrections.

The adiabatic potential energy surfaces calculated as functions of the elongation of the DNS and of the neck parameter were used to study classical trajectories for various heavy ion reactions by using dissipative forces and mass parameters obtained with the Werner-Wheeler aproximation [42]. The fusion probabilities in the adiabatic TCSM are much larger than those obtained from experimental data and show an incorrect isotopic dependence.

The reactions considered were for example the symmetric ones $^{90}Zr+^{90}Zr$, $^{100}Mo+^{100}Mo$, $^{110}Pd+^{110}Pd$, $^{124}Sn+^{124}Sn$ and $^{136}Xe+^{136}Xe$ and asymmetric ones. Therefore, it is concluded that a hindrance exists which prohibits the fast growth of the neck and the motion to smaller elongations and allows the DNS to survive a time comparable with the reaction time.

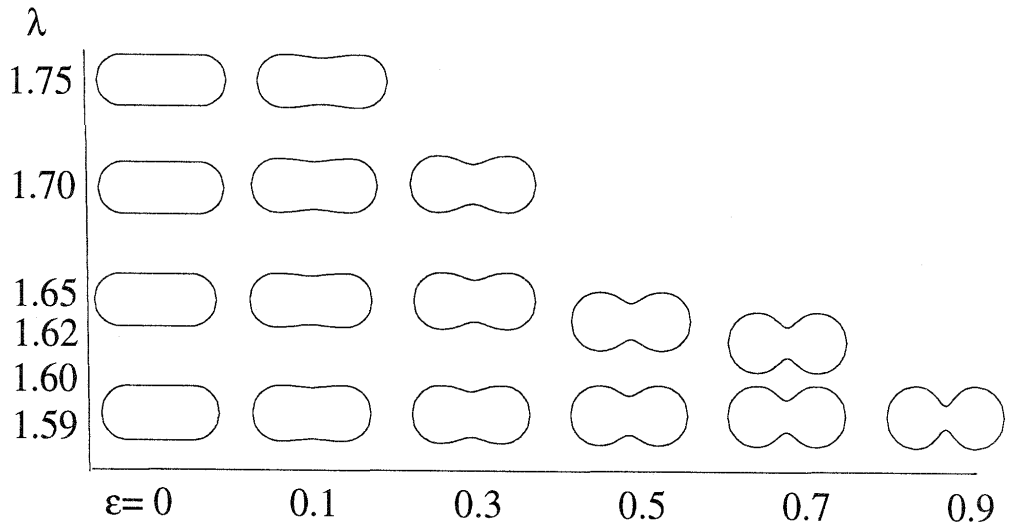

Figure 1-3: Shapes of the system $^{110}Pd + ^{110}Pd$ as functions of ε and λ.

Motivated by these results, we started to investigate possible factors which hinder the DNS to melt together in the elongation λ. We consider these factors to be diabatic effects in the potential energy surface [35] and a large mass parameter in the neck coordinate ε [43]. Investigating these factors, we try to find theoretical justifications for the basic assumptions of the model of fusion based on the DNS-concept. We would like to stress that the model of fusion, based on the DNS-concept, explains many experimental data concerning the production of superheavy elements and plays an important role for giving predictions for new experiments ([22],[27]).

In the present work, using the TCSM, we want to study the following:

- Diabatic potentials as a function of the relevant collective variables of the DNS for heavy-ion systems.
- Microscopic mass parameters for the relevant coordinates of the DNS formed in collisions of heavy nuclei taking the width of single-particle states into account.
- Whether the system has time for the growing of the neck.
- Whether the system has time for destroying the "memory" on the diabatic (structural) forbiddenness for the fusion in the elongation λ and to find the favorable fusion channel.
- Within which model it is possible to describe the experimental quasi-fission products of fusion reactions.

In the present chapter we have presented an introduction of experimental and theoretical knowledge in the field of transuranium and superheavy elements. A brief review about the model of fusion based on the DNS-concept as well as a comparison of this model with other theoretical models of fusion have been presented.

In chapter 2 we give a summary of the main ideas about diabaticity in heavy-ion collisions. Moreover, the methods of calculations of a diabatic basis in the TCSM are explained. The potential energy of the DNS as a function of the relevant collective variables of the diabatic TCSM is shown in chapters 3 and 4 for different heavy systems. In chapter 5 the calculation of microscopical mass parameters of the DNS formed in reactions with heavy nuclei is presented by using the adiabatic and diabatic TCSM and the width of the single-particle states. The competition between two possible fusion channels in elongation λ and in mass asymmetry η is studied for various heavy systems in chapter 6. In chapter 7 the quasi-fission process of the DNS is evaluated solving a transport master-equation for the exchange of nucleons between the parts of the DNS, which also takes the decay of the DNS in the elongation λ into account. A summary and the outlook of the work are given in chapter 8.

Chapter 2

The study of nucleus-nucleus collisions at energies of some few MeV/u above the interaction barrier stimulated the development of theoretical concepts for large-amplitude collective nuclear motion [44]. We note in particular the introduction of transport theories like the random-matrix approach [45], the one-body dissipation model [46, 47] and the linear response theory [48]. These theories assume (either explicitly or implicitly) a statistical equilibrium within the intrinsic degrees of freedom throughout the collision described by a few collective variables. Such a local equilibrium, however, is not expected to be realistic during the initial stage of a nucleus-nucleus collision, a process which starts from the approach of two nuclei in their ground states. Because of the long mean free path, the motion of the individual nucleons during the approach phase is governed by their self-consistent mean potential which evolves in time. Therefore, this stage should be well described by the time-dependent Hartree-Fock (TDHF) theory [49]. Effects from residual two-body collisions and the corresponding transition to local equilibrium were formulated in extensions of TDHF [50]. An alternative model was introduced in [51] by the concept of dissipative diabatic dynamics (DDD) as a time-dependent shell-model approach. This model takes into account simultaneously the coherent and incoherent forms of motion of the nucleons in nucleus-nucleus collisions. For sufficiently large collective velocities (typically the collective kinetic energy per nucleon needs to be larger than 0.03 MeV) the nucleons no longer adjust their wave functions adiabatically but diabatically, thereby preserving the nodal structure (character) of the wave functions. Adiabatic basis states are not always useful [52]. It was realized by Landau, Stueckelberg and Zener [53] that it is advantageous at

higher collective velocities to replace the adiabatic basis states at pseudo-crossings by diabatic states [54]. Diabatic states belong to crossing levels. This situation is illustrated in Fig. 2-1.

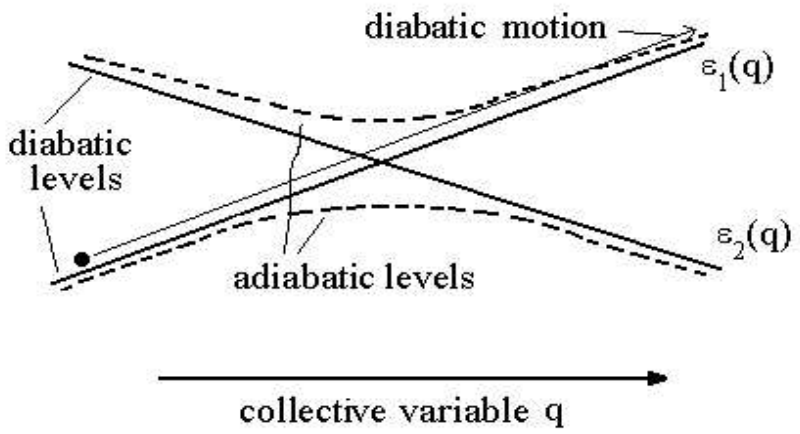

Figure 2-1: Diabatic and adiabatic levels at the Landau-Zener-Stückelberg (quasi-)crossing. In the diabatic motion the nucleon keeps the nodal structure (character) of the wave function.

Only for very small collective velocities, the nucleons are able to adjust their wave functions adiabatically and follow the adiabatic levels. At higher collective velocities, a nucleon occupying the lower level before the crossing with an unoccupied level will stay (while preserving the character of its wave function) on the diabatic level and finds itself on the upper level after the crossing. Quantitatively, this jump probability, which measures the degree of diabaticity, is given by [53]

$$J = \exp(-\frac{1}{\Delta}), \tag{2.1}$$

where

$$\Delta = \hbar \mid \partial(\epsilon_1 - \epsilon_2)/\partial q \mid \cdot \mid \dot{q} \mid /2\pi \mid H'_{12} \mid^2 . \tag{2.2}$$

The quantity Δ is proportional to the difference in the slopes of the diabatic levels and to

the collective velocity $\dot{q}$, and inversely proportional to the square of the static coupling H'_{12} between the diabatic states. A diabatic basis is advantageous if $J > 0.5$ and hence, $\Delta > 1.44$. The expression (2.1) is obtained in the linear two-state Landau-Zener model [55] which assumes that the motion of the system in the nonadiabaticity region is quasi-classical.

In the adiabatic TCSM one can observe the mutual repulsion of levels having the same z-component of total angular momentum j_z, which prevents crossings. It is due to the noncrossing rule obtained by Neumann and Wigner [56]. The noncrossing rule reads [55]: the eigenvalues of the Hamiltonian $H(q)$, taken to be functions of the coordinate q, do not cross if they belong to the same irreducible representations of the symmetry group of the Hamiltonian. The eigenvalues corresponding to different irreducible representations of this symmetry group may cross. The proof of the noncrossing rule is based on the following arguments: Let the Hamiltonian $H(q)$ have closely lying eigenvalues $E_1(q_0)$ and $E_2(q_0)$ corresponding to the eigenfunctions $\mid 1 >_0$and $\mid 2 >_0$ at a certain value q_0 of the collective coordinate, e.g., relative distance R_0 of the nuclei. Treating the Hamiltonian for q values close to q_0 as a perturbed $H(q_0)$

$$H(q) = H(q_0) + \frac{\partial H}{\partial q} \mid_{q=q_0} \cdot \delta q = H(q_0) + V, \tag{2.3}$$

it can be readily seen that the difference between the energy eigenvalues at point q is

$$\Delta E_{12}(q) = \left(\{ [E_1(q_0) + V_{11}] - [E_2(q_0) + V_{22}] \}^2 + 4 \mid V_{12} \mid^2 \right)^{1/2}, \tag{2.4}$$

where $V_{ik} =_0 < i \mid V \mid k >_0$. In order that the terms cross, both terms in the radical of (2.4) must go to zero simultaneously. If $\mid 1 >_0$ and $\mid 2 >_0$ belong to different irreducible representations of the $H(q)$ symmetry group, $V_{12} = 0$ and (2.4) can be converted to zero by the proper choice of δq. But when $\mid 1 >_0$ and $\mid 2 >_0$ belong to the same irreducible representations of the Hamiltonian symmetry group, $V_{12} \neq 0$ and generally speaking both terms in the radical of (2.4) cannot go to zero simultaneouly, since they are functions of only one parameter δq. The noncrossing rule uses a complete symmetry group of the Hamiltonian.

2.1 General considerations

We want to deal with the single-particle motion in a time-dependent mean field $U(x;q(t))$, where x denotes position, spin and isospin of the nucleon and $q \equiv \{q_n(t)\}$ a set of time-dependent collective parameters describing the shape of the nuclear system. The solution $\Psi_\beta(t)$ of the time-dependent Schrödinger equation with the Hamiltonian

$$H = T + U = - - \frac{\hbar^2 \nabla^2}{2m_0} + U(x,q) \tag{2.5}$$

can be expressed as an expansion [57]

$$\mid \Psi_\beta(t) >= \sum_\alpha c_{\alpha\beta}(t) \exp\left[-i\left\{\int_0^t dt' \epsilon_\alpha(t') - m_0 W(x;q,\dot{q})\right\}/\hbar\right] \mid \psi_\alpha(x,q) >, \tag{2.6}$$

in terms of some orthonormal stationary basis functions $\mid \psi_\alpha(x,q) >$ with the initial condition $c_{\alpha\beta}(t=0) = \delta_{\alpha\beta}$. In addition to the usual energy phase factor, a collective phase factor [58, 59] has been introduced which is common to all states α. In atomic collisions, the velocity potential W [55] is often allowed to depend on the atomic state α, so that the relative velocities can be accounted for in specific transfer reactions. Such a refinement can also become important for grazing nucleus-nucleus collisions. However, for central collisions which lead to compact nuclear shapes, a common phase factor seems to be more appropriate [57]. This choice has the advantage of leaving the stationary basis orthogonal and independent of the collective velocity.

Inserting the expansion (2.6) into the Schrödinger equation and projecting onto the state ψ_γ, we find the set of coupled first-order differential equations

$$i\hbar\, \dot{c}_{\gamma\beta} = \sum_\alpha c_{\alpha\beta} < \psi_\gamma \mid H' + U_1 + U_2 \mid \psi_\alpha > \exp\left[-i \int_0^t dt' \{\epsilon_\alpha(t') - \epsilon_\gamma(t')\}/\hbar\right] \tag{2.7}$$

with $\epsilon_\alpha =< \psi_\alpha \mid H \mid \psi_\alpha >$ for the determination of the expansion coefficients $c_{\alpha\beta}$. The coupling terms are given by

$$H' = H - H_0 = H - \sum_\alpha \mid \psi_\alpha > \epsilon_\alpha(q) < \psi_\alpha \mid, \tag{2.8}$$

$$U_1 = -i\hbar \left\{ \sum_n \dot{q}_n \partial/\partial q_n + \frac{1}{2} [\Delta, W] \right\}, \tag{2.9}$$

$$U_2 = \frac{1}{2} m_0 (\nabla W)^2 + m_0 \sum_n (\dot{q}_n \partial W/\partial q_n + \ddot{q}_n \partial W/\partial \dot{q}_n), \tag{2.10}$$

where H' is independent of the collective velocity $\dot{q}$. If we choose W to be linear in $\dot{q}$, we have all terms of U_1 linear in $\dot{q}$, too. Furthermore, the coupling U_2 becomes quadratic in $\dot{q}$ and proportional to the collective acceleration $\ddot{q}$, respectively. The optimal choice for the stationary basis states ψ_α is defined by minimizing the coupling so that the coefficients $c_{\alpha\beta}(t)$ keep close to the initial values $\delta_{\alpha\beta}$. We consider the adiabatic and diabatic choices which are convenient in different regions of the collective velocities.

The adiabatic basis states $\psi_\alpha^{ad} \equiv \chi_\alpha$ are determined by the vanishing of the static coupling H' and hence, are the eigenstates of the total single-particle Hamiltonian H. For a given H the adiabatic basis is uniquely defined. However, the dynamical couplings $< \chi_\beta \mid \dot{q}_n \partial/\partial q_n \mid \chi_\alpha >$ of U_1 have localized peaks around pseudo-crossings. Depending on the states χ_α, the pseudo-crossings occur at different points in the space of collective variables. Therefore, it is impossible to find a collective velocity potential W which can compensate the peaks of the couplings $< \chi_\beta \mid \dot{q}_n \partial/\partial q_n \mid \chi_\alpha >$, Eq. (2.9). Furthermore, dynamical couplings cannot be treated by perturbation theory [60]. This can be immediately seen from the expression (2.1) for the jump probability if the diabaticity parameter is rewritten as

$$\Delta = 2\hbar \mid < \chi_2 \mid \partial/\partial q \mid \chi_1 >_{q_c} \mid \cdot \mid \dot{q} \mid / \pi \mid H'_{12} \mid, \tag{2.11}$$

where the dynamical coupling between the adiabatic states at the crossing point $q = q_c$ enters into the numerator. Thus, the jump probability (2.1) cannot be expanded in powers of the dynamical coupling matrix element. Because of this, the adiabatic basis is only convenient for very small collective velocities so that the single-particle motion is purely adiabatic.

For larger velocities it is often more convenient to choose basis states ψ_α which have smaller

dynamical couplings. Diabatic basis states $\psi_\alpha^{diab} \equiv \phi_\alpha$ are defined [57] by the condition that the first-order dynamical coupling (2.9) vanishes. Introducing the decomposition $W = \sum_n \dot{q}_n$ $w_n(x,q)$, it is obtained [57]

$$-(\partial/\partial q_n) \mid \phi_\alpha >= \frac{1}{2}\left[\Delta, w_n\right] \mid \phi_\alpha >= \left\{(\nabla w_n)\cdot\nabla + \frac{1}{2}(\Delta w_n)\right\} \mid \phi_\alpha > \tag{2.12}$$

as the diabaticity criterion which is independent of $\dot{q}_n$ and hence allows to define stationary diabatic basis states. The relation (2.12) ascribes the change of any diabatic state with q_n to a collective displacement field ∇w_n which scales all wave functions in the same way.

The diabaticity criterion (2.12) does not rigorously determine a diabatic representation because the velocity field is not uniquely defined. Therefore, the following condition

$$< \phi_\beta \mid H' \mid \phi_\alpha > \simeq 0 \tag{2.13}$$

is added. This condition is appropriate whenever the collective velocities are sufficiently smaller than the Fermi velocity. The supplementary condition (2.13) then suggests to construct the diabatic basis states from adiabatic states by avoiding the dramatic changes of the wave functions near pseudo-crossings.

2.2 Construction methods

In atomic physics, a large variety of construction methods for diabatic representations have been considered [55, 61]. Within the TCSM, two methods for the construction of diabatic states were developed [57] for central nucleus-nucleus collisions. The method of maximum overlap is based on the construction of crossings of diabatic levels where pseudo-crossings occur in the adiabatic TCSM. The construction of the diabatic states as a function of the relative distance starts from the separated nuclei where adiabatic and diabatic states coincide. A diabatic state at a smaller relative distance is obtained from a linear combination of a few adiabatic states which maximizes the overlap with a diabatic state at somewhat larger relative distance. Using the so constructed states, one is able to obtain step by step the diabatic states for smaller relative distances. The method of maximum symmetry eliminates the symmetry-

violating parts SV from the total Hamiltonian H of the TCSM. Then the diabatic states are the eigenstates of the difference $H_d = H - SV$, which is taken as the diabatic TCSM-Hamiltonian in the case of equal nuclei (symmetric system). Since the symmetry of H_d is higher than that of H, the irreducible representations of the H_d symmetry group appear to be, generally speaking, reducible representations of the H symmetry group. Thus two different irreducible representations of the H_d symmetry group can contain the same irreducible representations of the H symmetry group. Therefore, in the general case the H_d eigenvalues possessing the same symmetry relative to the H symmetry group may cross. This crossing will become an avoided crossing if the perturbation SV, which is nondiagonal in the quantum numbers specifying the H_d eigenvalues, is taken into account. For slightly asymmetric systems, the diabatic states are defined by the expansion of the asymptotic states in terms of such maximum symmetry states. Keeping the expansion coefficients fixed as functions of the collective coordinate q, diabatic states are obtained with the desired property that their wave functions adjust to the shape of the TCSM potential by a minimum change in their structure. Diabatic levels obtained with this method agree with those from the maximum overlap procedure [57]. In the calculations we use the method of maximum symmetry because it turns out to be numerically easier to handle.

Chapter 3

The synthesis of transuranium and superheavy elements ([4], [7], [8]), the production of superdeformed nuclei and nuclei far from the line of stability stimulate the study of fusion processes in heavy ion collisions at low energies ($< \ 15\ MeV/u$). Existing theoretical models can be distinguished by the choice of the relevant collective variables in which the fusion occurs. The relative distance between the centers of nuclei R (or elongation of system) and the neck degree of freedom play an essential role in the macroscopic dynamical model (MDM) [16], which is based on an adiabatic approach to fusion. Without regarding the competition between complete fusion and quasi-fission, this model overestimates the fusion cross section of heavy nuclei [18]. Attempts were made to improve this model by including thermal fluctuations and the competition between complete fusion and quasifission in [62], but an agreement with the experimental data was not achieved for the reactions treated in this study. Corrections to these results could arise from nuclear structure effects in collisions with energies slightly above the Coulomb barrier. In a recent paper [42], the shell effects were incorporated by using the two-center shell model (TCSM) [40]. The study of the dynamics of fusion within the adiabatic TCSM overestimates the fusion probabilities for most symmetric and near symmetric reactions. Moreover, the isotopic dependence of the fusion probability resulted incorrectly. Therefore, hindrances for the growth of the neck and for the motion to smaller values of R should be assumed to explain the experimental data. This hindrance allows the dinuclear system (DNS) to keep a relatively small neck over a time comparable with the reaction time. Then the fusion proceeds as a motion of the DNS in mass asymmetry. Such a hindrance of the motion to smaller R is

explicitly assumed in the DNS model [34], which describes the experimental fusion data quite well. The nuclei in the DNS could be hindered to melt together in R due to diabatic effects or due to a specific behaviour of the mass parameters.

In this chapter we study the diabatic potentials for heavy nuclear systems as a function of the elongation λ, the neck coordinate ε and the mass asymmetric η using the method of maximum symmetry within the generalized TCSM [35]. In the previous calculations [57] a simplified version of the TCSM was used and the role of the neck coordinate was not taken into account. We will compare our results with nucleus-nucleus potentials obtained by using a double folding procedure for the nuclear interaction. The calculations are performed for the symmetric systems ^{90}Zr+^{90}Zr, ^{96}Zr+^{96}Zr, ^{100}Mo+^{100}Mo, ^{110}Pd+^{110}Pd, ^{130}Xe+^{130}Xe and ^{136}Xe+^{136}Xe. The asymmetric systems ^{110}Pd+^{136}Xe, ^{86}Kr + ^{160}Gd and ^{48}Ca+^{198}Hg are also studied. The applicability of the diabatic method will be discussed for collisions near the Coulomb barrier.

3.1 The diabatic potential

In a diabatic description the nucleons do not occupy the lowest free single-particle levels as in the adiabatic case, but remain in the diabatic levels during the collective motion of the nuclear system. As a result, the diabatic potential energy surface is raised with respect to the adiabatic potential energy surface and new potential barriers for collective variables may appear. The values of these barriers can be also estimated by calculations of the structural forbiddenness of fusion [36]. The concept of structural forbiddenness is based on the difference created by action of the Pauli principle between the state of the compound nucleus and the state of the separated heavy nuclei [63].

The total diabatic potential is defined as

$$V_{diab}(q) = V_{adiab}(q) + \Delta V_{diab}(q), \tag{3.1}$$

where the set of collective coordinates of the system is denoted by q. The adiabatic potential energy

$$V_{adiab}(q) = E_{LDM} + V_N + \delta E_{shell} + \delta E_{pair} - E^{CN}_{LDM} \tag{3.2}$$

is calculated within the TCSM using the liquid drop energy E_{LDM}, the Strutinsky prescription for the shell correction δE_{shell}, pairing correction δE_{pair} and the proximity nuclear potential V_N to improve the adiabatic energy for large elongations [42]. The adiabatic potential energy is normalised to the liquid drop energy E^{CN}_{LDM} of the spherical compound nucleus.

The diabatic contribution ΔV_{diab} is expressed as

$$\begin{aligned}
\Delta V_{diab}(q) &= \sum_\alpha \epsilon^{diab}_\alpha(q) n^{diab}_\alpha - \sum_\alpha \epsilon^{adiab}_\alpha(q) n^{adiab}_\alpha(q) \\
&= \sum_\alpha \epsilon^{diab}_\alpha(q)(n^{diab}_\alpha - n^{adiab}_\alpha(q)) + \sum_\alpha n^{adiab}_\alpha(q)(\epsilon^{diab}_\alpha(q) - \epsilon^{adiab}_\alpha(q)) \\
&\approx \sum_\alpha \epsilon^{diab}_\alpha(q)(n^{diab}_\alpha - n^{adiab}_\alpha(q)),
\end{aligned} \tag{3.3}$$

where the contribution from the second term with $(\epsilon^{diab}_\alpha(q) - \epsilon^{adiab}_\alpha(q))$ is assumed to be negligible because the adiabatic and diabatic single-particle levels differ only in the area of the pseudo-crossings of adiabatic states [57]. The diabatic occupation probabilities n^{diab}_α are determined by the configuration of the separated nuclei. The adiabatic occupation probabilities n^{adiab}_α vary with q according to the ground-state configuration where only the lowest levels are occupied. The diabatic levels ϵ^{diab}_α are classified by the quantum numbers $\alpha = j_z, l_z, s_z, n_\rho, n_z$ of the eigenstates of the diabatic Hamiltonian. We only used the diagonal elements of the symmetry-violating parts of the generalized TCSM Hamiltonian. Non-diagonal elements arise only from the spin-orbit potential V_{LS} (A.3), the centrifugal potential V_{L^2} (A.4) and the neck potential H_1 (A.16). The first two potentials contain l_x, l_y, s_x and s_y. The diabatic Hamiltonian is expressed as

$$H_d = H_0 + V_{l_z s_z} + V_{l_z^2} + \delta\!\!\!/, \tag{3.4}$$

where H_0 is the Hamiltonian of a two-center oscillator (A.15). The influence of the neck parameter ε is taken into account by means of the diagonal contribution of the difference

$$\delta\!\!\!/ \equiv H_1(\varepsilon) - H_1(\varepsilon = 1) = \frac{(\varepsilon - 1)}{2} m_0 \omega_z^2 z'^2 (1 + cz' + dz'^2), \tag{3.5}$$

where the coefficients c and d are determined by requiring that the potential and its derivative

are continuous with respect to z at $z = 0$. For $z < 0$ and $z > 0$, the oscillator frequencies ω_z must be determined numerically from the assumption of volume-conservation. With the method suggested we can find the diabatic levels close to the adiabatic levels (Fig. 3-1). Differences take place only near the crossing points. In contrast to Ref. [57], we can consider the diabatic effects for any neck parameter ε. This yields a better shape parametrisation of the DNS.

3.2 Results and discussion

In the calculations, we firstly consider symmetric collisions of spherical nuclei and then analyse asymmetric entrance channels, thermal and deformation effects. The diabatic contribution ΔV_{diab} as a function of the elongation is presented for the reaction ^{100}Mo+^{100}Mo in Fig. 3-2. The nuclei are considered as spherical with $\varepsilon = 0.74$, which supplies realistic shapes of the DNS for $\lambda = 1.5 - 1.6$. ΔV_{diab} consists of contributions from neutrons and protons. The diabatic contribution increases with decreasing λ or R because many diabatic levels cross the Fermi level (Fig. 3-3). In general, the diabatic contribution increases with the mass number A of the system because of the larger number of level crossings. The diabatic contribution ΔV_{diab} of many symmetric systems selected along the line of beta stability shows diabatic shell-structure effects [63, 64]. The role of these effects is demonstrated in Fig.3-4a by the diabatic contributions of neutrons and protons for the systems ^{90}Zr+^{90}Zr and ^{96}Zr+^{96}Zr. While the diabatic contributions of the protons are nearly the same in both the systems, the diabatic contributions of the neutrons are quite different. As a result, the total diabatic potential is more repulsive in the case of ^{90}Zr+^{90}Zr (Fig. 3-4b).

Further diabatic potentials are presented in Figs.3-4c and 3-5 for the systems ^{130}Xe+^{130}Xe, ^{136}Xe+^{136}Xe, ^{100}Mo+^{100}Mo and ^{110}Pd+^{110}Pd. The neck parameter is fixed at $\varepsilon = 0.74$ and the nuclei are considered as spherical. Excepting the potentials with the Xe isotopes (Fig. 3-4c), the diabatic potentials for all these systems have a pocket near to the touching configuration ($\lambda = 1.58$) in which the DNS could stand some time and evolve in mass asymmetry. For smaller elongations, the diabatic potential is strongly repulsive in all symmetric systems.
The diabatic potential is similar to the one calculated with the phenomenological double folding potential. In Fig. 3-5 we compare the diabatic potential of the system ^{110}Pd+^{110}Pd with the

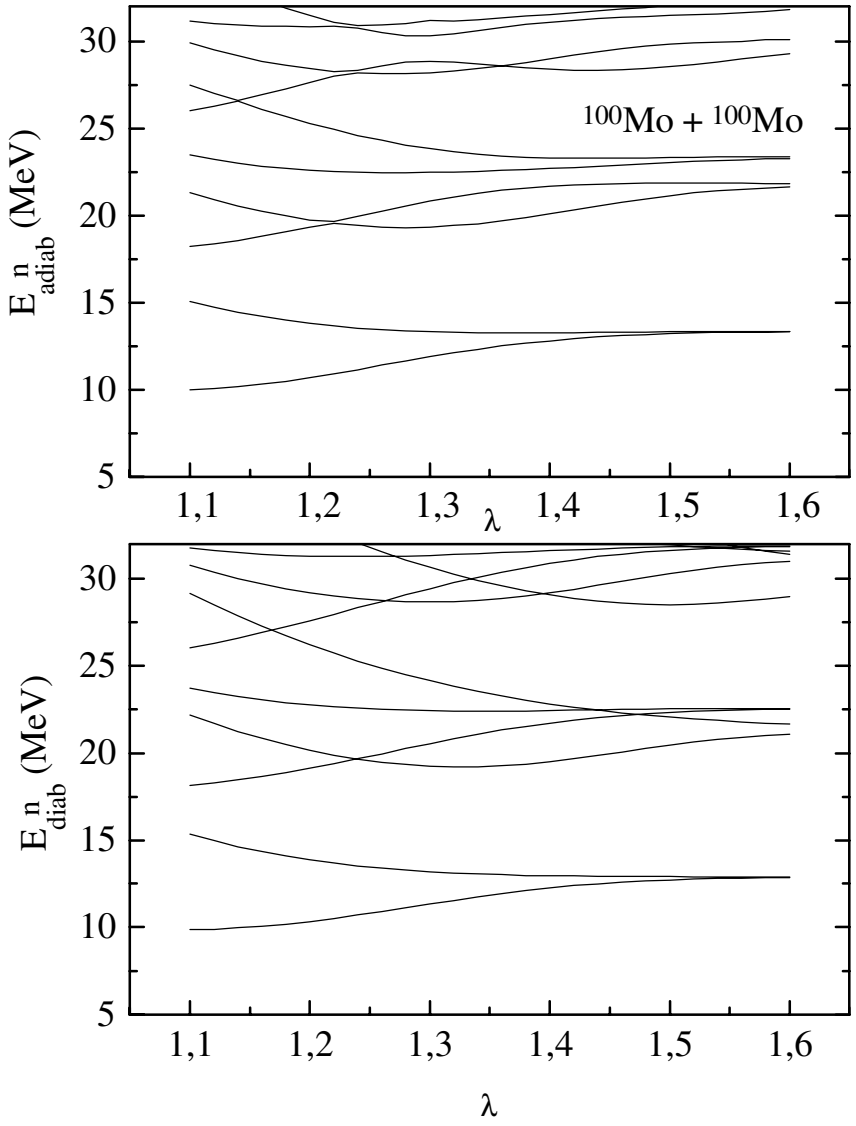

Figure 3-1: Diagrams of adiabatic (upper part) and diabatic (lower part) neutron levels with $j_z = 1/2$ for $^{100}Mo + ^{100}Mo$ as a function of elongation λ. The nuclei are considered as spherical with $\varepsilon = 0.74$. The adiabatic levels are calculated with the generalized TCSM Hamiltonian (A.14) and the diabatic levels with the diabatic Hamiltonian (3.4) using the maximum symmetry method.

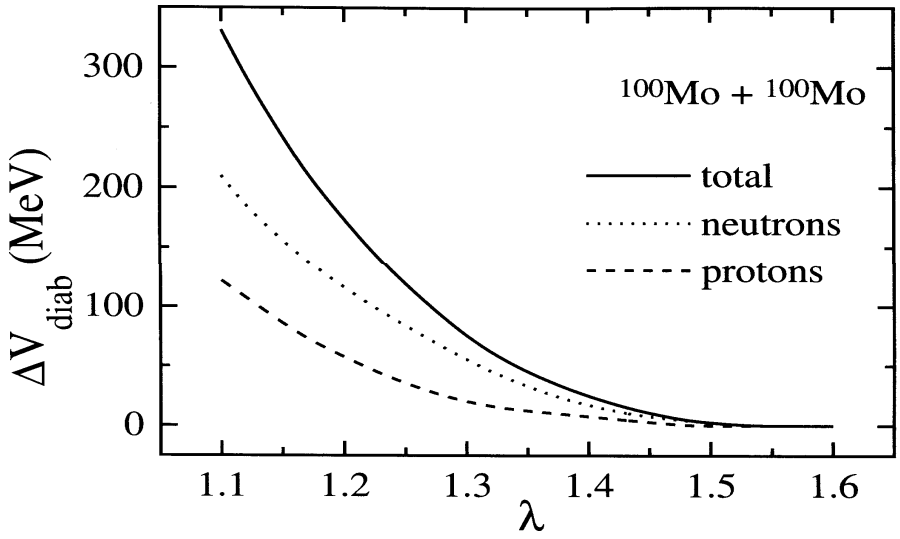

Figure 3-2: Diabatic contribution ΔV_{diab} as a function of elongation λ for the system ^{100}Mo+ ^{100}Mo (solid line). The neutron and proton diabatic contributions are shown by dotted and dashed lines, respectively. The nuclei are considered spherical with $\varepsilon = 0.74$.

phenomenological double folding potential [65]. A discrepancy with the adiabatic potential is seen for small elongations where the phenomenological potential is more repulsive than the diabatic one. The discrepancy becomes smaller if we take into account a decrease of ε with decreasing elongation. This is demonstrated for the system ^{110}Pd+^{110}Pd in Fig. 3-6, where the diabatic potential is shown as a function of ε for constant values of λ. The minimum of the diabatic potential moves to smaller values of ε with decreasing values of λ (or R).

Fig. 3-6 shows diabatic potentials for the systems ^{96}Zr+^{96}Zr and ^{90}Zr+^{90}Zr as a function of ε for $\lambda = 1.54$ near to the minimum of the pocket in λ. The diabatic contribution is smaller as a function of ε for the ^{96}Zr+^{96}Zr system than for the ^{90}Zr+^{90}Zr system (lower part of Fig. 3-7). The reason for this can be seen through an analysis of the single particle spectra (Fig. 3-8). In the case of ^{90}Zr+^{90}Zr, more diabatic levels with larger slopes cross the Fermi-level at larger values of ε. From Figs. 3-3 and 3-8 it follows that the diabatic contributions are larger with respect to the relative coordinate than with respect to the neck coordinate. This is explained by the number of crossings of diabatic states in the variation of both coordinates. In most systems

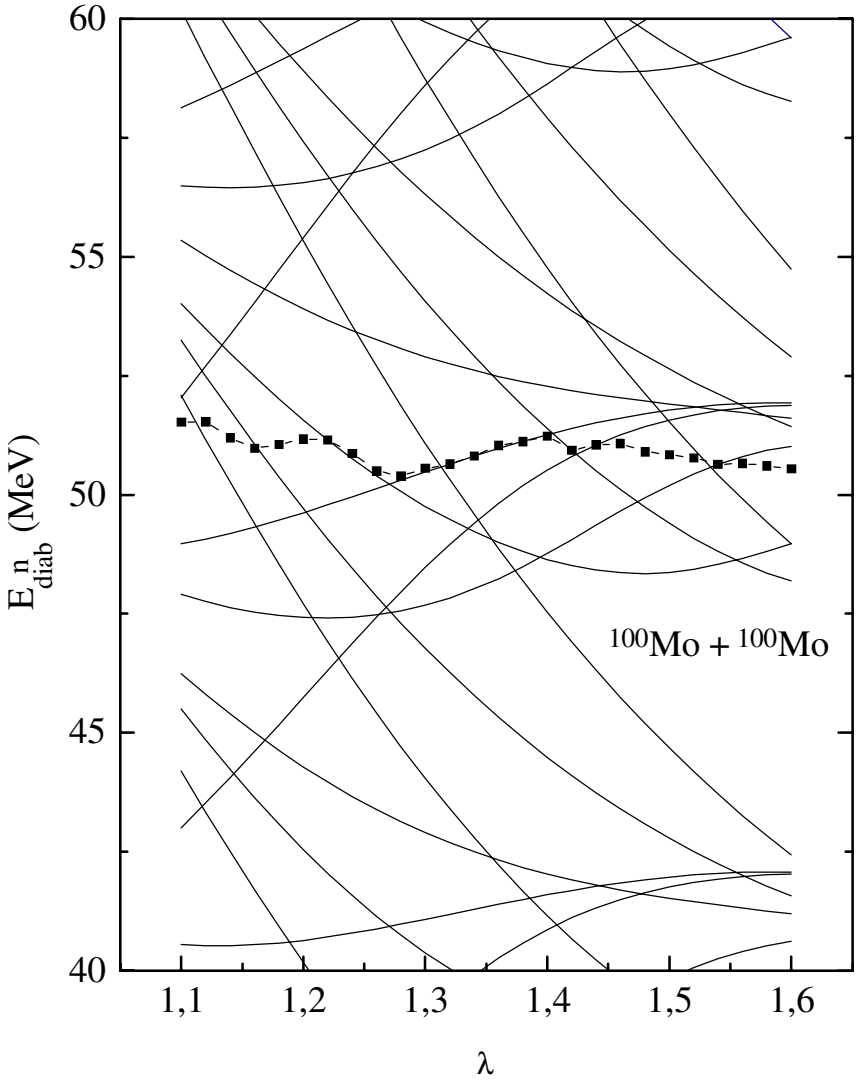

Figure 3-3: Diagram of diabatic neutron levels with $j_z = 1/2$ near the Fermi level (squares) for $^{100}Mo + ^{100}Mo$ as a function of λ. The nuclei are considered as spherical with $\varepsilon = 0.74$. The diabatic levels are calculated with the diabatic Hamiltonian (3.4) using the maximum symmetry method.

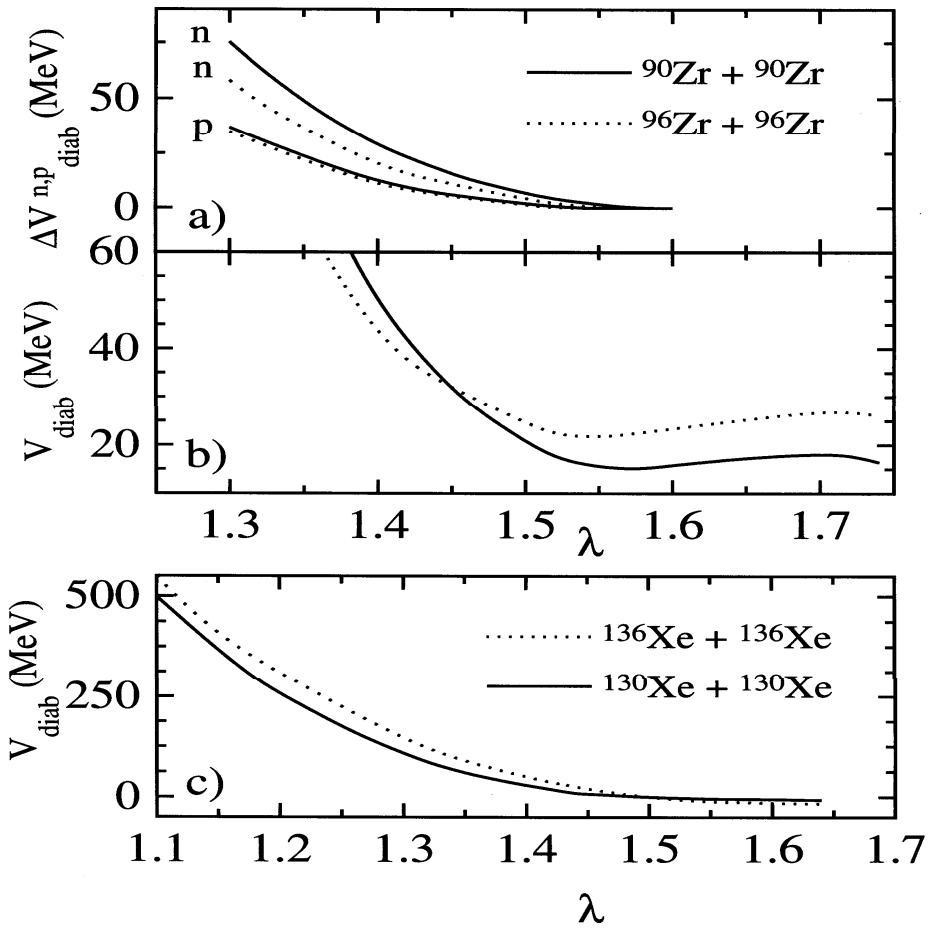

Figure 3-4: a) Diabatic contributions of protons and neutrons for the systems $^{90}Zr + ^{90}Zr$ (solid line) and $^{96}Zr + ^{96}Zr$ (dotted lines). Diabatic potentials for the systems b) $^{90}Zr + ^{90}Zr$ (solid line) and $^{96}Zr + ^{96}Zr$ (dotted line) and c) $^{130}Xe + ^{130}Xe$ (solid line) and $^{136}Xe + ^{136}Xe$ (dotted line). The nuclei are assumed as spherical with $\varepsilon = 0.74$.

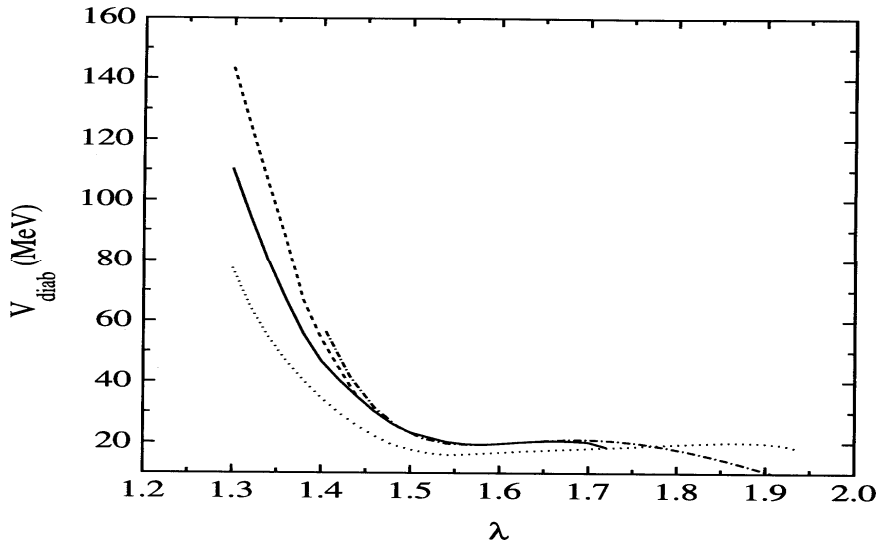

Figure 3-5: Diabatic potentials for the systems $^{100}Mo+^{100}Mo$ (dotted line) and $^{110}Pd+^{110}Pd$ (solid line). The phenomenological double folding potential for the system $^{110}Pd+^{110}Pd$ is shown by the dashed-dotted line. The discrepancy between this potential and the diabatic one becomes smaller if, by starting at the minimum of the pocket, the neck parameter ε is diminished with decreasing λ (dashed line for $^{110}Pd+^{110}Pd$).

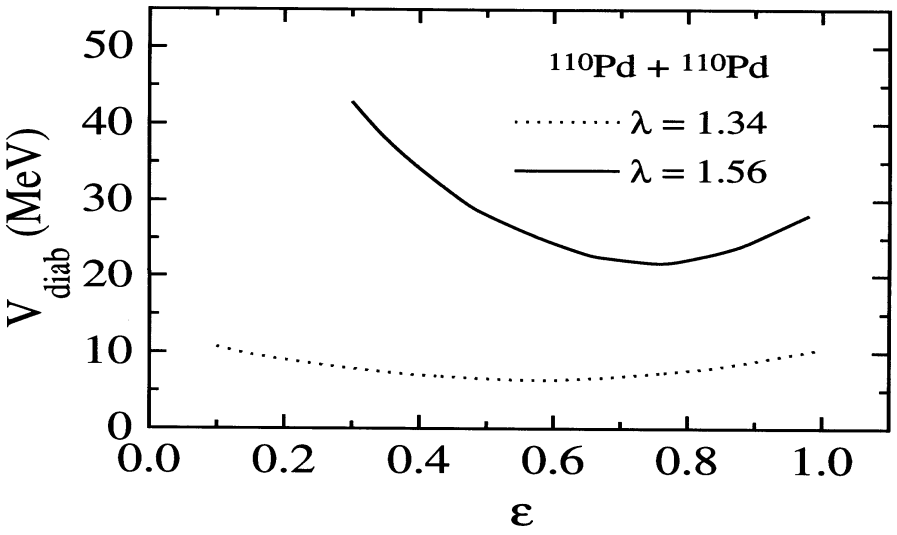

Figure 3-6: Diabatic potentials as a function of ε for the system $^{110}Pd+^{110}Pd$ at $\lambda = 1.34$ and 1.56.

considered, the diabatic potential has a minimum as a function of ε around $\varepsilon = 0.65 - 0.85$. Since the mass parameter in ε has been shown to be large [43], it strongly hinders the growth of the neck even for a small energy gain from the diabatic contributions during a variation of the neck coordinate.

Fig. 3-9 shows diabatic potentials as a function of λ for the asymmetric systems $^{110}Pd + ^{136}Xe$, $^{86}Kr + ^{160}Gd$ and $^{48}Ca + ^{198}Hg$, which lead to the same compound nucleus ^{246}Fm. These diabatic potentials are also strongly repulsive for smaller elongations and the quasi-fission barrier of the pocket becomes larger with the increase of the mass asymmetry η. In the upper part of Fig. 3-10, the diabatic contributions for the system ^{220}U(^{110}Pd+^{110}Pd) are shown for $\eta = 0$ and 0.5 at $\varepsilon = 0.74$. For an asymmetric clusterization of ^{220}U, the diabatic hindrance for the motion to smaller values of λ is smaller than for the symmetric configuration. This means that the evolution of the asymmetric DNS to the compound nucleus is more favored, which is supported by the experimental data. Since the diabatic effects are small near the touching of the nuclei, they are not important for the potential of the DNS as a function of the mass asymmetry at the touching configuration of the nuclei. The difussion process in the mass asymmetry η at the touching configuration of the nuclei starts after the formation of the initial DNS at the pocket of the potential in λ for a large fixed value of ε, e.g., $\varepsilon = 0.74$. This slow difussion process is studied using an adiabatic potential which will be presented in chapter 4.

The dependence of the diabatic contribution on the temperature is presented in the lower part of Fig. 3-10 for the system ^{220}U(^{110}Pd+^{110}Pd). For this calculation, we take the occupation probabilities n_α^{diab} given by the Fermi-distribution at finite temperature for the touching configuration of the nuclei. This temperature could be related to the excitation of the nuclei in the approaching phase of the collision. The initial excitation energy of the system decreases the repulsive character of the diabatic contribution due to smaller occupation numbers of the diabatic states under the Fermi-level. If these states are occupied and cross the Fermi-level from below, they increase the repulsive contributions of the potential, while occupied states above the Fermi-level, crossing it from above with decreasing λ, diminish the diabatic contributions.

The diabatic contributions increase with prolate deformations and decrease for oblate deformations (Fig. 3-11). However, in order to conclude about an advantageous fusion with oblate nuclei, the corresponding mass parameters should first be analysed.

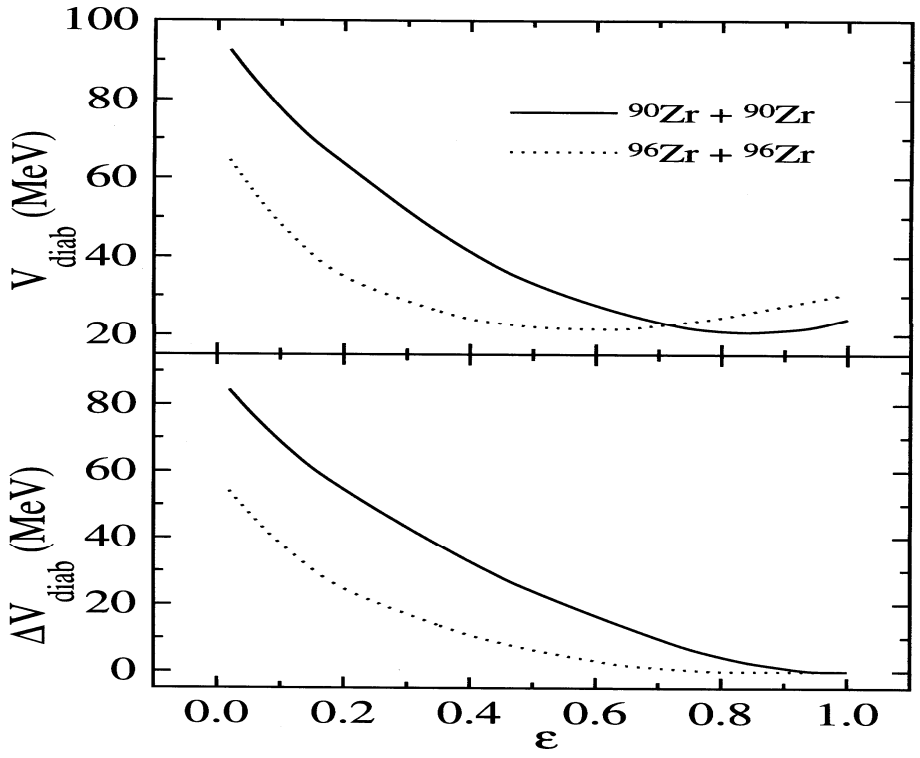

Figure 3-7: The same as in Fig. 3-6 for the systems $^{90}Zr+^{90}Zr$ and $^{96}Zr+^{96}Zr$ for $\lambda = 1.54$, which is near to the minimum of the pocket in λ (upper part). The diabatic contributions for these systems are presented as a function of ε in the lower part.

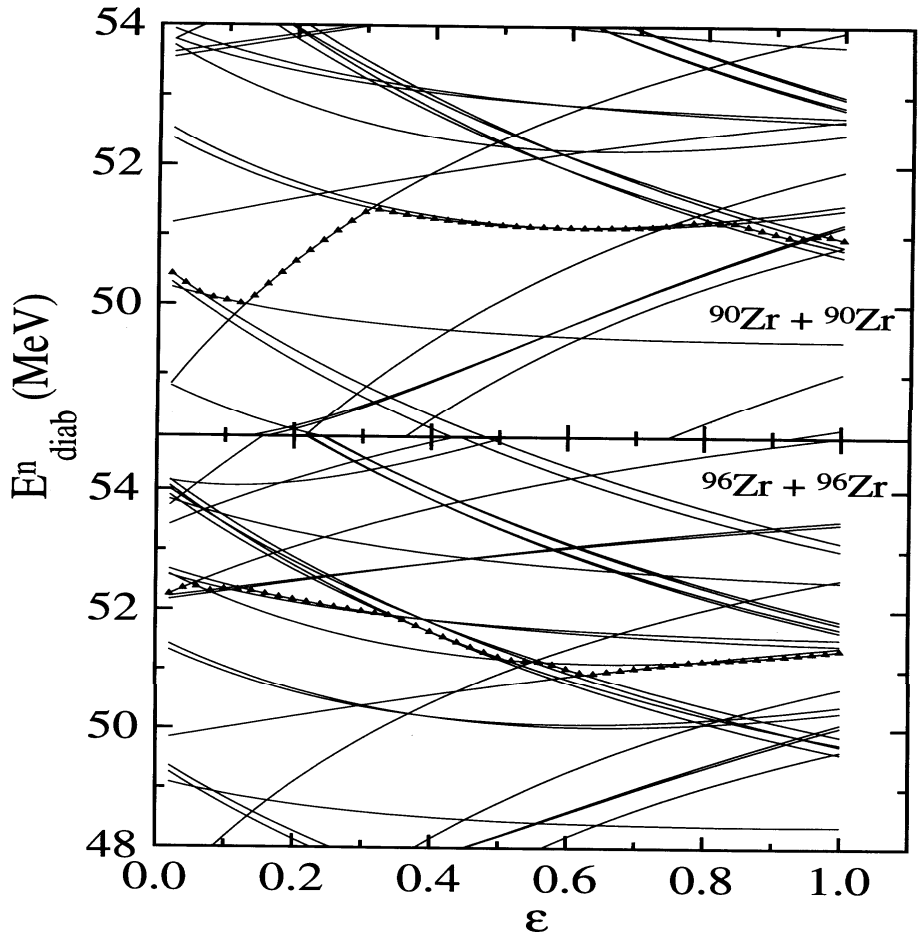

Figure 3-8: Diabatic neutron single-particle spectra as a function of ε for the systems $^{90}Zr+^{90}Zr$ (upper part) and $^{96}Zr+^{96}Zr$ (lower part) for $\lambda = 1.56$, corresponding roughly to the minimum of the pocket. The Fermi level is indicated by triangles.

The estimated collective velocities in λ and ε are large enough to consider diabatic effects in the DNS. We estimated the minimal excitation energy per nucleon ε^* for the applicability of the diabatic treatment. The value of ε^* must fulfill the following inequality [52]

$$\varepsilon^* \geq (1.4 \times 10^{-22}\mathrm{MeV\,s})\frac{2\pi|H_{\alpha\beta}|^2}{\hbar|\partial\epsilon_{\alpha\beta}/\partial q|\kappa}, \tag{3.6}$$

where κ is the mean distance in q between two subsequent crossings. The numerical factor in (3.6) is obtained by using the Fermi-gas model for estimating the decay time due to residual two-body collisions [52]. From the study of the diabatic and adiabatic levels of the systems considered, we obtained ε^* $\geq$0.03 MeV for the relative motion in R and $\varepsilon^* \geq 0.07$ MeV for the motion in the neck coordinate ε. Therefore, the diabatic effects are already important for relatively small excitation energies of 6–14 MeV. For the relative motion, the averange values of the coupling $|H_{\alpha\beta}|$ and of the difference $|\partial\epsilon_{\alpha\beta}/\partial R|$ in the slopes of the crossing levels are 0.17 MeV and 1.52 MeV/fm, respectively. The value of the coupling $|H_{\alpha\beta}|$ is estimated as the half of the difference of energies of the adiabatic levels α, β at the pseudo-crossing point. For the motion in the neck coordinate, we obtained $|H_{\alpha\beta}| = 0.2$ MeV and $|\partial\epsilon_{\alpha\beta}/\partial\varepsilon| = 0.77$ MeV. Since in Ref. [52] the diabatic single particle spectra were calculated with another Hamiltonian, a larger minimal value of ε^* was obtained.

In the present chapter we studied diabatic potentials as a function of elongation, neck coordinate and mass asymmetry for various heavy systems. The calculations were performed using the maximum symmetry method with the generalized TCSM. The diabatic effects give rise to hindrances for the growth of the neck and for the motion to smaller relative distances. The diabatic potentials as a function of the elongation are similar to the phenomenological double folding potentials used in the DNS model of fusion, which describes the experimental data quite well. For the asymmetric DNS, the diabatic hindrance for the motion to smaller elongations is smaller than for the symmetric DNS and, therefore, its evolution to the compound nucleus in λ is more favored. The quasi-fission barrier becomes larger with the increase of the mass asymmetry in the entrance channel. The temperature decreases the repulsive character of the diabatic potential. The diabatic TCSM supports the model of fusion based on the DNS concept, where a hindrance for the motion to smaller values of λ is assumed. The diabatic

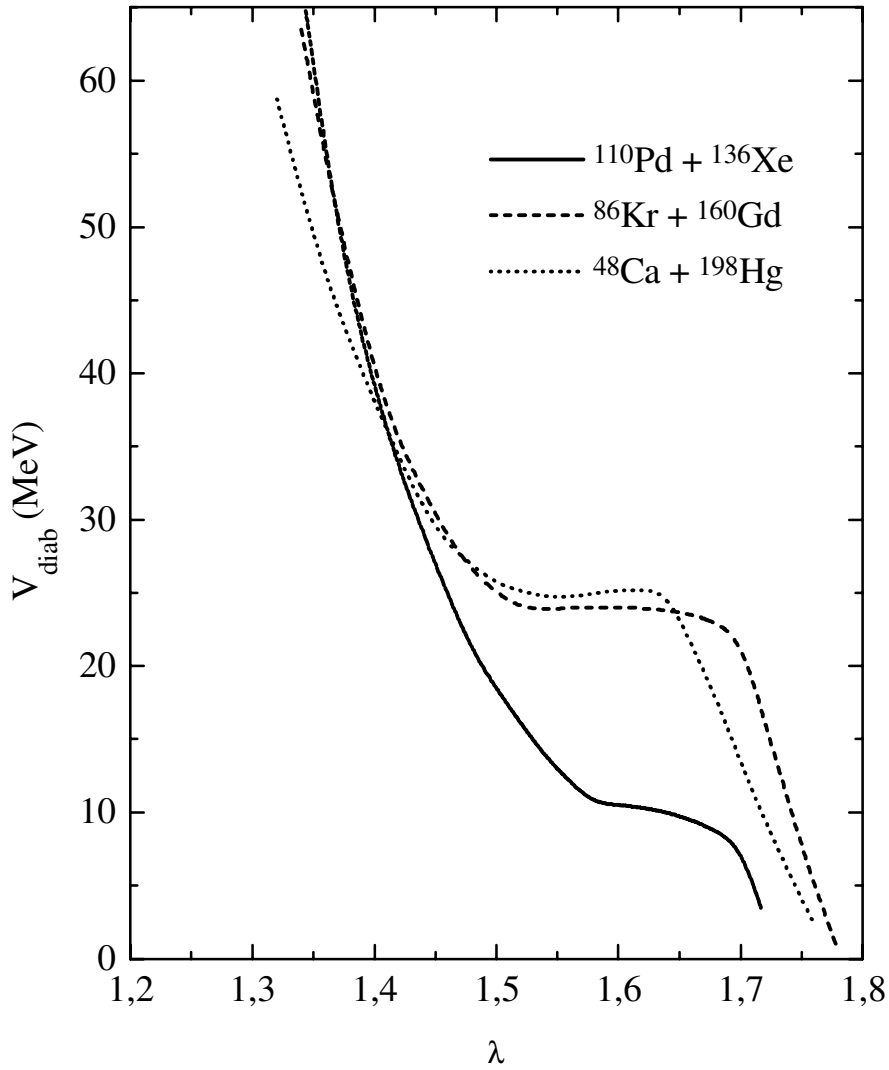

Figure 3-9: Diabatic potentials for the asymmetric systems $^{110}Pd+^{136}Xe$ ($\eta = 0.1$, solid line), $^{86}Kr+^{160}Gd$ ($\eta = 0.3$, dashed line) and $^{48}Ca+^{198}Hg$ ($\eta = 0.6$, dotted line) which lead to the same compound nucleus ^{246}Fm. The nuclei are considered as spherical with $\varepsilon = 0.74$.

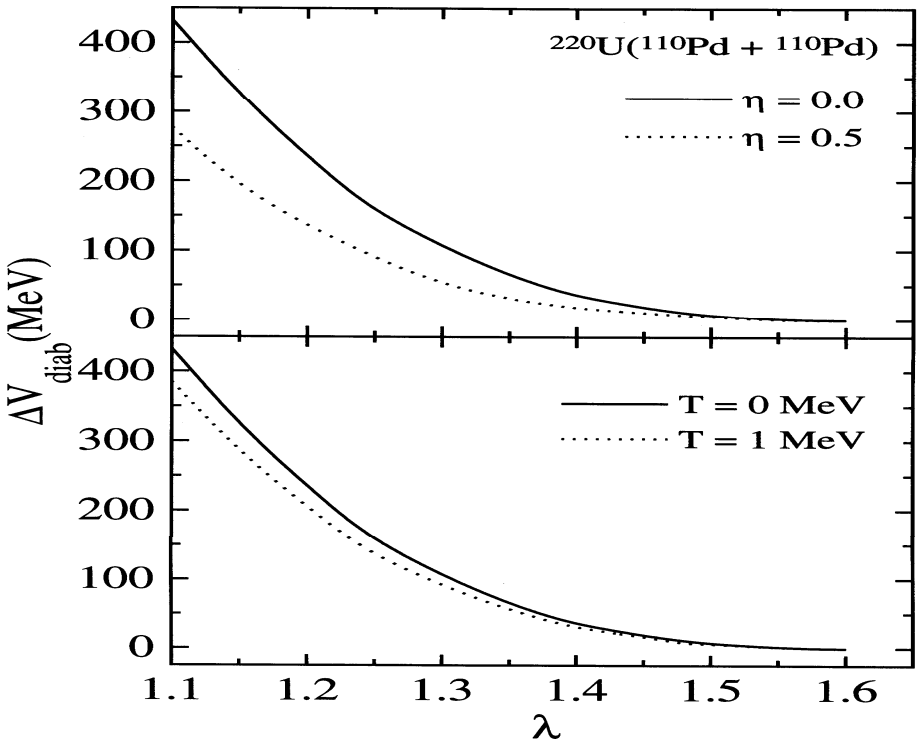

Figure 3-10: Diabatic contributions as a function of λ for the mass asymmetries $\eta = 0$ (dotted line) and 0.5 (solid line) in the system $^{110}Pd+^{110}Pd$ at $\varepsilon = 0.74$ (upper part). The dependence on temperature is shown for $\eta = 0$ in the lower part. $T = 0MeV$: solid line, $T = 1MeV$: dotted line.

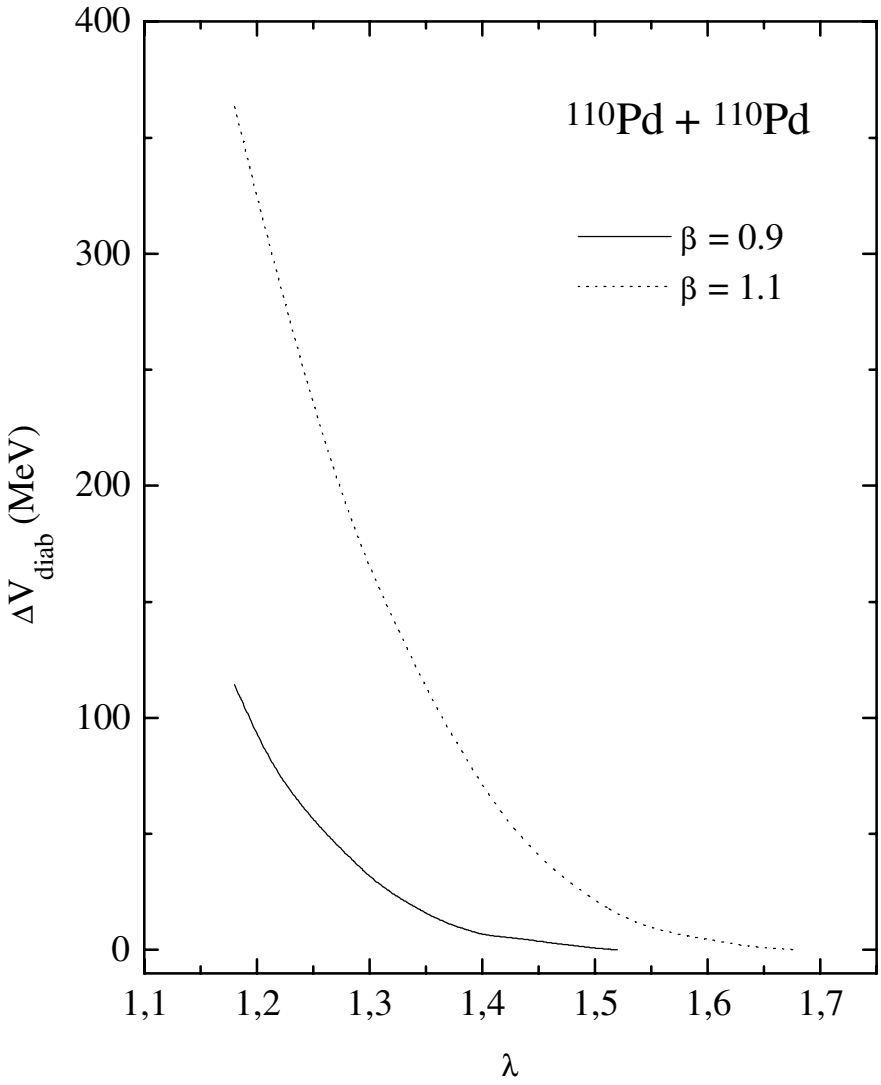

Figure 3-11: Diabatic contributions as a function of λ for oblate ($\beta = 0.9$, solid line) and prolate ($\beta = 1.1$, dotted line) nuclei in the system $^{110}Pd + ^{110}Pd$. The neck parameter ε is 0.74.

effects give a justification for the use of the DNS in heavy ion collisions at low energies.

Chapter 4

The evolution of the dinuclear system (DNS) proceeds along a large number of trajectories in the configuration space. The mass (charge) asymmetry $\eta = (A_1 - A_2)/(A_1 + A_2)$ ($\eta_Z = (Z_1 - Z_2)/(Z_1 + Z_2)$) ($A_1$ (Z_1) and A_2 (Z_2) are the mass (charge) numbers of two nuclei) and the distance R between the centers of nuclei (or the elongation λ of the system) are assumed to be the most important degrees of freedom in the DNS [18, 34]. The preferable fusion channel in the DNS model [18, 34] is the evolution of the DNS to a compound nucleus by nucleon transfer from a light nucleus to a heavy one, the motion to larger η at the touching configuration of the nuclei. In this model the melting of nuclei in the relative distance R is strongly hindered. This hindrance can be explained by a structural forbiddenness effect [36], by diabatic effects for the motion of the system to smaller relative distance [35, 66] and by a large microscopical mass parameter for the growth of the neck [43]. The dynamics of the DNS is ruled by the potential energy surface which depends on the isotope composition, on the structure of the fragments determining the transfer processes and collective excitations, and on the division of the excitation energy between the nuclei.

In this chapter, we compare the potential energy U as a function of η at the touching configuration of the nuclei (*driving potential*) obtained with different methods. The value of R for the touching configuration is determined by η and by deformations of the DNS nuclei.

The similarity of the potential energy U as a function of η at the touching configuration of the nuclei calculated within different approaches can indicate the stability of the results obtained in the DNS model.

Using a small overlap of the DNS nuclei, the value of U is calculated as the sum of asymptotic binding energies of the nuclei and the nucleus-nucleus potential [34, 65] in the phenomenological treatment. Since the DNS nuclei retain their individual properties, in this approach the shell effects enter U through the binding energies of the two nuclei.

In the microscopical consideration, the DNS potential energy as a function of η can be calculated within the adiabatic TCSM using the Strutinsky method. Contrary to the phenomenological approach, in the TCSM-method we do not need the calculation of the nucleus-nucleus interaction. There is an alternative microscopical method where the energy of the DNS as a function of η is calculated using the rate of probability of nucleon transfer between the DNS nuclei. In this method, which we call "alternative microscopical method" to distinguish it from the TCSM-method, the energy contains not only the potential energy, but the contribution from the kinetic energy. Therefore, this driving potential could deviate from the driving potentials calculated phenomenologically and within the TCSM.

In Sect. 4-1, methods of calculation of the driving potential in the phenomenological approach, within the TCSM and in the alternative microscopical approach are presented. The isotopic dependence of the phenomenological driving potential was analysed in [67]. In Sect. 4-2, we check whether this dependence is the same for the driving potential calculated within the TCSM. The isotopic dependence of the fusion barrier in mass asymmetry is studied. The effect of the deformation of the DNS nuclei on the potential energy is demonstrated.

4.1 Methods of calculation of the driving potential

4.1.1 Phenomenological method

The phenomenological driving potential is calculated as in [34, 65]

$$U(R, \eta, \eta_Z) = B_1 + B_2 + V(R, \eta, \eta_Z) - B_{12}, \tag{4.1}$$

where B_1, B_2, and B_{12} are the binding energies of the fragments and the compound nucleus, respectively, and are calculated with liquid-drop masses for large excitation energies and with realistic masses [68] for small excitation energies. The value of $U(R, \eta, \eta_Z)$ is normalised to the binding energy B_{12} of the compound nucleus. The nucleus-nucleus potential $V(R, \eta, \eta_Z)$ in (4.1) includes the Coulomb and nuclear terms. The nuclear part of the nucleus-nucleus potential is calculated using a double-folding procedure [65]. The phenomenological driving potential is obtained as $U(\eta) = U(R_m, \eta, \eta_Z)$, where $R_m = R_1 + R_2$+0.5 fm (R_i is the radius of the nuclei) is the distance between the centers of interacting nuclei corresponding to the minimum of the pocket in the nucleus-nucleus potential $V(R, \eta, \eta_Z)$. For heavy systems and small values of the angular momentum, the influence of the rotational energy is negligible [34, 69]. Deformation effects are taken into account in the calculation of $V(R, \eta, \eta_Z)$ [34]. The heavy nuclei in the DNS, which are deformed in the ground state, are treated with the parameters of quadrupole deformation taken from Refs. [70, 71]. The light nuclei of the DNS are assumed to be deformed only if the energy of their 2^+ state is smaller than 1.5 MeV. As known from experiments on sub–barrier fusion of lighter nuclei [72], these states are easily populated. For the collision energies considered here (above and near the Coulomb barrier), the relative orientation of the nuclei in the DNS follows the minimum of the potential energy.

4.1.2 TCSM-method

The driving potential is calculated using the adiabatic TCSM (3.2) because the diabatic effects are small near the touching configuration of the nuclei. Since we consider small excitation energies $(20 - 30 MeV)$, for which the shell effects remain important, the dependence of δU_{shell} and δU_{pair} on the temperature is disregarded here. The isotopic composition of the nuclei forming the DNS is chosen with the condition of N/Z- equilibrium in the system. The deformations $\beta_i = a_i/b_i$ of the DNS nuclei are calculated from their semiaxes a_i and b_i (see Appendix). The semiaxes a_i and b_i of the nuclei can be related to the parameter of the quadrupole deformation [70, 71] using the known expansion of the nuclear surface in spherical functions. The neck parameter ε is 0.74, which supplies realistic shapes of the DNS for the touching configuration of the nuclei ($\lambda = 1.5 - 1.6$) .

4.1.3 Alternative microscopical method

Since the isotopic composition of the nuclei forming the DNS is chosen with the condition of the N/Z-equilibrium in the system, mass and charge evolutions (neutrons and protons transfer) are related to each other. The charge number Z of the light fragment is used instead of the charge asymmetry η_Z. The potential is obtained by an iteration procedure [33, 73]

$$\tilde{U}(Z+1) = \tilde{U}(Z) + T \cdot \ln\left(\frac{\Delta_{Z+1}^{(-)}}{\Delta_Z^{(+)}}\right), \tag{4.2}$$

where the microscopic transport coefficients $\Delta_Z^{(\pm)}$ [74]

$$\begin{aligned} \Delta_Z^{(+)} &= \frac{1}{\Delta t}\sum_{\alpha,\beta} \mid g_{\alpha\beta}(R) \mid^2 n_\beta^Z(T)(1-n_\alpha^Z(T))\frac{\sin^2[\Delta t(\tilde{\epsilon}_\alpha^Z - \tilde{\epsilon}_\beta^Z)/2\hbar]}{(\tilde{\epsilon}_\alpha^Z - \tilde{\epsilon}_\beta^Z)^2/4}, \\ \Delta_Z^{(-)} &= \frac{1}{\Delta t}\sum_{\alpha,\beta} \mid g_{\alpha\beta}(R) \mid^2 n_\alpha^Z(T)(1-n_\beta^Z(T))\frac{\sin^2[\Delta t(\tilde{\epsilon}_\alpha^Z - \tilde{\epsilon}_\beta^Z)/2\hbar]}{(\tilde{\epsilon}_\alpha^Z - \tilde{\epsilon}_\beta^Z)^2/4} \end{aligned} \tag{4.3}$$

characterise the rate of probability of the proton transfer from a heavy to a light nucleus ($\Delta_Z^{(+)}$) or in the opposite direction ($\Delta_Z^{(-)}$). The DNS temperature T is calculated using the Fermi-gas expression $T = \sqrt{E^*/a}$ with the excitation energy E^* of the DNS and with level-density parameter $a = A_{tot}/12$ MeV^{-1}, where A_{tot} is the total mass number of the system. In the expression (4.3), "α" and "β" are the quantum numbers characterising the single-particle states in light and heavy nuclei respectively, $n_\alpha(T)$ ($n_\beta(T)$) are the temperature-dependent occupation numbers of the single-particle states in a light (heavy) nucleus, $g_{\alpha\beta}$ are the matrix elements for the nucleon transition from nucleus to nucleus because of the action of the mean fields of the reaction partners [33, 73]. The time interval $\Delta t = 1.5 \times 10^{-22} s$ must be larger than the relaxation time of the mean field but considerably smaller than the characteristic evolution time of the macroscopic quantities. The mutual influence of the mean fields of the reaction partners leads to the renormalisation of the single-particle energies $\tilde{\epsilon}_{\alpha(\beta)}$ of the nuclei [33, 73]. Peculiarities of the structure of interacting nuclei are explicitly taken into account in the transport coefficients (4.3), which are calculated using realistic schemes of single particle levels. For the single-particle spectrum, the spectrum for a spherically symmetric Woods-

Saxon potential $V_i(i = 1, 2)$ that contains central, spin-orbit and Coulomb (for the protons) interactions is used. The single-particle wave function $\psi_i(i = \alpha, \beta)$ is obtained using the same Woods-Saxon potential $V_i(i = 1, 2)$. The matrix elements $g_{\alpha\beta}(R)$ are presented in [75], where the analytical method of their calculation has been suggested (see also Appendix of the Ref. [33]). The total single-particle potential of the DNS $[V_1(r) + V_2(r - R)]$ is used to calculate the matrix element for nucleon transfer $g_{\alpha\beta}(R) = \frac{1}{2} \int dr \psi^*_\beta(r)[V_1(r) + V_2(r - R)]\psi_\alpha(r - R)$.

The expression (4.2) is obtained in [33, 73] assuming that the probability of the different DNS configurations in Z is stationary and reaches a statistical equilibrium for a temperature T. In this approach, the decay of the DNS configurations in the relative distance R is not considered when the system evolves in the variable Z.

4.2 Results and discussion

4.2.1 Isotopic dependence of the driving potential

Figs. 4-1 to 4-5 show the isotopic dependence of the driving potentials $U(\eta)$ calculated with the TCSM-method for the heavy systems Hg, Pb, Po, Th and Fm, respectively. From these figures, we can see that the driving potential is sensitive to the mass number of the dinuclear systems. Such behaviour was also observed in [73] for the potentials obtained with the alternative microscopical method and with the phenomenological method. In general, it is observed that the heavier the isotope, the larger is the fusion barrier in η. Many of the fusion characteristics are given by the static potential energy surface. It provides the information about the energy threshold for fusion, which determines the optimal bombarding energy. In the DNS model, the inner fusion barrier in mass asymmetry supplies the hindrance for complete fusion. The top of this barrier coincides with the maximum (Businaro-Gallone point) of the DNS potential energy as a function of mass asymmetry. The fusion barrier B_η in η for a reaction under consideration is defined as the difference between the potential energies of the initial DNS and of the DNS in the Businaro-Gallone maximum. If the excitation energy is sufficient to overcome this barrier, then the fusion in the mass asymmetry degree of freedom occurs. From these Figures, we can also observe that the Businaro-Gallone point moves towards larger asymmetries with the increase of the mass number of the compound nucleus. From Fig. 4-5, we see that according

to the DNS concept [18, 34], cross sections for the synthesis of the heaviest elements in nearly symmetric reactions are very small due to large fusion barriers in mass asymmetry and, correspondingly, due to small fusion probabilities, for example in the reactions ^{128}Sn+^{126}Sn$\rightarrow^{254}$Fm and ^{132}Sn+^{132}Sn$\rightarrow^{264}$Fm.

Table 4-1 shows the fusion barriers B_η^{TCSM} in η calculated with the TCSM-method for the reactions which produce the systems of the Figs. 4-1 to 4-5. These barriers are compared with the experimental surplus of energy $\Delta B^{\rm exp} = B^{\rm exp} - B_{Bass}$ above the Bass barrier B_{Bass} [76]. The value of $B^{\rm exp}$ is defined [4] as the value of the bombarding energy for a fusion probability 0.5. The Bass potential [77] is an empirical nucleus-nucleus potential derived from a geometric interpretation of fusion data above the Coulomb barrier for systems with $Z_1 \times Z_2 = 64 - 850$. As shown in Table 4-1, the isotopic trends of the fusion barrier, calculated with the TCSM-method, agree with the experimental data. The experimentally observed hindrance of the fusion roughly increases with a growing Coulomb repulsion between the colliding nuclei, but also their shell structure and isotopic composition play a major role [78, 79, 80]. The energy thresholds for fusion increase and, correspondingly, the fusion probabilities decrease [79, 80] when the neutron number of projectile or target increasingly deviates from a magic number in the reactions $^{90,96}Zr + ^{90,96}Zr$, $^{90,96}Zr + ^{100}Mo$, $^{94,100}Mo + ^{100}Mo$ and $^{90,96}Zr + ^{124}Sn$. This effect is simply explained by the deformation of the nuclei in the initial DNS and in the DNS at the top of the barrier in η and by the shell effects in dependence of the DNS potential energy on η [34, 67]. In these calculations, we did not average the inner fusion barrier in mass asymmetry over all possible orientations of colliding nuclei as we usually do in the calculations of fusion and evaporation residue cross sections, taking the half of the deformation parameters of the nuclei in the entrance channel. They are not always in good agreement with $\Delta B^{\rm exp}$ because these data are not directly measurable but are obtained with model assumptions about the fusion, the surviving probabilities and the Bass barrier.

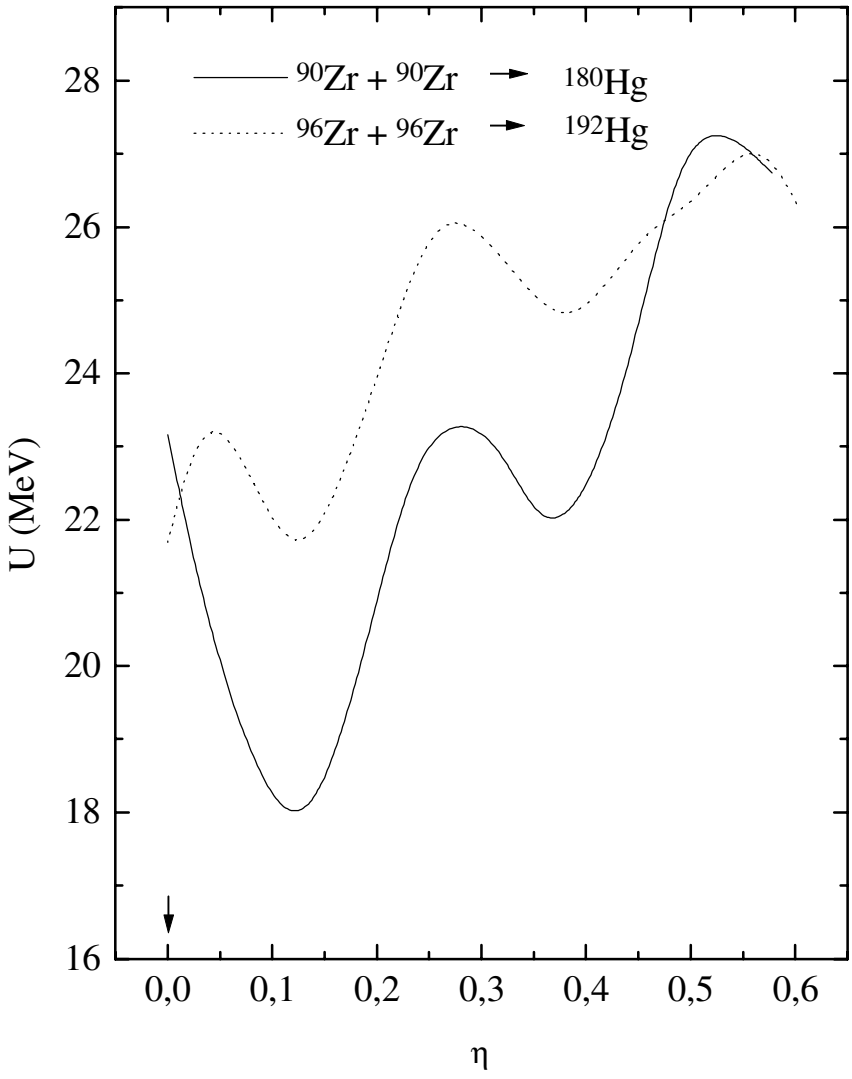

Figure 4-1: Driving potentials calculated with the TCSM-method for the systems ^{180}Hg (solid line) and ^{192}Hg (dotted line), which are produced by the reactions $^{90}Zr+^{90}Zr$ and $^{96}Zr+^{96}Zr$, respectively. The injection point for these reactions is indicated by an arrow.

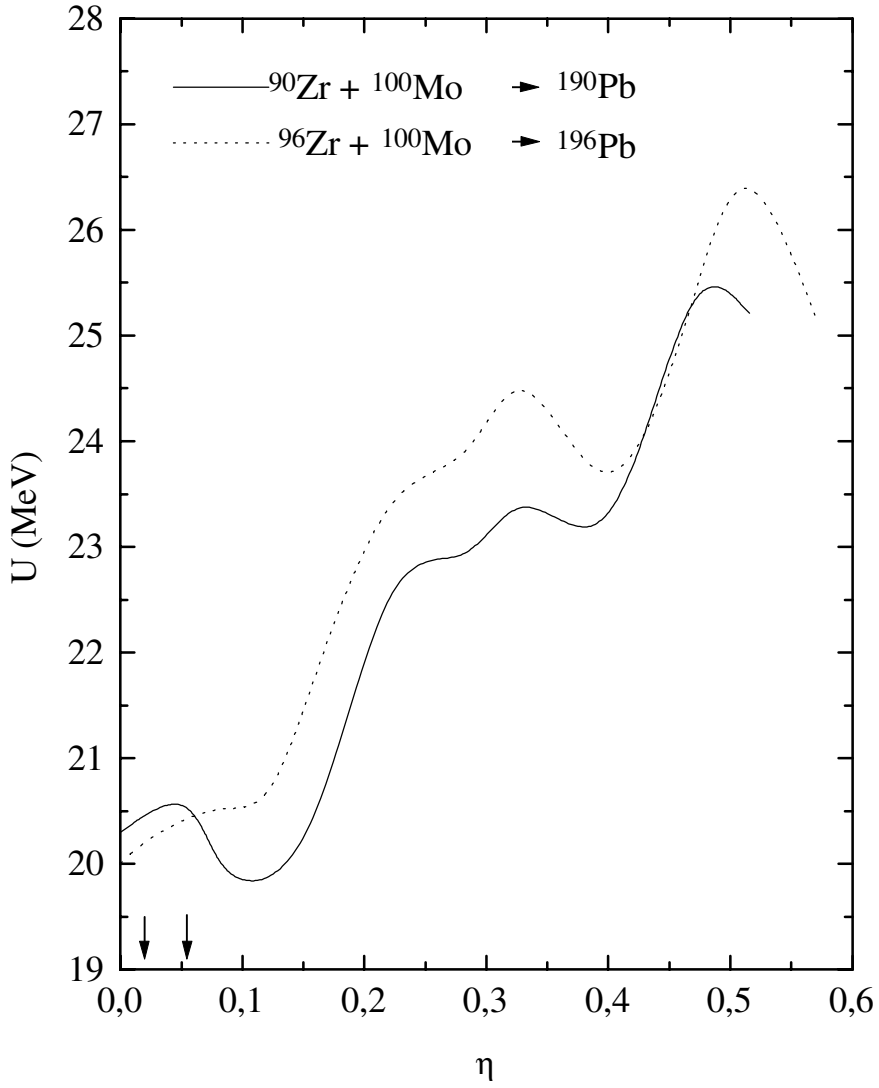

Figure 4-2: The same as in Fig. 4-1 for the systems ^{190}Pb (solid line) and ^{196}Pb (dotted line), which are produced by the reactions $^{90}Zr +^{100} Mo$ and $^{96}Zr +^{100} Mo$, respectively.

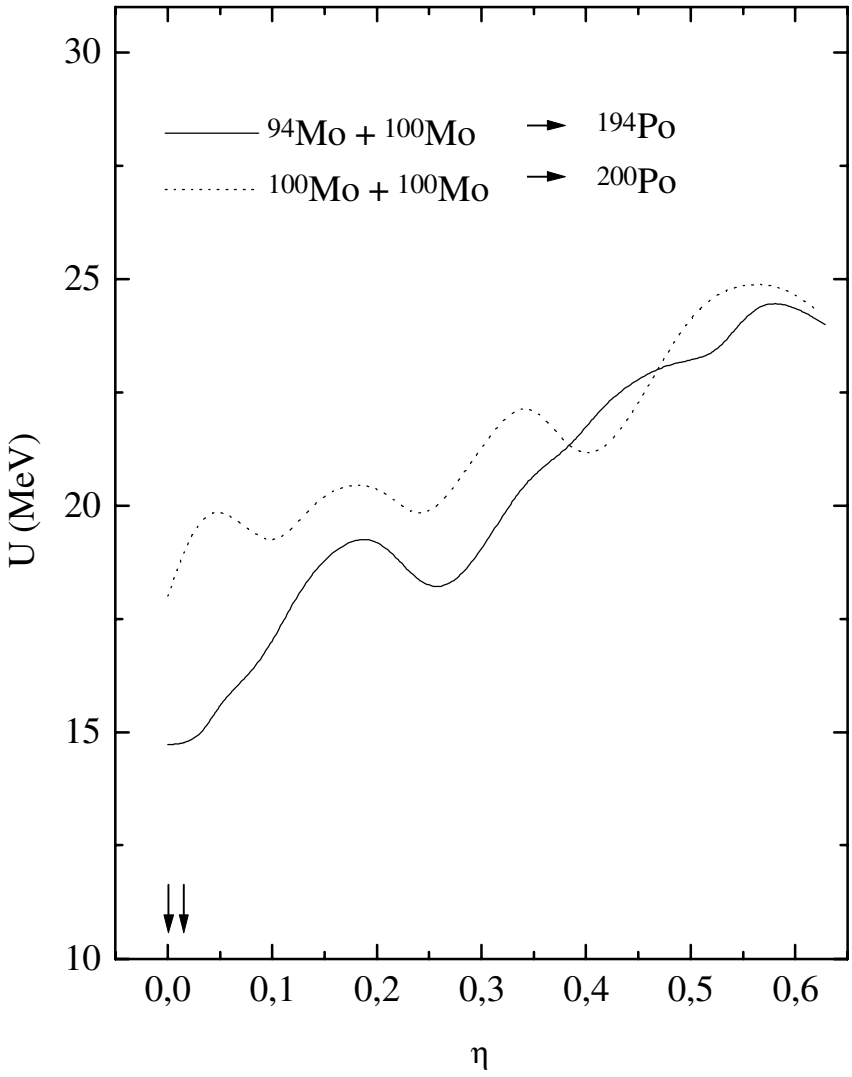

Figure 4-3: The same as in Fig. 4-1 for the systems ^{194}Po (solid line) and ^{200}Po (dotted line), which are produced by the reactions $^{94}Mo +^{100} Mo$ and $^{100}Mo +^{100} Mo$, respectively.

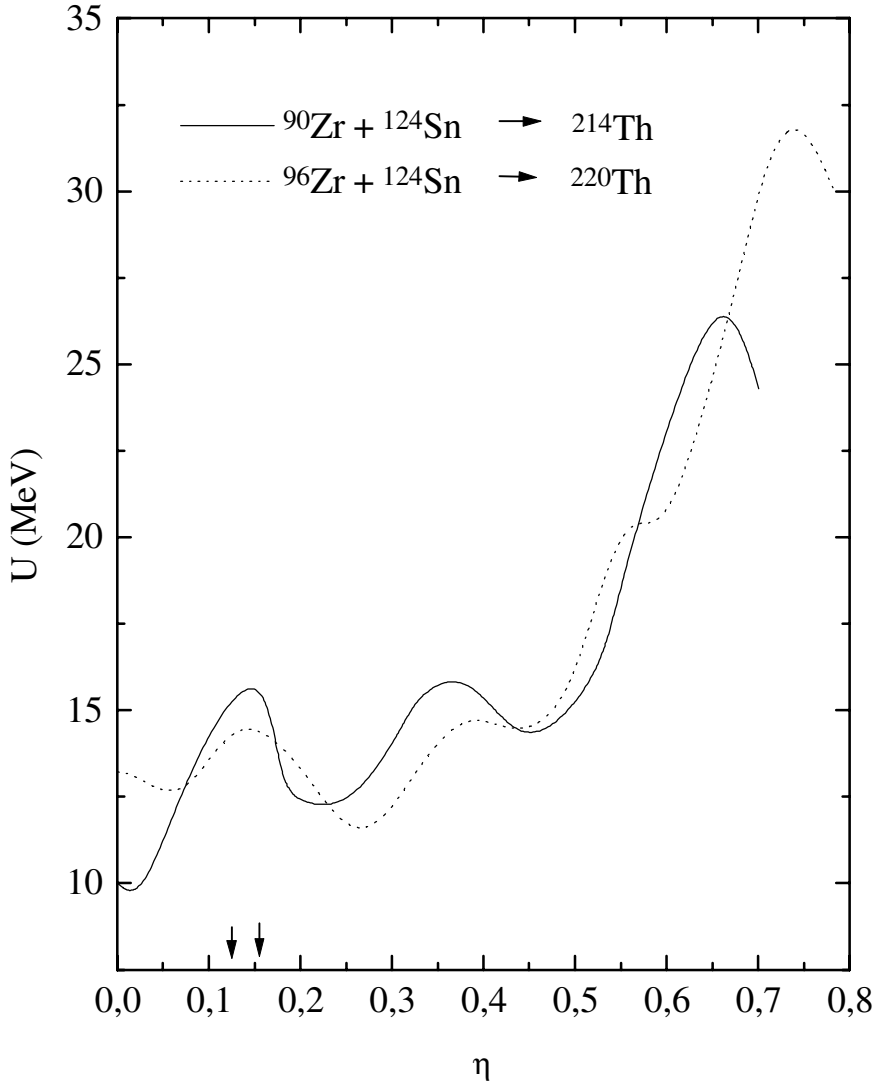

Figure 4-4: The same as in Fig. 4-1 for the systems ^{214}Th (solid line) and ^{220}Th (dotted line), which are produced by the reactions $^{90}Zr +^{124} Sn$ and $^{96}Zr +^{124} Sn$, respectively.

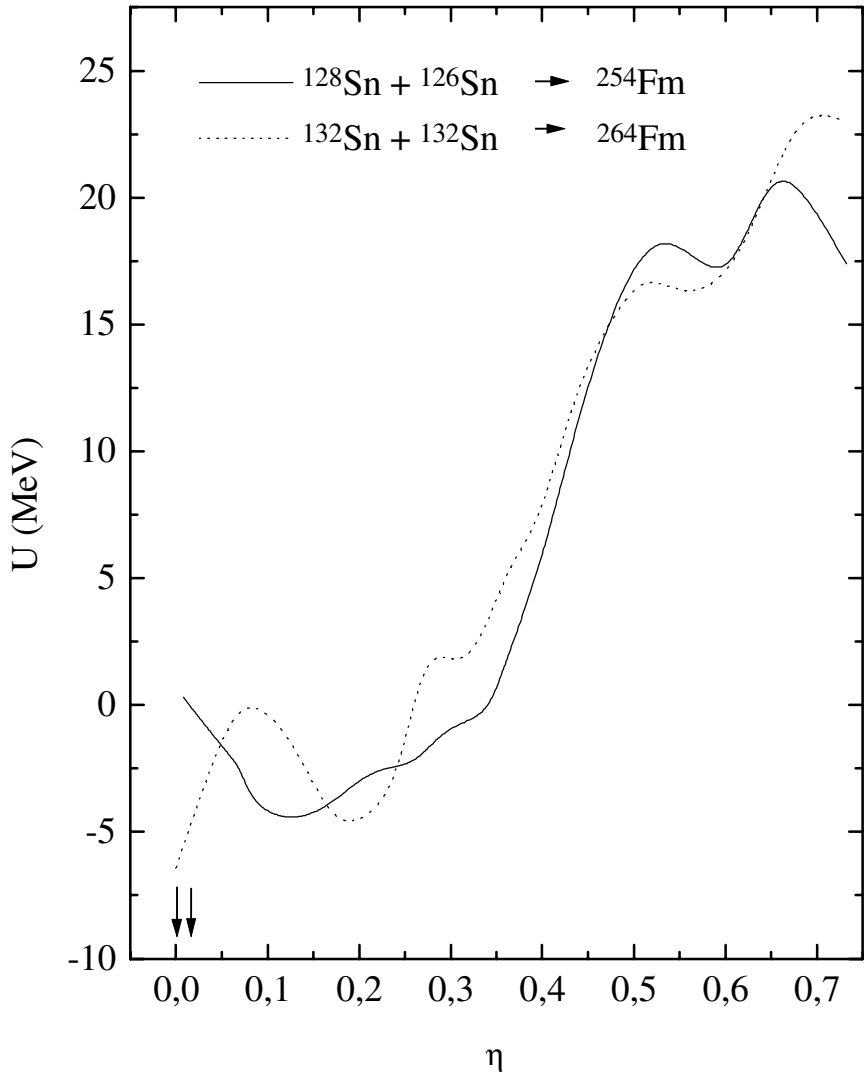

Figure 4-5: The same as in Fig. 4-1 for the systems ^{254}Fm (solid line) and ^{264}Fm (dotted line), which are produced by the reactions $^{128}Sn +^{126} Sn$ and $^{132}Sn +^{132} Sn$, respectively.

Table 4-1: Fusion barriers B_η^{TCSM} are compared with the experimental surplus of energy $\Delta B^{\exp}$ above the Bass barrier.

Reactions	$B_\eta^{TCSM}(MeV)$	$\Delta B^{\exp}(MeV)$
$^{90}Zr + ^{90}Zr \rightarrow ^{180}Hg$	4	$0.0^{+0.5}_{-0.5}$
$^{96}Zr + ^{96}Zr \rightarrow ^{192}Hg$	6	$4.2^{+1.2}_{-1.2}$
$^{90}Zr + ^{100}Mo \rightarrow ^{190}Pb$	5	$5.1^{+1.0}_{-1.0}$
$^{96}Zr + ^{100}Mo \rightarrow ^{196}Pb$	7	$9.5^{+1.0}_{-1.0}$
$^{94}Mo + ^{100}Mo \rightarrow ^{194}Po$	10	$16.3^{+1.0}_{-1.0}$
$^{100}Mo + ^{100}Mo \rightarrow ^{200}Po$	7	$12.2^{+0.5}_{-0.5}$
$^{90}Zr + ^{124}Sn \rightarrow ^{214}Th$	11	$20.3^{+4.0}_{-4.0}$
$^{96}Zr + ^{124}Sn \rightarrow ^{220}Th$	17	$26.7^{+5.0}_{-3.0}$
$^{128}Sn + ^{126}Sn \rightarrow ^{254}Fm$	22	-
$^{132}Sn + ^{132}Sn \rightarrow ^{264}Fm$	30	-

4.2.2 Comparison of driving potentials calculated with different methods

Figs. 4-6 a) and 4-7 a) show the driving potential calculated with the TCSM-method, with the phenomenological method and with the alternative microscopical method for the systems ^{180}Hg and ^{246}Fm, which are produced in the reactions $^{90}Zr + ^{90}Zr$ and $^{76}Ge + ^{170}Er$, respectively. Here, the nuclei forming the DNS are considered as spherical and the driving potential calculated with the alternative microscopical method is shown for a temperature $T = 1\ MeV$. The driving potentials are given as a function of the charge Z of the light nucleus of the DNS. We can observe that the driving potential calculated with the TCSM-method is qualitatively similar to the driving potentials calculated with the phenomenological and the alternative microscopical methods.

The phenomenological driving potential, where the shell effects are taken into account only through the asymptotic binding energies, reveals more structures [73] than the ones calculated with the TCSM-method or with the alternative microscopical method. Experiments ([28]-[32]) confirm the assumption that during the collision, the individual properties of the colliding nuclei are conserved and the shell effects play an essential role. For instance, there are local maxima corresponding to the closed-shell nuclei [28] in the charge and mass distributions of the reaction

products. However, in the driving potential calculated with the phenomenological method the peculiarities of the single-particle spectra of the DNS nuclei are not taken into account explicitly.

The shell effects in the driving potentials calculated with the TCSM-method and the alternative microscopical method reflect the influence of peculiarities of the single-particle spectra near the Fermi surface on the nucleon exchange process. For this reason, these driving potentials can carry more information about the DNS evolution in η than the driving potential calculated with the phenomenological method. It is obvious that the position of the initial configuration η_i defines the evolution direction of the DNS in η. The driving potentials calculated with the TCSM- and with the alternative microscopical methods have few local minima. The absence of local minima for some magic nuclei in the dinuclear system can be explained by the shell structure of the conjugated nucleus and the influence of the neutron subsystem.

The effect of the deformations of the nuclei on the driving potential is presented in Figs. 4-6b) and 4-7b) for the dinuclear systems ^{180}Hg and ^{246}Fm, respectively. Here, the driving potential calculated within the TCSM and the phenomenological potential are shown.We assume that the deformations take the effects of polarisation of the nucleus induced by the mean-field of the other nucleus into account. The potential energy of the DNS with prolate nuclei is smaller than the potential energy with spherical nuclei (Figs. 4-6a) and 4-7a)) because the Coulomb energy becomes larger for spherical nuclei. In this case, the fusion barrier in η gets smaller than the one obtained with spherical nuclei. For oblate deformations of the nuclei, the potential energy and the fusion barrier in η are larger than for spherical nuclei. In reality, some averaging over the orientations of the nuclei has to be carried out in the initial DNS. The deformation effects produce fluctuations of the value of the fusion barrier in η around the value obtained for spherical nuclei. In the present version of the TCSM, the intrinsic symmetry axes of the deformed nuclei lie along the internuclear axis. For arbitrary orientations of the intrinsic symmetry axes of the deformed nuclei, a more general TCSM [81] should be used. Calculations with the method suggested in [65] reveal a weak dependence of the potential on the orientations of the nuclei. In order to completely take into account the deformation effect in the driving potential calculated with the alternative microscopical method, the single-particle levels should be taken for deformed nuclei. For the sake of simplicity, we use the single-particle levels of spherical nuclei in the present calculations. However, the fit of the Fermi surface by the

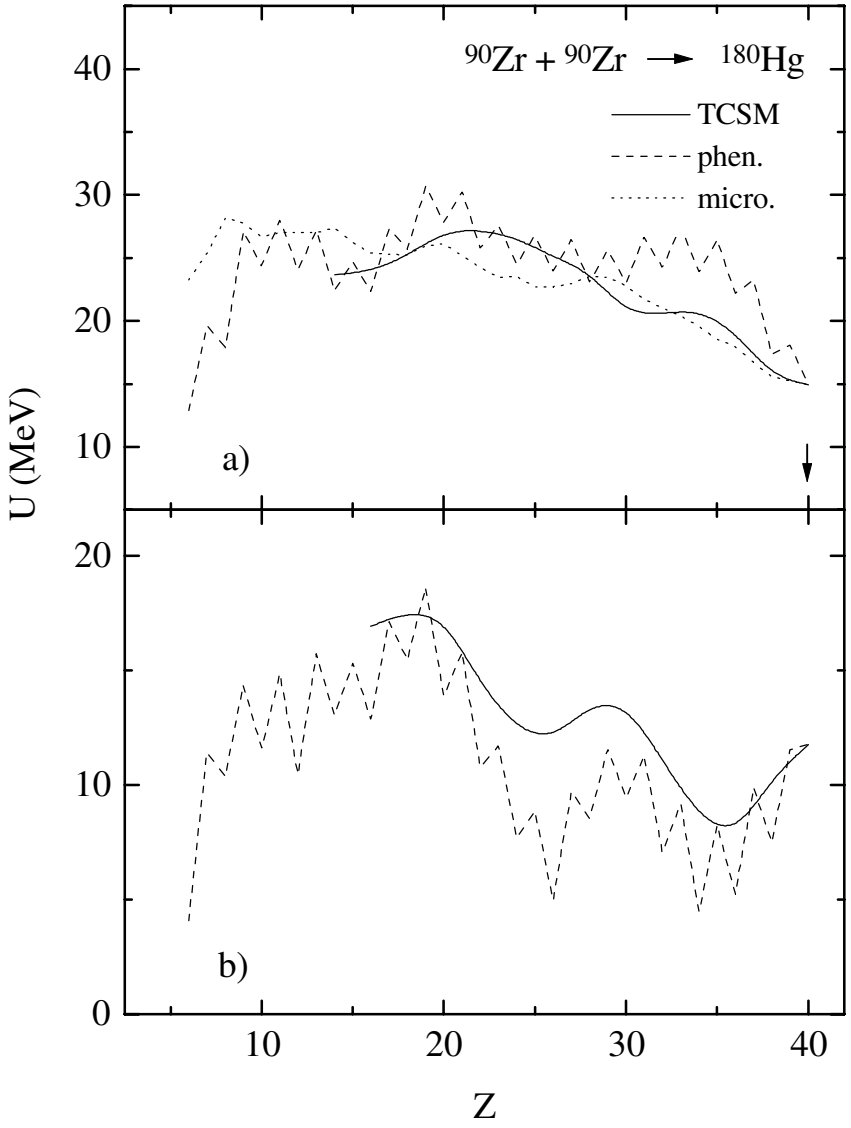

Figure 4-6: a) Driving potentials for the system ^{180}Hg as a function of the charge number Z of the light nucleus of the DNS: potential calculated with the TCSM-method (solid line), the phenomenological potential (dashed line) and the potential calculated with the alternative microscopical method for $T = 1MeV$ (dotted line). The nuclei are considered as spherical. The arrow indicates the reaction $^{90}Zr + ^{90}Zr$. b) The same as in a) but with deformed nuclei in the driving potential calculated with the TCSM- and with the phenomenological methods. The deformations are taken from Refs. [70, 71]

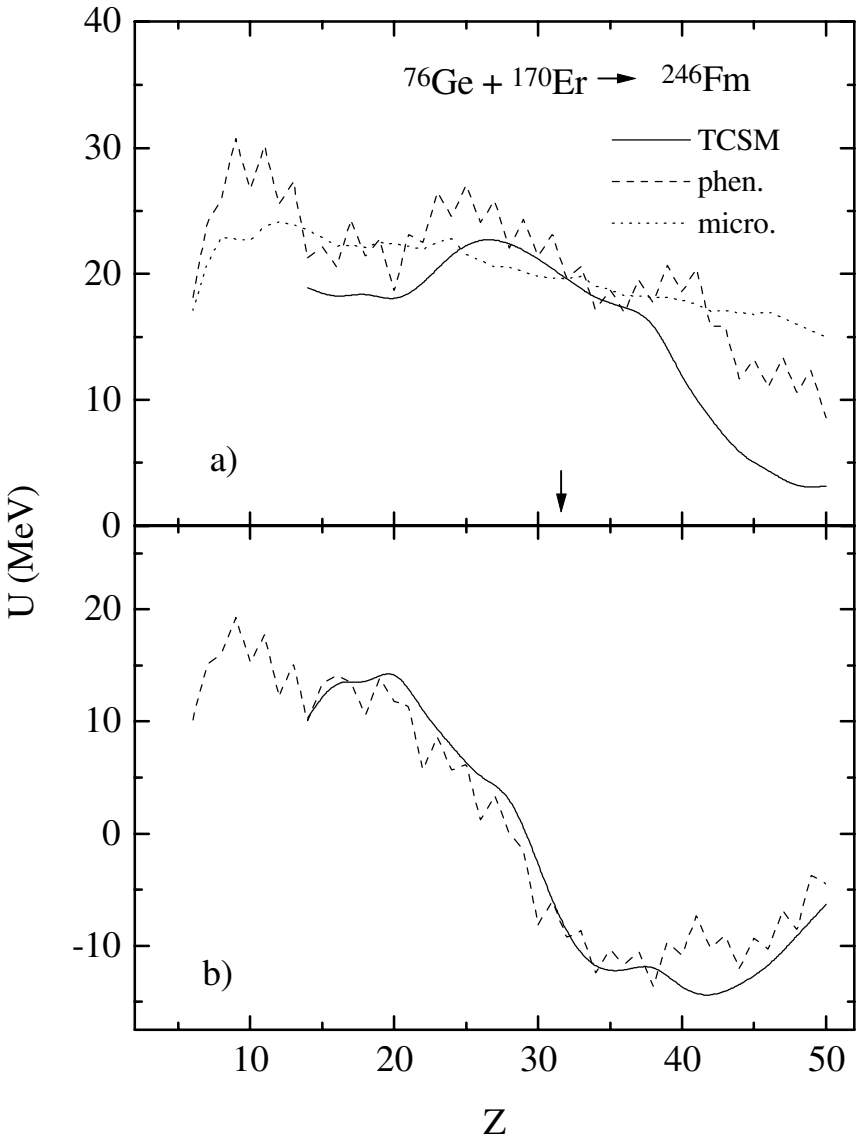

Figure 4-7: The same as in Fig. 4-6 for the system ^{246}Fm, which is produced by the reaction $^{76}Ge +^{170} Er$.

experimental separation energy allows us to partly take the deformation effects into account in the driving potential calculated with the alternative microscopical method.

In this chapter, we have studied the isotopic dependence of the driving potential of various heavy DNS using the TCSM-method. The isotopic dependence of the energy threshold for the complete fusion in mass asymmetry calculated with the TCSM-method agrees with the isotopic behaviour of the experimental surplus of energy $\Delta B^{\exp}$ above the Bass barrier. The similarity of the driving potentials calculated with the TCSM-method and with the phenomenological approach is demonstrated. The description of the DNS evolution in η at the touching configuration of the nuclei weakly depends on the method of calculation of the potential energy. The structures in the driving potentials show the strong influence of the shell effects on the evolution of the DNS. In chapter 7, we will study the correlation between the distribution of quasi-fission products and the driving potential.

Chapter 5

The present fusion models can be distinguished by the choice of the relevant collective variables along which fusion mainly occurs. While many models study the fusion in R at a practically fixed value of η, the DNS model [34] considers the DNS evolution in mass asymmetry by nucleon or cluster transfers as the main path to the compound nucleus. The DNS model assumes basically that the neck degree of freedom is fixed in the evolution in η and the nuclei are hindered from melting together by a variation in the relative distance R. In this chapter, we study dynamical restrictions for the growth of the neck in the DNS and suggest proper methods of the calculation of the DNS inertia tensor.

There are various macroscopical and microscopical approaches to calculating the inertia tensor [82]. The macroscopical approaches (see, for example, [16, 83]) are based on the hydrodynamical model of the nucleus. A calculation of the inertia tensor with a theory for quantum fluid dynamics is suggested in Ref. [84]. By using a random-matrix model to describe the coupling between a collective nuclear variable and intrinsic degrees of freedom, and with the help of the functional integral approach, mass parameters are derived in Ref. [85]. In the linear response theory [86, 87] the inertia tensor is found for fissioning nuclei. The microscopical approaches mainly use the cranking type expression and perform calculations in different single particle bases applying adiabatic [40, 88] or diabatic [57] two-center shell models. Difficulties in the cranking type calculations arise for collective motions with large amplitudes, for example, in fusion or fission, due to pseudo–crossings or crossings of levels in the single particle spectrum. Some publications disregard the contributions from the crossings (pseudo–crossings), which

means a neglect of effects of configuration changes on the mass parameters during the evolution of the nuclear shape in spite of the fact that the collective inertia is strongly influenced by level crossings (pseudo–crossings) [89, 90]. In order to overcome this problem, two–body collisions should be regarded which lead to a width of the single particle levels and an effective reduction of the level crossing effects. For example, calculations of the nuclear inertia in a generalized cranking model with pairing correlations yielded masses of about one order of magnitude larger than the ones without pairing [91].

One of the aims of this chapter is to obtain analytical expressions for mass parameters using models and methods which include residual interaction effects. In sect. 5.1, the mass parameters are obtained within the linear response theory, taking the fluctuation-dissipation theorem and the width of single particle states into account. The same mass parameters are also derived by Fermi's golden rule and by smoothing the single particle spectrum in the mean–field cranking formula. In sect. 5.2, the mass parameters for the relevant collective variables (mass asymmetry, elongation, neck and deformation parameters) of the DNS and strongly deformed nuclear systems are evaluated in the two-center shell model with adiabatic and diabatic bases.

5.1 Microscopical inertia

5.1.1 Derivation from collective response function

Let us consider a nuclear system described by a single collective coordinate Q and intrinsic single particle coordinates x_i (with the conjugated momentum p_i) and assume the following effective Hamiltonian [86]

$$\hat{H}(x_i, p_i, Q) = \hat{H}(x_i, p_i, Q_0) + (Q - Q_0)\hat{F}(x_i, p_i, Q_0)$$

$$+\frac{1}{2}(Q - Q_0)^2 < \frac{\partial^2 \hat{H}(x_i, p_i, Q)}{\partial Q^2} >_{Q_0, T_0} . \tag{5.1}$$

The shape of the nuclear mean field is changed with the collective coordinate Q that introduces the coupling between Q and the nucleonic degrees of freedom x_i. Eq. (5.1) is obtained by expanding the Hamiltonian to second order in the vicinity of Q_0 (local harmonic approx-

imation). In the second order term the "nucleonic" part appears only as an average of the corresponding operator. Consistently with the harmonic approximation, this average is to be built with that density operator for the nucleons $\widehat{\rho}_{qs}(Q_0)$ which in the quasi-static picture is to be calculated with the Hamiltonian at Q_0, namely, $\hat{H}(x_i, p_i, Q_0)$. The operator $\widehat{\rho}_{qs}(Q_0)$ is the canonical distribution for the temperature T_0. The coupling term between the collective and intrinsic motion is proportional to the first order in $\delta Q = Q - Q_0$ with an operator $\hat{F}$ given by the derivative of the mean field with respect to Q in the neighborhood of Q_0.

The local motion in the Q variable can be described in terms of the so-called collective response function $\chi_{coll}(\omega)$ [86] (see Appendix). In the linear response theory [86], the mass coefficient for a slow collective motion can be expressed as [86, 87, 92, 93]

$$M(Q) = \frac{1}{2k^2}\frac{\partial^2(\chi_{coll}(\omega))^{-1}}{\partial\omega^2}|_{\omega=0} = (1+\frac{C(0)}{\chi(0)})^2[M^{cr} + \frac{\gamma^2(0)}{\chi(0)}], \tag{5.2}$$

where

$$M^{cr} = \frac{1}{2}\frac{\partial^2\chi(\omega)}{\partial\omega^2}|_{\omega=0} = \frac{1}{2}\frac{\partial^2\chi'(\omega)}{\partial\omega^2}|_{\omega=0} \tag{5.3}$$

is the inertia in the zero-frequency limit of the second derivative of the intrinsic response function. M^{cr} can be shown to be similar to the one of the cranking model [86]. Here a response function $\chi(\omega)$ for "intrinsic" motion appears and measures how, at some given Q_0 and temperature T_0, the nucleonic degrees of freedom react to the coupling term $\hat{F}\delta Q$. The intrinsic response function $\chi(\omega) = \chi'(\omega) + i\ \chi''(\omega)$ is written in terms of the reactive $\chi'(\omega)$ and dissipative $\chi''(\omega)$ parts [86]. $\chi(0)$ and $C(0)$ are the zero-frequency limit of the intrinsic response function and stiffness, respectively (see Appendix). For many applications, the value of $C(0)/\chi(0) \ll 1$. The additional term $\gamma^2(0)/\chi(0)$ in Eq. (5.2) gives a positive contribution to M where $\gamma(0)$ is the friction coefficient defined as [86]

$$\gamma(0) = -i\frac{\partial\chi(\omega)}{\partial\omega}|_{\omega=0} = \frac{\partial\chi''(\omega)}{\partial\omega}|_{\omega=0} = \frac{1}{2T_0}\psi''(0). \tag{5.4}$$

The dissipative part of the intrinsic response function $\chi''(\omega)$ is connected with the dissipative part of the correlation function $\psi''(\omega)$ through the fluctuation-dissipation theorem [86]

$$\chi''(\omega) = \frac{1}{\hbar}\tanh(\frac{\hbar\omega}{2T_0})\psi''(\omega). \tag{5.5}$$

In the case of an independent particle model, the correlation function $\psi^{''}(\omega)$ is expressed as [86]

$$\psi^{''}(\omega) = \pi\hbar \sum_{j,k} |F_{jk}|^2 n(\epsilon_j)[1 - n(\epsilon_k)][\delta(\hbar\omega - \epsilon_{kj}) + \delta(\hbar\omega + \epsilon_{kj})]. \tag{5.6}$$

Here, $\epsilon_{kj} = \epsilon_k - \epsilon_j$ is the difference of single particle energies, $n(\epsilon_j)$ are the occupation numbers and $F_{jk} =< j|\hat{F}|k >$ the single particle matrix elements of the operator $\hat{F}$. The $\psi^{''}(\omega)$ has a singularity of δ–function type at $\omega = 0$

$$\psi^{''}(\omega) = 2\pi\psi^{\mathbf{0}}\delta(\hbar\omega) + \psi^{''}_R(\omega), \tag{5.7}$$

with $\psi^{''}_R(\omega)$ being regular at $\omega = 0$. $\psi^{''}_R(\omega)$ is given by a sum like the one in (5.6) but with the restriction $j \neq k$. At $j = k$, we find the contributions from the diagonal matrix elements

$$\psi^{\mathbf{0}} = \sum_k |F_{kk}|^2 n(\epsilon_k)[1 - n(\epsilon_k)] = T_{\mathbf{0}} \sum_k \left|\frac{\partial n(\epsilon)}{\partial \epsilon}\right|_{\epsilon=\epsilon_k} \left(\frac{\partial \epsilon_k}{\partial Q}\right)^2. \tag{5.8}$$

The last part in (5.8) was derived with a Fermi distribution for the occupation numbers, which is characterized by the temperature $T_{\mathbf{0}}$. The value of $T_{\mathbf{0}}$ does not effectively go to zero with decreasing excitation energy because each single particle level has a width due to the two-body interaction. Indeed at zero excitation energy, the distribution of the occupation numbers deviates from a step function at least due to pairing correlations. In order to obtain a smooth correlation function $\psi^{''}(\omega)$, we substitute the δ–functions in Eq (5.6) by the Lorentzian $\Gamma/[\pi((\hbar\omega \pm \epsilon_{kj})^2 + \Gamma^2)]$. The Lorentzian function with the double single particle width 2Γ is applied because $\hbar\omega$ is the transition energy between two single particle states [86]. Then using Eqs. (5.4)-(5.8), we can write the friction coefficient in the following form

$$\gamma(0) = \gamma^{diag}(0) + \gamma^{nondiag}(0), \tag{5.9}$$

where

$$\gamma^{diag}(0) = \frac{\hbar}{\Gamma} \sum_k \left|\frac{\partial n(\epsilon)}{\partial \epsilon}\right|_{\epsilon=\epsilon_k} \left(\frac{\partial \epsilon_k}{\partial Q}\right)^2. \tag{5.10}$$

For smaller temperatures $T_{\mathbf{0}} < 2$ MeV, which are of interest here, $\gamma^{diag}(0)$ is much larger than

$\gamma^{nondiag}(0)$ [86]. The zero-frequency limit of the intrinsic response function defined as [86]

$$\chi(0) = \lim_{\epsilon \to 0} \int_{-\infty}^{+\infty} \frac{d\omega}{\pi} \frac{\chi''(\omega)}{\omega - i\epsilon} = \lim_{\epsilon \to 0} \int_{-\infty}^{+\infty} \frac{d\omega}{\hbar\pi} \frac{\tanh(\frac{\hbar\omega}{2T_0})\psi''(\omega)}{\omega - i\epsilon} \tag{5.11}$$

is expressed as follows

$$\chi(0) = \chi^{diag}(0) + \chi^{nondiag}(0), \tag{5.12}$$

where

$$\chi^{diag}(0) = \sum_k \left| \frac{\partial n(\epsilon)}{\partial \epsilon} \right|_{\epsilon=\epsilon_k} \left(\frac{\partial \epsilon_k}{\partial Q} \right)^2. \tag{5.13}$$

With realistic assumptions $\gamma^{diag}(0) \gg \gamma^{nondiag}(0)$ and $\chi^{diag}(0) \gg \chi^{nondiag}(0)$ and neglecting $C(0)/\chi(0)$, we can divide the mass parameter (5.2) as

$$M = M^{diag} + M^{nondiag}. \tag{5.14}$$

The contribution of the diagonal matrix elements of $\hat{F}$ to M are

$$M^{diag} = \frac{(\gamma^{diag}(0))^2}{\chi^{diag}(0)} = \frac{\hbar^2}{\Gamma^2} \sum_k \left| \frac{\partial n(\epsilon)}{\partial \epsilon} \right|_{\epsilon=\epsilon_k} \left(\frac{\partial \epsilon_k}{\partial Q} \right)^2. \tag{5.15}$$

If the single particle widths are properly taken into account, the nondiagonal contributions to the inertia are [88]

$$M^{nondiag} = M^{cr} = \hbar^2 \sum_{k \neq k'} \frac{|F_{kk'}|^2}{\epsilon_{kk'}^2 + \Gamma^2} \frac{n(\epsilon_k) - n(\epsilon_{k'})}{\epsilon_{k'} - \epsilon_k}. \tag{5.16}$$

The main contribution to M is the diagonal part M^{diag} (e.g., $< M_{\lambda\lambda}^{diag} > \sim 10^2 < M_{\lambda\lambda}^{nondiag} >$ for the fission of ^{240}Pu [91]), because it dominates for collective variables which are responsible for changes of the nuclear shape of the system [89, 90, 91, 94]. Note that the calculation of M^{diag} is simpler than $M^{nondiag}$. For the case that the pairing residual interaction is regarded and only diagonal matrix elements in the cranking formula are taken into account, Eq. (5.16) was obtained with $\Gamma = \Delta$ (Δ is the pairing gap) in Ref. [91, 95]. Starting with an equation for the

single particle density matrix extended with an approximate incorporation of particle collisions in the relaxation time approach, the authors of Ref. [96] derived an expression similar to (5.16) (with $\Gamma = \hbar/\tau$, τ is the relaxation time) but with a negative sign. This negative sign arises from the fact that the condition of self-consistency between collective and nucleonic dynamics, which is important for a correct calculation of the mass parameters, was disregarded in [96]. It was stressed in [86, 97] that within the linear response theory the diagonal component of the friction parameter originates from the "heat pole" of the correlation function $\psi''(\omega)$ and vanishes when the system is ergodic. As shown in Ref. [98], the well necked DNS-type configurations are not ergodic and stable against chaos. Even at zero excitation energy, the level crossings at the Fermi surface lead to considerable mass flow [89, 90, 94] and the diagonal component of the correlation function $\psi''(\omega)$ (or mass parameter) does not vanish.

Besides the mass and friction coefficients, the diffusion coefficients D_{kl} $(k, l = (Q, P))$ must also have a component diagonal in the matrix elements of $\hat{F}$ because they are connected with correlation functions. For example, the diffusion coefficient in momentum is defined as [86]

$$D_{PP} = \frac{1}{2}\psi''(\omega = 0) = T_0\gamma(0). \tag{5.17}$$

5.1.2 Derivation from Fermi's golden rule

By setting $\hat{H}_I = (Q - Q_0)\hat{F}(x_i, p_i, Q_0)$ as perturbation (see Eq. (5.1)), the decay rate of a collective state $|n>$ with energy E_n to the collective state $|m>$ with energy E_m is given in lowest order according to Fermi's golden rule

$$\begin{aligned} w(n \to m + \hbar\omega) &= \frac{2\pi}{\hbar}| < m|Q - Q_0|n > |^2 \\ &\times \int d(\hbar\omega)| < \hbar\omega|\hat{F}|0 > |^2\delta(E_n - E_m - \hbar\omega)\rho_{qs}(\hbar\omega). \end{aligned} \tag{5.18}$$

Here, the integral is taken over the final states of the intrinsic system with the density ρ_{qs}. $|0>$ and $|\hbar\omega>$ are the intrinsic states associated with the collective states $|n>$ and $|m>$, respectively.

The half-decay width is obtained from Eq.(5.18) as

$$\Gamma_n = \hbar \sum_m w(n \to m + \hbar\omega). \tag{5.19}$$

With the fluctuation-dissipation theorem for small temperatures we have [99]

$$| < \hbar\omega | \hat{F} | 0 > |^2 \rho_{qs}(\hbar\omega) d(\hbar\omega) = \frac{2}{\pi} \frac{\hbar\omega}{2} R(\omega) d\omega \tag{5.20}$$

with the relaxation function defined as $R(\omega) = \chi^{''}(\omega)/\omega$. Using the properties of the response function $\chi^{''}(\omega)$ [86] and a Taylor expansion

$$R(\omega) = \frac{\chi^{''}(\omega)}{\omega} = \frac{1}{\omega} \left[\chi^{''}(\omega = 0) + \left. \frac{\partial \chi^{''}(\omega)}{\partial \omega} \right|_{\omega=0} \omega + \frac{1}{2} \left. \frac{\partial^2 \chi^{''}(\omega)}{\partial \omega^2} \right|_{\omega=0} \omega^2 + ... \right], \tag{5.21}$$

we calculate the integral in (5.18). We then replace $w(n \to m + \hbar\omega)$ in (5.19) by (5.18). Considering the standard formula for mass M_n ($E_n \neq E_m$)

$$M_n = \frac{\hbar^2}{2} (\sum_m | < m | Q - Q_0 | n > |^2 [E_n - E_m])^{-1}, \tag{5.22}$$

which is obtained from the relation $M_n = \hbar^2 (< n | [\widehat{q}, [\widehat{q}, \widehat{H}]] | n >)^{-1}$[94], we obtain by setting $\Gamma = \Gamma_n$ and $M = M_n$

$$M = \frac{\hbar}{\Gamma} \frac{\partial \chi^{''}(\omega)}{\partial \omega} |_{\omega=0} = \frac{\hbar}{\Gamma} \gamma(0). \tag{5.23}$$

Large temperatures in (5.20) effectively lead to a temperature dependence of Γ in (5.23). Since $\gamma(0)$ in Eq. (5.9) contains the terms with the diagonal matrix elements of the operator $\hat{F}$, the mass parameter M also has the diagonal component M^{diag} (5.15). So, the contributions to the mass parameter can be again classified as those with diagonal and nondiagonal matrix elements, respectively.

That the mass parameter is proportional to the friction coefficient (see Eq. (5.23)), has an analogy in the hydrodynamic model. For multipole moments ν of the nucleus with $\nu > 1$, the

following ratio in the limit of an irrotational flow was derived in [100]

$$M_\nu^{irr}/\gamma_\nu^{irr} = \frac{3A^{2/3}}{8\pi(2\nu+1)(\nu-1)r_0}\frac{1}{\beta}, \tag{5.24}$$

where β is the coefficient of the two-body viscosity and $r_0 = 1.2$ fm.

5.1.3 Derivation from the mean–field cranking formula

Using the single particle spectrum ϵ_α and the corresponding wave functions $|\alpha>$, one can obtain the mass parameter with the cranking formula [94]

$$M^{cr} = \hbar^2 \sum_{\alpha\neq\beta} |<\alpha|\frac{\partial}{\partial Q}|\beta>|^2 \frac{n(\epsilon_\alpha)-n(\epsilon_\beta)}{\epsilon_\beta-\epsilon_\alpha}. \tag{5.25}$$

In reality the Hamiltonian of the system contains a residual two-body interaction between the nucleons in addition to the mean field. The residual coupling distributes the strength of single particle states over more complicated states. This spectral smoothing has the effect that the sum over α and β appearing in (5.25) also includes diagonal terms with $\alpha = \beta$. Let us prove this statement.

The Eq.(5.25) can be rewritten as

$$M^{cr} = \hbar^2 \sum_{\alpha\neq\beta} \int d\epsilon_1 \delta(\epsilon_1-\epsilon_\alpha) \int d\epsilon_2 \delta(\epsilon_2-\epsilon_\beta) |<\epsilon_1|\frac{\partial}{\partial Q}|\epsilon_2>|^2 \frac{n(\epsilon_1)-n(\epsilon_2)}{\epsilon_2-\epsilon_1}. \tag{5.26}$$

Next we use the following replacements

$$\int d\epsilon_1 g(\epsilon_1) \to \sum_{k_1}, \quad \int d\epsilon_2 g(\epsilon_2) \to \sum_{k_2}, \tag{5.27}$$

$$\delta(\epsilon-\epsilon_k) \to \rho_k(\epsilon) = \frac{1}{2\pi}\frac{\Gamma}{(\epsilon-\epsilon_k)^2+(\Gamma/2)^2} \tag{5.28}$$

and the approximation

$$D^2 |<k_1|\frac{\partial}{\partial Q}|k_2>|^2 \approx |F_{k_1 k_2}|^2. \tag{5.29}$$

Here, $D = 1/g$ is the average energy distance between single particle states. We then express

the mass (5.26) as

$$M^{cr} = \frac{\hbar^2\Gamma^2}{4\pi^2} \sum_{\alpha\neq\beta,k_1,k_2} \frac{|F_{k_1k_2}|^2}{[\epsilon^2_{\alpha k_1} + (\Gamma/2)^2][\epsilon^2_{\beta k_2} + (\Gamma/2)^2]} \frac{n(\epsilon_{k_1}) - n(\epsilon_{k_2})}{\epsilon_{k_2} - \epsilon_{k_1}}. \tag{5.30}$$

The energy spreading of the single particle states is taken into account in Eq.(5.30). A line broadening happens if collisions of particles and holes with the background result in single particle and single hole strength functions that are concentrated around the original single particle energies. The quantity $D\rho_k$ determines the average strength function for a particle in state k [101]. In the limit $\epsilon_{k_1} = \epsilon_{k_2} = \epsilon_k$, for $\epsilon_\alpha \approx \epsilon_k$ and $\epsilon_\beta \approx \epsilon_\alpha$, i.e. when two neighboring levels near the level k are considered, and $8/\pi^2 \approx 1$, Eq.(5.30) leads to Eq.(5.15). Thus, diagonal terms in the mass parameters appear because of the finite width of the single particle levels due to the residual interaction.

5.2 Results of the calculations

5.2.1 The adiabatic two-center shell model

Since collisions above the Coulomb barrier are discussed, we firstly consider spherical nuclei with $\beta_i = 1$ and then analyse the deformation effects.

In order to calculate the width of the single particle states, we use the expression [86, 102]

$$\Gamma_k = \frac{1}{\Gamma_0} \frac{(\epsilon_k - \epsilon_F)^2 + (\pi T_0)^2}{1 + [(\epsilon_k - \epsilon_F)^2 + (\pi T_0)^2]/c^2}. \tag{5.31}$$

Here, ϵ_F is the Fermi energy. Both parameters Γ_0 and c are known from experience with the optical model potential and the effective masses [86]. Their values are in the following ranges: $0.030\,\mathrm{MeV}^{-1} \leq {\Gamma_0}^{-1} \leq 0.061\,\mathrm{MeV}^{-1}$, $15\,\mathrm{MeV} \leq c \leq 30\,\mathrm{MeV}$. The quadratic dependence of the numerator can be obtained from the collision term in the Landau theory of Fermi liquid [103] and has been also verified within a microscopic approach based on an effective interaction of Skyrme type [104]. Since each single particle state has its own width, Eq. (5.15) is generalised as ($Q_i = \lambda, \eta, \eta_Z, \varepsilon, \beta_1, \beta_2$):

$$M^{diag}_{ij} = \hbar^2 \sum_k \frac{f_k}{\Gamma^2_k} \frac{\partial\epsilon_k}{\partial Q_i} \frac{\partial\epsilon_k}{\partial Q_j}. \tag{5.32}$$

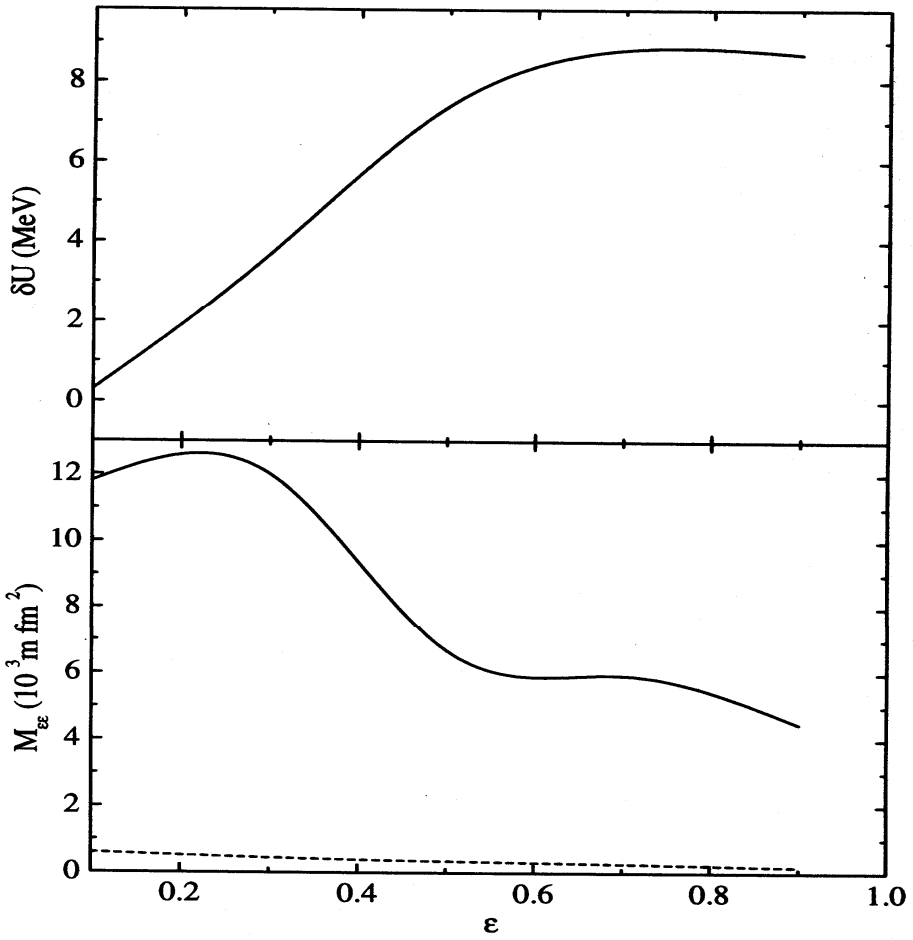

Figure 5-1: Dependence of the mass parameter $M_{\varepsilon\varepsilon}$ (lower part) and of the shell correction δU (upper part) on ε for the system $^{110}Pd + ^{110}Pd$ at $\lambda = 1.6$. In the calculation of $M_{\varepsilon\varepsilon}$, an excitation energy of $30MeV$ of the DNS and adiabatic single-particle states are used. The mass parameter $M_{\varepsilon\varepsilon}^{WW}$ calculated in the Werner-Wheeler approximation is presented by a dashed line in the lower part. Units: $m\ fm^2$ with m = nucleon mass.

For the Fermi occupation numbers $n(\epsilon_k)$, the function

$$f_k = -\frac{dn_k}{d\epsilon_k} = \frac{1}{4T_0}\cosh^{-2}\left(\frac{\epsilon_k - \epsilon_F}{2T_0}\right) \tag{5.33}$$

has a bell-like shape with a width T_0 and is peaked at the Fermi energy ϵ_F.

Various calculations of the mass parameter for the motion in λ were carried out with expressions similar to Eq. (5.32), for example in [88, 91, 95]. When the system adiabatically moves towards the compound nucleus, the value of $M_{\lambda\lambda}$ increases approximately by a factor 10–15 in our and other calculations. In this section, we concentrate on the calculation of the mass parameter $M_{\varepsilon\varepsilon}$ for the motion of the neck to test whether the DNS exists long enough with a relatively small neck. The dependence of $M_{\varepsilon\varepsilon}$ on ε is presented in Fig. 5-1 for the system ^{110}Pd+^{110}Pd at $\lambda = 1.6$, which corresponds to the touching configuration in this symmetric reaction. The obtained values of $M_{\varepsilon\varepsilon}$ have the same order of magnitude as in [88], where the pairing correlations were taken into account. The value of $M_{\varepsilon\varepsilon}$ increases by a factor 2.5 when the system falls into the fission-type valley [42]. This valley is observed in the adiabatic potential energy surface for $\varepsilon = 0 - 0.2$ and $\lambda = 1.6 - 1.7$. This increase reflects the decrease of the shell correction δU with ε towards $\varepsilon \to 0$. Smaller values of δU correspond to larger masses because the mass parameter is proportional to some effective level density g_{eff} at the Fermi energy. The expression (5.15) could be written as $M^{diag} \approx \frac{\hbar^2}{\Gamma^2}\left\langle\frac{\partial\epsilon_k}{\partial Q}\right\rangle^2_{aver} g_{eff}$. The effective level density g_{eff} is in inverse proportion to the shell correction δU [95].

In order to obtain a nuclear shape for the touching configuration of the nuclei similar to the one obtained in the DNS model, the neck parameter ε should be set about 0.75 [42]. With this value of ε, the neck radius and the distance between the centers of the nuclei are approximately equal to the corresponding quantities in the DNS.

For the parameter c in Eq. (5.31), we use the "standard" value 20 MeV since the masses (5.32) depend only weakly on this parameter. Setting the parameter $\Gamma_0^{-1} = 0.045\,\mathrm{MeV}^{-1}$ in (5.32) and comparing our results with M_{ij}^{WW} obtained in the Werner-Wheeler approximation for a touching configuration of the nuclei with the excitation energy $30MeV$ ($T_0 = 1.3MeV$), we find $M_{\lambda\lambda} = M_{\lambda\lambda}^{WW}$, $M_{\varepsilon\varepsilon} \approx (20-30)M_{\varepsilon\varepsilon}^{WW}$, $M_{\lambda\varepsilon} \approx 0.4M_{\lambda\varepsilon}^{WW}$ and $M_{\lambda\varepsilon}/\sqrt{M_{\lambda\lambda}M_{\varepsilon\varepsilon}} \ll 1$, practically independent of the mass number of the system. Therefore, we can conclude that

the microscopical mass parameter of the neck is much larger than the one in the Werner-Wheeler approximation, and the nondiagonal component $M_{\lambda\varepsilon}$ is small. Since at the touching configuration the slope of the single-particle levels is small and changes slowly with decreasing elongation λ, the microscopical mass parameter in λ is close to its smooth, hydrodynamical value. In contrast, a large amount of internal reorganisation occurs at the level crossings with decreasing ε and leads to a large neck inertia of the initial DNS. So, the value of $M_{\varepsilon\varepsilon}$ is larger than the one in the hydrodynamical model, due to large values of $\partial\epsilon_k/\partial\varepsilon$. The restriction for the growth of the neck may be understood by analysing the single particle spectrum as a function of ε [42]. Well necked-in shapes with large ε have single particle spectra with a good shell structure. The levels show a larger number of avoided level crossings with decreasing ε.

The time-dependence of the neck parameter calculated with the microscopical and Werner-Wheeler mass formulas are compared in the upper part of Fig. 5-2. The lower part of Fig. 5-2 shows trajectories in the (ε, λ)-plane, calculated with microscopic and Werner-Wheeler masses. An adiabatic potential energy surface is used in all these calculations [42]. Since there are no suitable barriers at smaller values of λ and ε in the adiabatic potential which hinder a growth of the neck, the neck parameter and system length decrease steadily to smaller values, faster in the case with the Werner-Wheeler masses and much slower with the microscopical masses. The experiments on fusion of heavy nuclei cannot be explained as a melting with increasing neck together with a decreasing λ in an adiabatic potential [42]. It seems that there is an intermediate situation between the adiabatic and diabatic limits for the collective motion. The study of the transition between diabatic and adiabatic regimes gives a potential energy surface which contains quite high barriers for the motion to smaller λ and ε [35, 66]. Therefore, the dynamical calculations with the adiabatic potential energy show a maximal possible growth of the neck. Since the moment of inertia is large in heavy nuclear systems, we disregard the dependence of the potential energy on the angular momentum in dynamical calculations. Indeed, in the fusion reactions with massive nuclei the low angular momenta ($< 20\ \hbar$) only contribute to the evaporation residue cross sections. The isotopic composition of fusioning nuclei forming a DNS is chosen by the condition of a N/Z-equilibrium in the system, and η_z follows η [42]. In processes developing in shorter times, η_z could be considered as an independent collective variable.

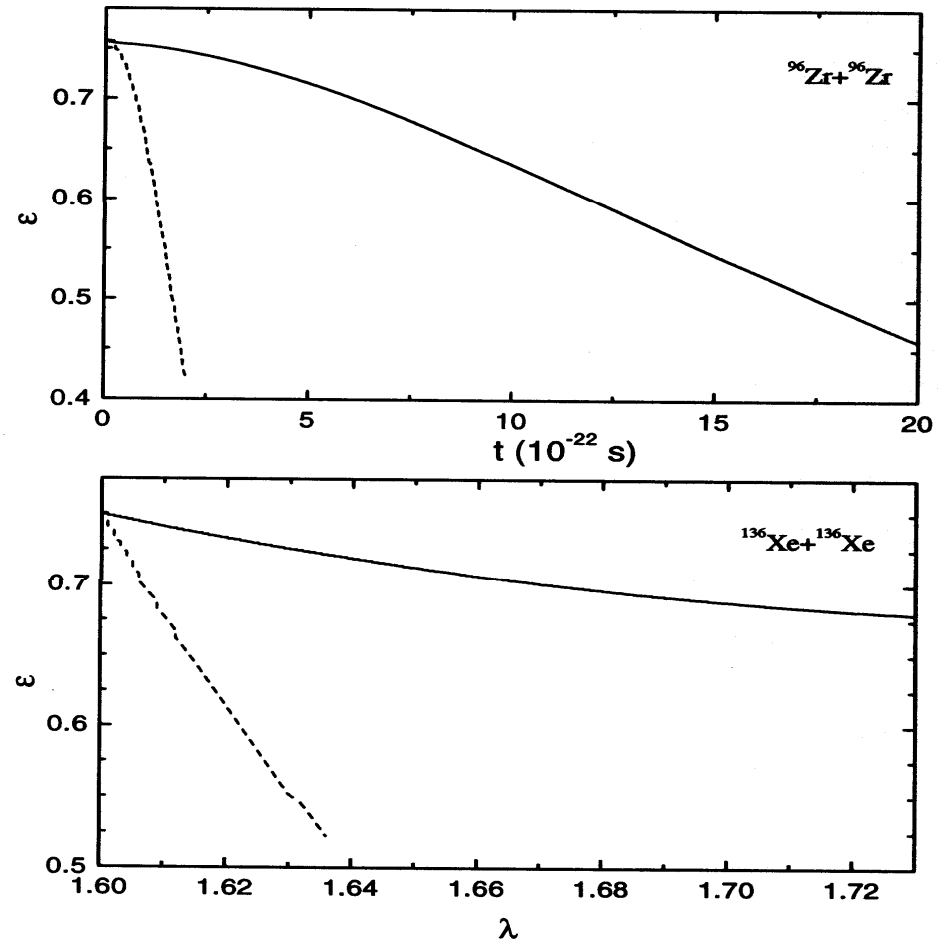

Figure 5-2: Upper part: Time-dependence of the neck parameter ε for the system $^{96}Zr+^{96}Zr$ calculated with microscopical (solid curve) and Werner-Wheeler (dashed curve) mass parameters. Lower part: Trajectories in the (λ, ε)-plane, calculated for the system $^{136}Xe+^{136}Xe$ with microscopical mass parameters (solid curve) and with Werner-Wheeler mass parameters (dashed curve). The end points of the solid and dashed curves in the drawing are at time $t = 2 \times 10^{-21} s$ and $t = 2 \times 10^{-22} s$, respectively.

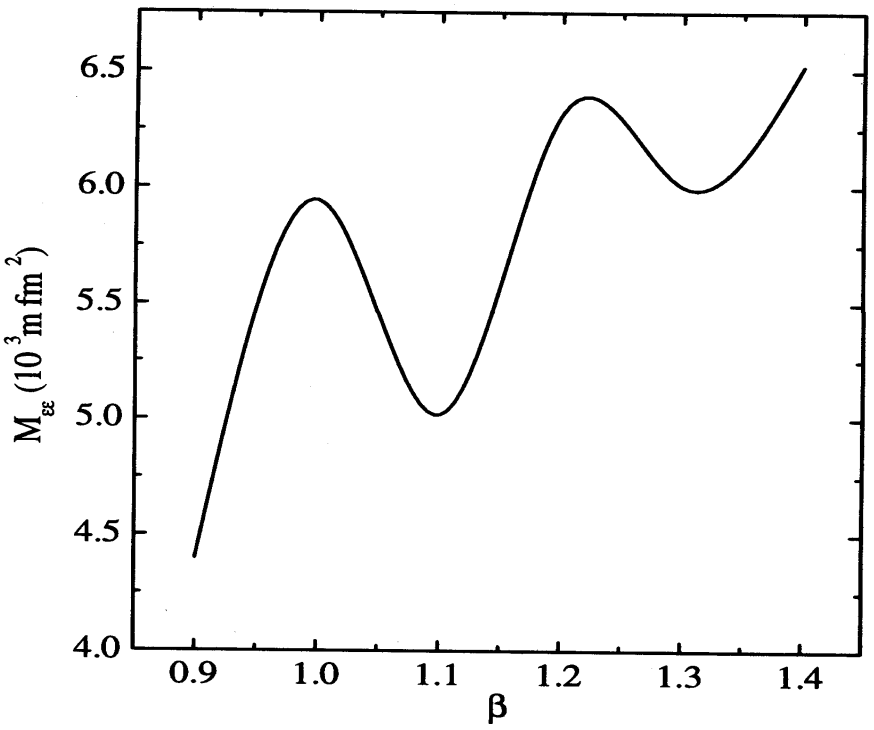

Figure 5-3: Mass parameter $M_{\varepsilon\varepsilon}$ as a function of deformation β, calculated for the system $^{110}Pd + ^{110}Pd$ at the touching configuration with excitation energy $30MeV$ and adiabatic single-particle states. Units: $m\ fm^2$ with m = nucleon mass.

As a result of Fig. 5-2, we find that the microscopical mass parameters keep the system near the entrance configuration for a sufficient long time comparable with the time of reaction even in an adiabatic potential. Therefore, this situation justifies the assumption of a fixed neck as we assume it in the DNS model [34]. When the DNS configuration exists a long time, then thermal fluctuations in the mass asymmetry coordinate play the essential role in the fusion process. Indeed, these fluctuations are responsible for the fusion in the DNS model. Thus, the dynamical restriction for the growth of the neck can be caused partly by a large microscopical mass parameter for the neck motion, partly by the potential energy surface intermediate between diabatic and adiabatic limits.

In the adiabatic two-center shell model, the mass parameter $M_{\varepsilon\varepsilon}$ slightly increases with the deformation parameters β_i of the two nuclei in the symmetric system ^{110}Pd+^{110}Pd as shown in Fig. 5-3. The small variation of $M_{\varepsilon\varepsilon}$ is due to the shell structure. Therefore, the relatively large value of $M_{\varepsilon\varepsilon}$ is a general result for collisions of both spherical and deformed nuclei. Fig. 5-4 shows the mass parameter $M_{\varepsilon\varepsilon}$ at the touching configuration of symmetric systems $\eta = 0$ with $\beta_i = 1$ as a function of the mass number $A = A_1 + A_2 = 2A_1$. The mass $M_{\varepsilon\varepsilon}$ increases with the mass of the system. It slightly decreases with increasing mass asymmetry of the DNS.

5.2.2 The diabatic two-center shell model

Let us now consider the calculation of the mass parameters (5.32) with the diabatic single particle energies obtained with the method of maximum-symmetry in the diabatic two-center shell model [35, 57]. In the diabatic motion, the nucleons do not occupy the lowest single particle states as in the adiabatic case, but remain in their diabatic states. In comparison to the calculations with the adiabatic single particle levels, the numerical procedure with diabatic single particle levels is much easier because each level has a complete set of quantum numbers and the drawing of the levels as a function of a collective variable is simpler and unique.

Due to the nonzero width of the single particle states, the distribution of single particle strength over more complicated states is a Lorentzian distribution $\rho_k(\epsilon)$ as introduced in Eq. (5.28) instead of the δ-function $\delta(\epsilon - \epsilon_k)$ [86]. The occupation number $\widetilde{n}(\epsilon_k)$ of a state k with energy ϵ_k and the corresponding value of $\widetilde{f}_k$ are obtained, respectively, from functions

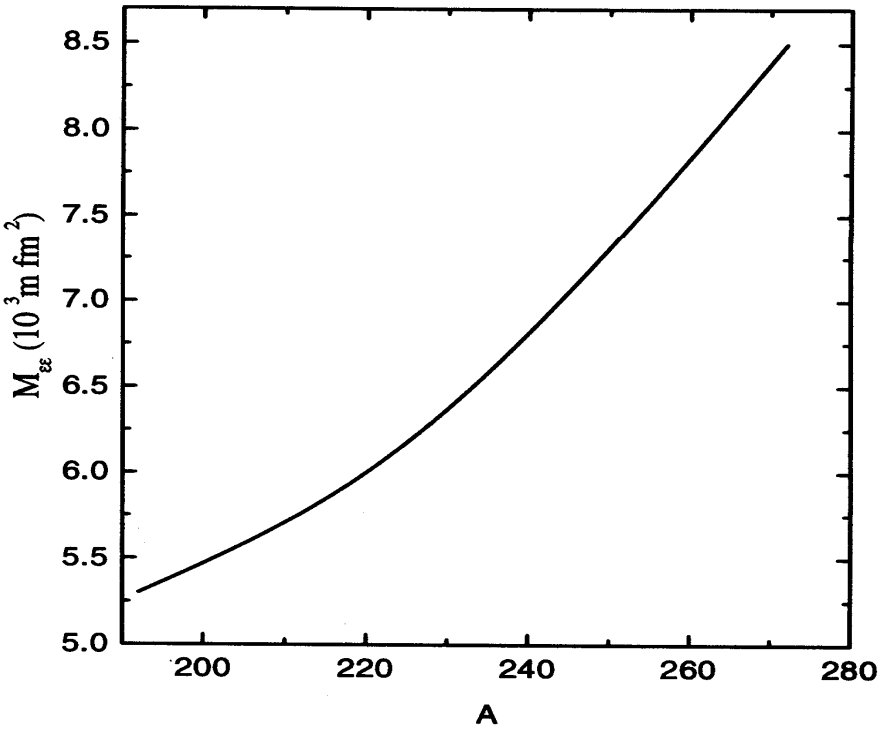

Figure 5-4: Mass parameter $M_{\varepsilon\varepsilon}$ as a function of the mass number $A = A_1 + A_2 = 2A_1$ for symmetric systems ($\eta = 0$) calculated with adiabatic single-particle states for $\beta_i = 1, \lambda = 1.6$, and $\varepsilon = 0.75$. Units: $m\ fm^2$ with m = nucleon mass.

$n(\epsilon)$ and $dn(\epsilon)/d\epsilon$ calculated with zero width of the levels

$$\widetilde{n}(\epsilon_k) = \int n(\epsilon)\rho_k(\epsilon)d\epsilon, \tag{5.34}$$

$$\widetilde{f}_k = -\int \frac{dn(\epsilon)}{d\epsilon}\rho_k(\epsilon)d\epsilon. \tag{5.35}$$

The Lorentzian distribution increases the diffuseness of the Fermi-distribution. The Fermi distribution which is given at the touching configuration of the nuclei in the DNS is destroyed if the further motion of the system runs diabatically. To treat the diabatic case, we use the following function $n(\epsilon)$ for an arbitrary configuration of the system

$$n(\epsilon) = \sum_{l=0}^{N} a_l \left(\vartheta(\epsilon - \epsilon_l) - \vartheta(\epsilon - \epsilon_{l+1})\right), \tag{5.36}$$

where $\vartheta(x)$ is the Heavyside's function and ϵ_l the energy of single particle state l with the occupation number a_l. Here, the numbers $l = 0, ..., N$ count the single particle states in the region of the Fermi level. The values ϵ_0 and ϵ_{N+1} are the low and high limits of the single particle energies. For lower and higher energies, the occupation numbers are one and zero, respectively. Therefore, we assume $a_0 = 1$ and $a_N = 0$ in (5.36). The derivative $dn(\epsilon)/d\epsilon$ is expressed as

$$-\frac{dn(\epsilon)}{d\epsilon} = (1 - a_1)\delta(\epsilon - \epsilon_1) + \sum_{l=2}^{N-1}(a_{l-1} - a_l)\delta(\epsilon - \epsilon_l) + a_{N-1}\delta(\epsilon - \epsilon_N). \tag{5.37}$$

We then obtain $\widetilde{f}_k$ with (5.35) as follows

$$\widetilde{f}_k = (1 - a_1)\rho_k(\epsilon_1) + \sum_{l=2}^{N-1}(a_{l-1} - a_l)\rho_k(\epsilon_l) + a_{N-1}\rho_k(\epsilon_N). \tag{5.38}$$

In the calculations we assume the same average width for each Lorentzian $\rho_k(\epsilon)$. The diabatic occupation numbers a_l are fixed at the touching configuration of the system using a Fermi distribution for a smaller temperature $T_0^* < T_0$. The value of T_0^* is chosen in such a way that the occupation numbers $\widetilde{n}(\epsilon_k)$ (5.34) and the values of $\widetilde{f}_k$ (5.35) obtained at the touching configuration of the nuclei, using either the exact expresions (Fermi distribution and (5.33)) or

the approximate expressions (Eqs. (5.36) and (5.37)), are nearly equal in both cases.

Similar results as in the adiabatic two-center shell model are obtained. The mass parameters $M_{\lambda\lambda}$ and $M_{\varepsilon\varepsilon}$ depend weakly on the mass asymmetry η and on the deformations β of the nuclei ($\beta = \beta_1 = \beta_2$ for ^{110}Pd+^{110}Pd) at the touching configuration. This result is presented in Fig. 5-5. One can observe a minimum of $M_{\lambda\lambda}$ as a function of β in the reaction ^{110}Pd+^{110}Pd around the ground state deformation of ^{110}Pd ($\beta \approx 1.2$). Since we regard the widths of single-particles states, the mass parameters depend more smoothly on the mass asymmetry η than the mean field cranking masses. In comparison to Ref. [84], where the hydrodynamical-type treatment was used, the shell effects are here more transparent in the present consideration because all peculiarities of the single particle spectra are taken into account. Let us consider the fragmentation $^{86}Kr +^{134} Ba$ ($\eta = 0.2$) in the system ^{220}U where the number of neutrons in the fragments is close to the magic numbers 50 and 82, respectively, and the single particle levels have a smaller slope with respect to λ than in the neighbouring combinations. We find a smaller contribution to $M_{\lambda\lambda}$ from $M_{\lambda\lambda}^{diag}$ and a local minimum in the dependence of $M_{\lambda\lambda}$ on η (Fig. 5-5). For $\eta < 0.6$, the dependence of the mass parameter $M_{\lambda\lambda}$ on η is consistent with the results of Ref. [84]. The shape parametrisation of the TCSM is not appropriate for $\eta > 0.7$. Therefore, we cannot calculate $M_{\varepsilon\varepsilon}$ at the moment for such large mass asymmetries, where a strong increase of $M_{\varepsilon\varepsilon}$ with η is expected in accordance with Ref. [84].

The mass parameter $M_{\varepsilon\varepsilon}$ increases about two times with decreasing ε from 1.0 to 0.5 or with increasing neck as shown in Fig. 5-6 and depends weakly on the mass number A. In the reactions ^{110}Pd+^{110}Pd and ^{48}Ca+^{172}Hf, which lead to the same compound nucleus ^{220}U, the difference between the corresponding values of $M_{\varepsilon\varepsilon}$ becomes larger for small values of ε. Such a behaviour correlates with the fact that the diabatic contribution to the potential energy grows faster with decreasing ε in symmetric configurations than in asymmetric ones [35].

For fixed $\varepsilon = 0.75$, the mass $M_{\lambda\lambda}$ grows with decreasing elongation λ on average as shown in Fig. 5-6 and is 5 times larger than the reduced mass at $\lambda \approx 1.3$. The dependence of $M_{\lambda\lambda}$ on λ has fluctuations around an average upwards trend which are more pronounced with an increasing total mass number A of the system (Fig. 5-6) and at smaller temperatures (Fig. 5-7). The average trend is connected with an increase of the average slope of the single particle levels with decreasing λ or ε and with the enlarged number of crossings between the diabatic levels.

Such a behaviour correlates with the diabatic contributions to the potential energy [35]. The fluctuations arise from the factor $\tilde{f}_k / \Gamma_k^2$ in Eq. (5.32) and are related to the increasing number of crossings between the single particle levels near the Fermi level with decreasing λ [35].

The choice of the width of the single particle levels is crucial for the value of M^{diag} in both the diabatic and adiabatic cases within a reasonable variation. If instead of $\Gamma_0^{-1} = 0.045$ MeV^{-1}, the value of Γ_0^{-1} is taken as 0.03 MeV^{-1}at the lower limit , the value of $M_{\varepsilon\varepsilon}$ becomes 2.25 times smaller, but remains larger than $M_{\varepsilon\varepsilon}^{WW}$ by about one order of magnitude. For larger temperatures, the average width Γ increases and the function $\tilde{f}_k / \Gamma_k^2$ becomes smoother. The mass parameter $M_{\varepsilon\varepsilon}$ depends on temperature T_0 mainly due to the width Γ_k of the single-particle levels ($\Gamma_k \sim T_0^2$). The value of $M_{\varepsilon\varepsilon}$ decreases with T_0^{-4}. One- and two-body interactions [96] contribute to the nondiagonal and diagonal parts of the mass parameter, respectively. Whereas the one-body contribution to mass (nondiagonal part) is relatively insensitive to the temperature of the system, the two-body contribution to mass (diagonal part) increases strongly with decreasing temperature. The two-body interaction is considered in our calculations using the width of the single-particle levels [86]. So, we can observe in Fig. 5-7 that $M_{\varepsilon\varepsilon}^{diag}(T_0 = 1MeV)/M_{\varepsilon\varepsilon}^{diag}(T_0 = 1.5MeV) \sim 5$ on average for the values of $\varepsilon = 0.5 - 1$. We found that the contribution of the diagonal part $M_{\varepsilon\varepsilon}^{diag}$ to $M_{\varepsilon\varepsilon}$ is the largest at quite a high excitation energy of $30MeV$ $(T_0 = 1.3MeV)$ of the DNS in fusion reactions. For comparison, the excitation energies of the initial DNS are smaller than $20MeV$ $(T_0 < 1.0MeV)$ in $Pb-$ and $Bi-$ based cold fusion reactions. Hot fusion reactions of heavy nuclei have excitation energies of the initial DNS smaller than $40MeV$ $(T_0 = 1.5MeV)$ and a rapid decrease of the survival probability of the compound nucleus with increasing excitation energy. Finally, we should stress that the mass parameter $M_{\varepsilon\varepsilon}$ remains always much larger (e.g., $20-30$ times for $T_0 = 1.3MeV$) in fusion reactions than the mass calculated with the hydrodynamical Werner-Wheeler approximation for $T_0 = 1 - 1.5MeV$.

The mass parameters at the touching configuration of the nuclei are the same in the adiabatic and diabatic descriptions because the single particle levels and occupation numbers are practically the same in these two limits. It is known that the mass parameters are smaller in the diabatic case for a zero width of single particle levels than in the adiabatic case [57]. We found values for the mass parameters $M_{\lambda\lambda}$ and $M_{\varepsilon\varepsilon}$ within the diabatic TCSM which are closer

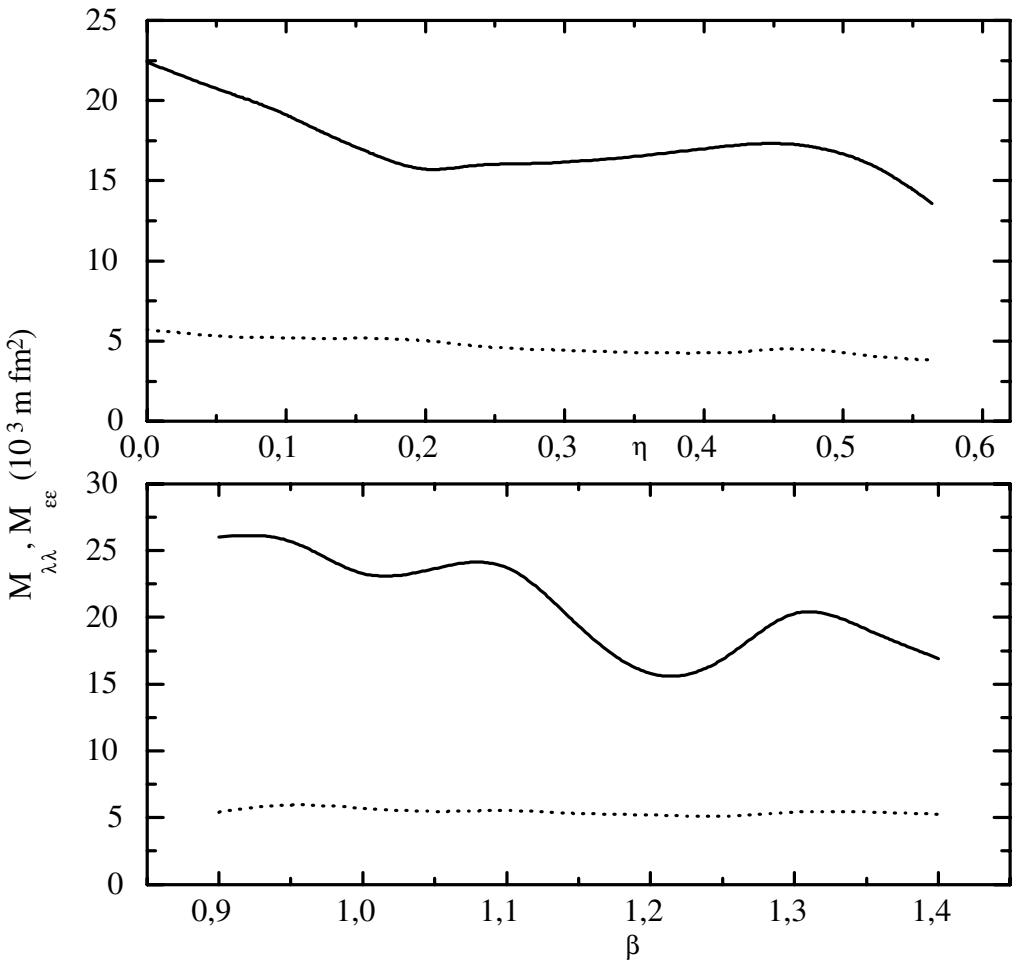

Figure 5-5: Upper part: Mass parameters $M_{\lambda\lambda}$ (solid line) and $M_{\varepsilon\varepsilon}$ (dotted line) as functions of mass asymmetry η at the touching configuration for DNS which leads to the same compound nucleus ^{220}U. The value of the neck coordinate is $\varepsilon = 0.75$, and the excitation energy of the DNS is $30MeV$. The calculation is done with spherical nuclei. Lower part: The same as in the upper part, but as a function of deformation β for the reaction $^{110}Pd+^{110}Pd$ ($\eta = 0$). Diabatic single-particle states are used. Units: $m\ fm^2$ with m = nucleon mass.

to the ones obtained in adiabatic calculations because we took the width Γ_k of single-particle states into consideration. This is observed in Figs. 5-1 and 5-6 comparing the values of $M_{\varepsilon\varepsilon}$ at the touching configuration of the nuclei for the reaction $^{110}Pd + ^{110}Pd$. Due to the effect of the width of the single-particle states, the occupation probabilities for single-particle levels with zero widths are distributed over more levels. This effect partially destroys the difference between the diabaticity and adiabaticity at crossings (or pseudo-crossings) of the single-particle levels. We want to stress that the differences between the diabatic and adiabatic single-particle levels appear only near the crossing points. Moreover, the distribution of the diabatic occupation numbers $\widetilde{n}(\epsilon_k)$ and the derivatives $\widetilde{f}_k$ approaches the ones obtained in the adiabatic case for fixed values of ε, λ and excitation energy of the system (Fig. 5-8). Since we showed the similarity of the data obtained with adiabatic and diabatic levels using the same width, we can use diabatic single particle states in further calculations of mass parameters in order to simplify the numerical procedure.

The obtained mass parameter for the neck degree of freedom is much larger than the one obtained in the hydrodynamical model with the Werner-Wheeler approximation. By applying the microscopical mass parameters we find a relatively stable neck during the time of reaction. In addition, a large energy threshold due to the diabatic (structural) forbiddenness effect [35, 36] hinders the motion to smaller internuclear distances. Therefore, the DNS configuration exists long enough, and thermal fluctuations in the mass asymmetry coordinate could develop and lead to fusion and quasifission, which are the essential reactions in the DNS concept.

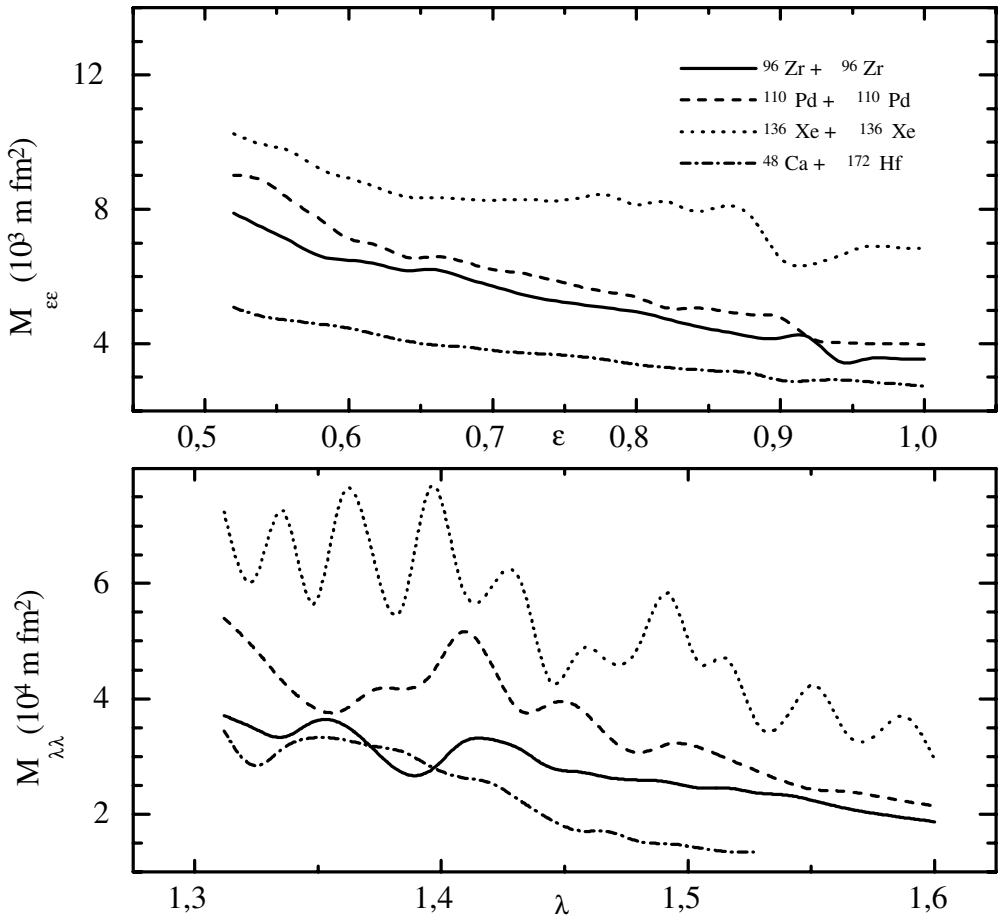

Figure 5-6: Upper part: $M_{\varepsilon\varepsilon}$ as a function of the neck coordinate ε at the touching configuration for the reactions: $^{96}Zr + ^{96}Zr$ (solid line), $^{110}Pd + ^{110}Pd$ (dashed line), $^{136}Xe + ^{136}Xe$ (dotted line) and $^{48}Ca + ^{172}Hf$ (dashed-dotted line). The excitation energy of the DNS in these reactions is $30MeV$. Lower part: The same as in the upper part, but for $M_{\lambda\lambda}$ as a function of the elongation λ. Diabatic single-particle states are used. Units: $m\ fm^2$ with m = nucleon mass.

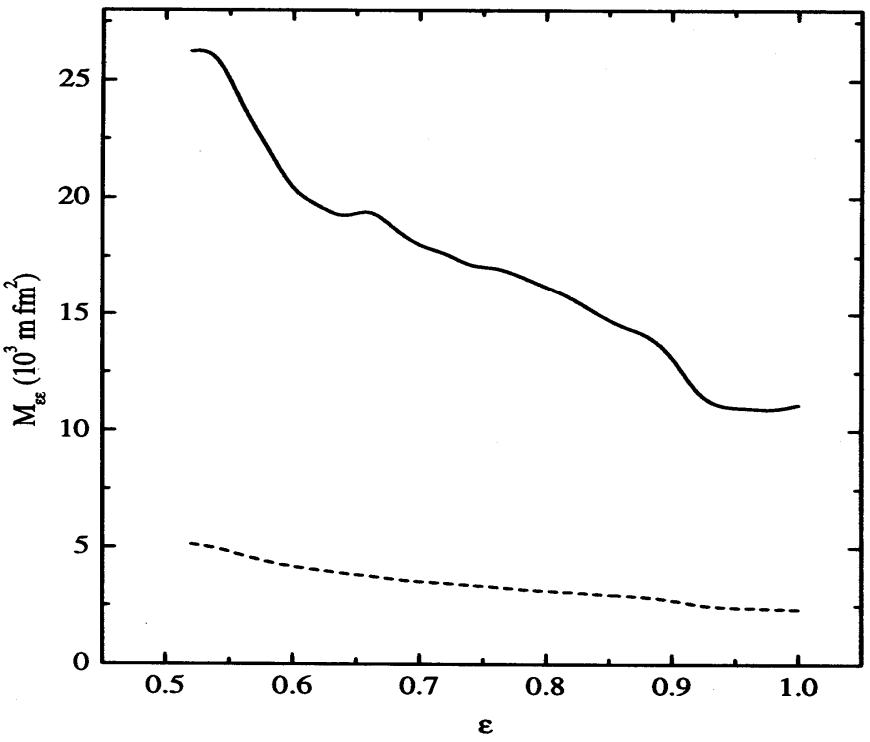

Figure 5-7: Mass parameter $M_{\varepsilon\varepsilon}$ as a function of ε at the touching configuration in the $^{110}Pd + ^{110}Pd$ reaction for temperatures $T_0 = 1MeV$ (solid line) and $1.5MeV$ (dashed line). Diabatic single-particle states are used. Units: $m\ fm^2$ with m = nucleon mass.

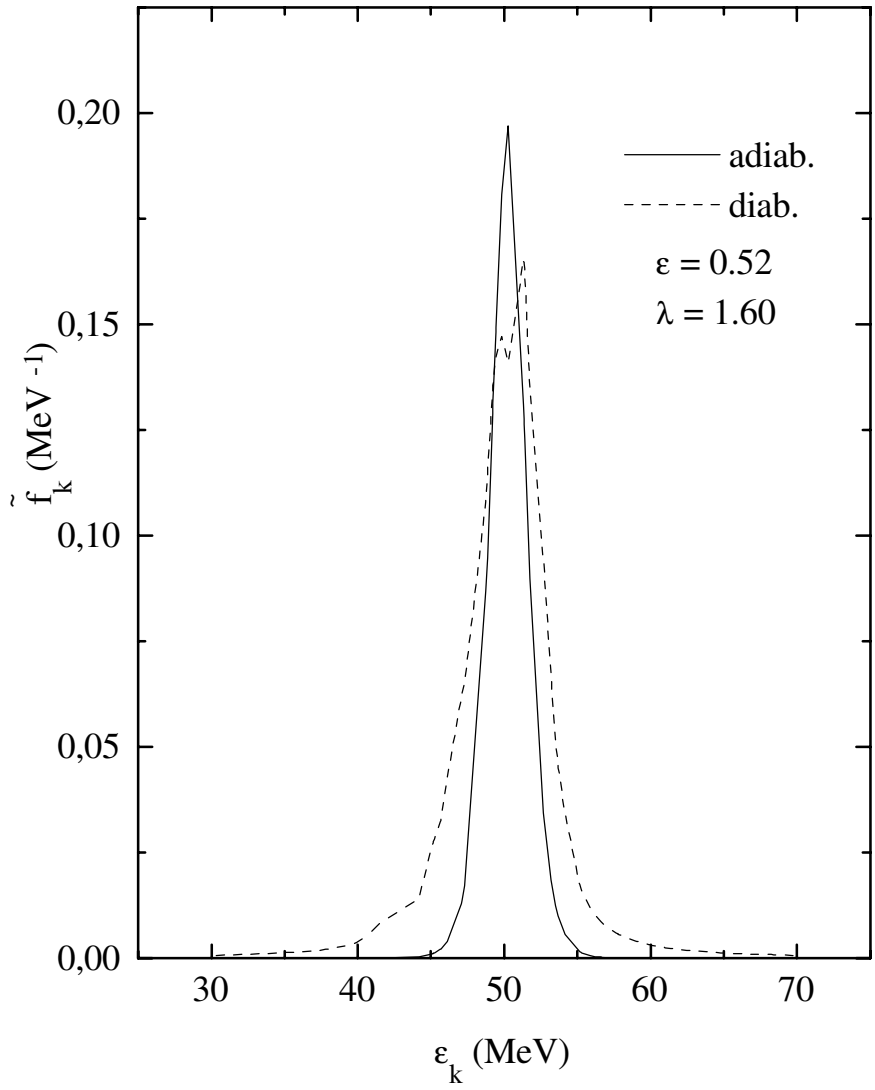

Figure 5-8: Derivatives $\widetilde{f}_k$ of the adiabatic (solid line) and diabatic (dashed line) neutron occupation numbers $\tilde{n}\ (\epsilon_k)$ as a function of the single-particle energies ϵ_k for the system ^{110}Pd+^{110}Pd which moves in the neck coordinate ε. The nuclei are in the touching configuration ($\lambda = 1.6$) and are considered as spherical. The value of ε is 0.52.

Chapter 6

In most reactions studied in chapter 3 [35] the diabatic potential has a minimum in the neck parameter ε around $\varepsilon = 0.65$–0.85. Due to the large inertia and friction coefficient in the neck coordinate ε obtained in chapter 5 [43], the DNS configurations with fixed neck parameters have a long lifetime in comparison to the reaction time. In contrast to the Ref. [42], where the fusion probability through the fission-type valley with small ε was considered, fusion probabilities P_{CN} obtained for fixed large ε depend correctly on the initial value of η in the entrance channel [34]. As in Ref. [42], the adiabatic treatment of fusion in λ yields fusion probabilities which are considerably overestimated in comparison to the experimental data although a fixed large neck ε is considered. The reason of this overestimate is clearly seen in Fig. 6-1, where the adiabatic potentials for different fragmentations leading to the same compound nucleus ^{246}Fm are shown as a function of λ at $\varepsilon = 0.75$. In contrast to experiment the hindrance of fusion in these potentials is practically absent ($P_{CN} \approx 1$) because there is no fusion barrier for the motion to smaller elongations λ. The diabatic effects in the entrance phase of the collision studied in chapter 3 strongly hinder the motion of the system to smaller elongations λ. The study of the transition from the diabatic potential to the adiabatic one in the motion of the system in λ during the lifetime of the dinuclear system allows us to conclude whether the fusion is possible in the elongation coordinate.

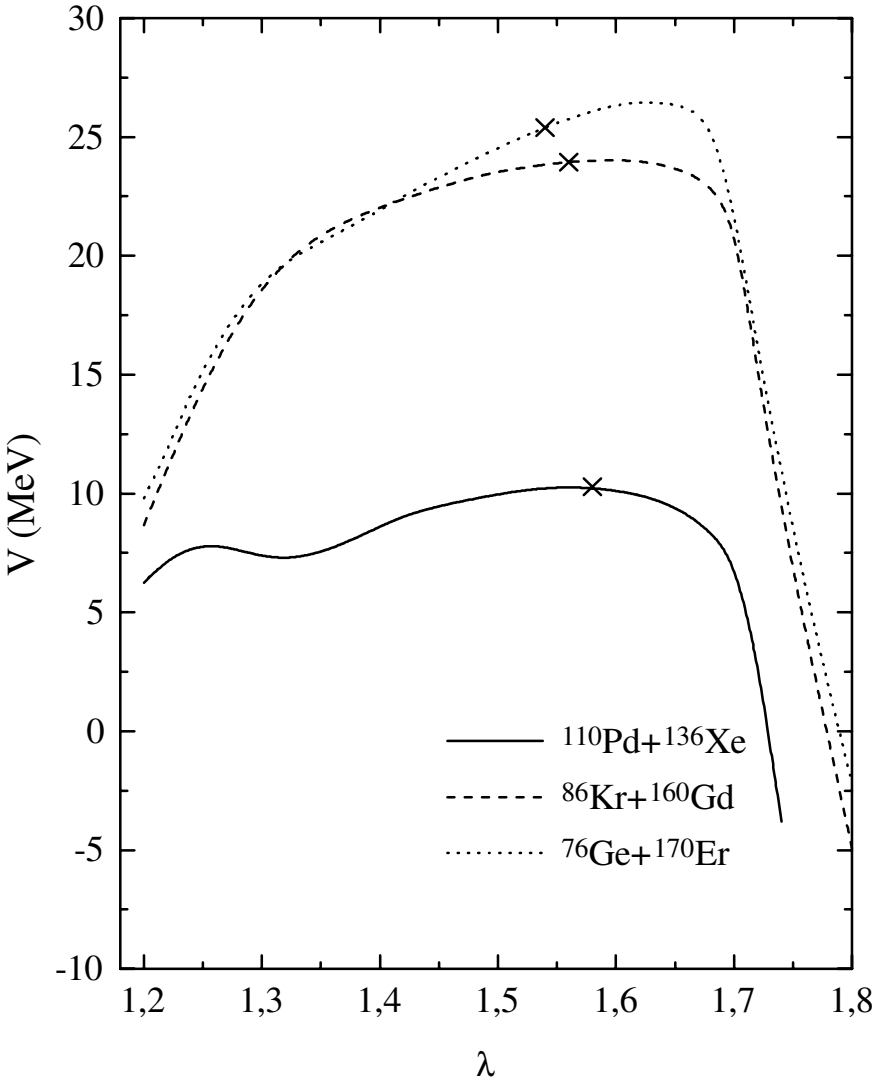

Figure 6-1: Adiabatic potentials as a function of λ calculated within the TCSM for different combinations leading to the same compound nucleus ^{246}Fm. The nuclei are considered as spherical and the neck parameter $\varepsilon = 0.75$. The crosses denote the touching configurations.

It will be interesting to study the competition between two possible fusion channels. The first one (λ–channel) describes the transition of two nuclei into the compound nucleus with a decreasing elongation and assumes a fixed mass asymmetry η during the fusion. The second channel, named η–channel, describes the evolution of the DNS to the compound nucleus as a change of the mass asymmetry η by nucleon transfer from the light nucleus to the heavy one at the touching configuration of the nuclei. Nuclei are considered as spherical with $\varepsilon = 0.74$ which corresponds to realistic shapes of the DNS for λ =1.5–1.6. The comparison of the fusion probability calculated in both channels will allow us to find the favorable fusion channel.

In the present chapter we will study whether the system has time for destroying the "memory" about the diabatic hindrance [35, 36]. This time is necessary to reorganize the density of the system for the transition from the initial diabatic potential $V_{diab}(\lambda)$ to the adiabatic one $V_{adiab}(\lambda)$. The time dependence of the transition of the potential can be related to the effective relaxation time $\tau(\lambda, t)$ [105, 106]

$$V(\lambda,t) = V_{diab}(\lambda)\exp(-\int_0^t \frac{dt}{\tau(\lambda,t)}) + V_{adiab}(\lambda)[1-\exp(-\int_0^t \frac{dt}{\tau(\lambda,t)})]. \tag{6.1}$$

A time-dependent dynamical potential $V(\lambda, t)$ was originally introduced in Refs.[105, 106] from a phenomenological ansatz and applied to study the effects of local equilibrium in dissipative heavy-ion collisions. Eq. (6.1) may be rewritten as

$$V(\lambda,t) = V_{adiab}(\lambda) + \Delta V_{diab}(\lambda,t) \tag{6.2}$$

with $\Delta V_{diab}(\lambda,t) = (V_{diab}(\lambda) - V_{adiab}(\lambda))\exp(-\int_0^t \frac{dt}{\tau(\lambda,t)})$. The additional part $\Delta V_{diab}(\lambda, t)$ can be microscopically obtained from the diabatic excitation of particle-hole states

$$\Delta V_{diab}(\lambda,t) \approx \sum_\alpha \epsilon_\alpha^{diab}(\lambda)[n_\alpha^{diab}(\lambda,t) - n_\alpha^{adiab}(\lambda)], \tag{6.3}$$

where the $\epsilon_\alpha^{diab}(\lambda)$ are diabatic single–particle energies as a function of the elongation λ of the TCSM. The adiabatic occupation numbers $n_\alpha^{adiab}(\lambda)$ vary with λ according to a Fermi distribution with a temperature $T(\lambda) = \sqrt{E^*(\lambda)/a}$ ($a = A/12MeV^{-1}$), where the excitation energy $E^*(\lambda)$ is determined from total energy conservation. The exponential factor in (6.1) is

due to the dependence of the diabatic occupation probabilities n_α^{diab} on time expressed by the relaxation equations [51, 52, 57]

$$\frac{dn_\alpha^{diab}(\lambda,t)}{dt} = -\frac{1}{\tau(\lambda,t)}[n_\alpha^{diab}(\lambda,t) - n_\alpha^{adiab}(\lambda)], \tag{6.4}$$

which is known in the relaxation-time approximation. Due to the residual two-body interactions, the diabatic occupation probabilities approach a local (fixed λ) equilibrium with an average relaxation time

$$\tau(\lambda,t) = \frac{2\hbar}{<\Gamma(\lambda,t)>}. \tag{6.5}$$

The factor 2 assumes that two subsequent collisions are sufficient to establish equilibrium for fixed values of the collective variable λ (local equilibrium). Here, we use a minimal value of this factor (or minimal possible value of τ) in comparison to Refs. [51, 52, 57] where this factor was chosen as 3–4. From the (6.1) it is clear that the effective time τ necessary to reorganize the densities of the system corresponds to a mean value of various relaxation times associated with the shape degrees of freedom of the system. This effective relaxation time τ is larger than the average single-particle decay time ($\frac{\hbar}{<\Gamma>}$) due to the effect of a self-consistency between collective and intrinsic degrees of freedom [86, 107]. The width in Eq. (6.5)

$$<\Gamma(\lambda,t)> = \sum_\alpha \overline{n}_\alpha^{diab}(\lambda,t)\Gamma_\alpha(\lambda) / \sum_\alpha \overline{n}_\alpha^{diab}(\lambda,t) \tag{6.6}$$

is an average width of the particle-states above the Fermi level ($\overline{n}_\alpha^{diab} = n_\alpha^{diab}$ for $\epsilon_\alpha^{diab} > \epsilon_F$) and of the hole-states under the Fermi level ($\overline{n}_\alpha^{diab} = 1 - n_\alpha^{diab}$ for $\epsilon_\alpha^{diab} \leq \epsilon_F$).

For the widths Γ_α, the expression (5.31) is used. In the calculations we take the standard value c=20 MeV and consider the cases with two extreme values of Γ_0^{-1}: $0.030 MeV^{-1}$and $0.061 MeV^{-1}$. The results depend weakly on the value of the parameter c. From (5.31), one can see that for very large free energies $\epsilon_\alpha^{diab} - \epsilon_F$ the broadening of single-particle widths due to intrinsic excitation energy of the system plays no essential role in contrast to the case when the excited system is near the equilibrium state [108]. Although one may define a local excitation energy during the decay of the diabatic potential to the adiabatic one, the concept of temperature is less meaningful as the system is not locally equilibrated or thermalized [109].

More detailed investigations are required to clarify these points. In the calculations, we do not consider thermal effects in the values of Γ_α.

The adiabatic potential energy V_{adiab} is calculated using the expression (3.2), but taking into account the dependence of the shell correction and the pairing correction on the excitation energy $E^*(\lambda)$. Shell effects are damped exponentially $\delta U_{shell} = \delta U_{shell}(E^* = 0)\exp(-\zeta E^*)$ if the system is excited with the excitation energy E^*. The parameter ζ is chosen as $\zeta^{-1} = 5.48A^{\frac{1}{3}}/(1 + 1.3A^{-\frac{1}{3}})\ MeV$ [110]. The pairing corrections are taken as follows $\delta U_{pair} = 0$ for $E^* \geq E_c$ and δU_{pair}=$\delta U_{pair}(E^* = 0)[1 - E^*/E_c]^2$ for $E^* < E_c$ [78] with $E_c = 10MeV$. We neglect the dependence of potential energy on the angular momentum in the reactions considered [18, 20, 22, 34, 38] because in fusion reactions with heavy nuclei only low angular momenta ($< 20 - 30\,\hbar$) contribute [78, 111].

The potential energy of the DNS in the touching configuration of the nuclei was calculated as a function of the mass asymmetry η within the adiabatic TCSM because the diabatic effects are very small near this configuration [35]. The diabatic potential practically coincides with the adiabatic one in the touching configuration of the nuclei. Therefore, the values of the fusion barrier in the η-channel and the quasi-fission barrier are practically independent of time. Indeed, the motion in η proceeds with nucleon exchanges between the levels near the Fermi surfaces of the DNS nuclei. For smaller elongations ($\lambda < \lambda_t$) the diabatic potential is considerably higher than the adiabatic potential. As shown in Refs. [35, 36], the diabatic potential measures the structural forbiddenness which reflects the action of the Pauli principle. For the motion in η at the touching configuration of the nuclei, the structural forbiddenness is absent and thus diabatic contributions to the potential energy are negligible.

In order to study the competition between the fusion channels in λ and η, we use the fusion rate $\Lambda^\lambda_{fus}(t)$ ($\Lambda^\eta_{fus}(t)$) through the inner fusion barrier B^λ_{fus} (B^η_{fus}) in λ (η) and the quasi-fission rate $\Lambda^\lambda_{qf}(t)$ to calculate the fusion probability in λ–channel (η–channel)

$$P^{\lambda(\eta)}_{fus} = \int_0^{t_0} \Lambda^{\lambda(\eta)}_{fus}(t)dt, \tag{6.7}$$

where the lifetime t_0 of the DNS is obtained with the condition

$$\int_0^{t_0} [\Lambda^{\lambda}_{fus}(t) + \Lambda^{\eta}_{fus}(t) + \Lambda^{\lambda}_{qf}(t)]dt = 1. \tag{6.8}$$

The rate of probability $\Lambda^{\lambda}_{qf}(t)$ through the external barrier in λ determines the quasi-fission process (the decay of the system). The height B^{λ}_{qf} of this barrier monotonically decreases with the mass asymmetry of the DNS because the Coulomb repulsion increases with decreasing η and leads to very shallow pockets in the nucleus-nucleus potential for the near symmetric configurations. Therefore, the quasi-fission probability for a symmetric and near symmetric DNS is much larger than for an asymmetric one. The reactions considered in this chapter are symmetrical or near symmetrical and, correspondingly, their initial DNS configurations are in or near the minimum of the potential energy of the systems as a function of λ and η. In this case the main contribution to the quasi-fission channel comes from the initial or near initial configurations which have approximately the same quasi-fission barrier B^{λ}_{qf}. Indeed, in reactions with heavy nuclei the experimental data do not show relaxation in η and have their maximal yields of the quasi-fission products near the initial DNS [112, 113]. All these facts allow us to calculate the quasi-fission rate for the initial DNS with a Kramers-type expression. It was proved in calculations with the multidimensional Fokker-Planck equation that the use of the value B^{λ}_{qf} for the initial DNS is a good approximation even for asymmetric reactions [34]. The quasi-fission decay process in λ determines the lifetime of the DNS mainly because the barrier B^{λ}_{qf} is smaller than the barrier B^{η}_{fus} in η. The lifetimes t_0 obtained for the reactions considered are comparable with the experimentally extracted characteristic fusion times of $10^{-21} - 10^{-20} s$ [114]. Since the effect of the transient times for stationary rates of probability over the fusion and quasi-fission barriers is weak [34] and their contribution is of the order of the accuracy of the calculation of the barrier heights, we use the one-dimensional Kramers expression [115] ($^{Kr}\Lambda^{j}_{i}$, $i =$"fus" or "qf" and $j =$"λ" or "η") which is a quasi–stationary solution of the Fokker-Planck equation for the corresponding rate of probability

$$^{Kr}\Lambda^{j}_{i} = \frac{\omega_j}{2\pi\omega^{B^j_i}} \left(\sqrt{(\frac{\Gamma}{2\hbar})^2 + (\omega^{B^j_i})^2} - \frac{\Gamma}{2\hbar} \right) \exp(-\frac{B^j_i}{T(\lambda_t)}). \tag{6.9}$$

Here, B_i^j denotes the height of the fusion barriers $B_{fus}^{\lambda}(t)$ and B_{fus}^{η}, and quasi-fission barrier B_{qf}^{λ}. The values of B_{fus}^{η} and B_{qf}^{λ} are practically independent of time. The initial DNS of the reactions considered here are in or near the minimum of the total potential energy of the system as a function of λ and η. Moreover, they are in thermodynamic equilibrium because the diabatic and adiabatic potentials practically coincide. The temperature $T(\lambda_t)$ is calculated using the expression $T(\lambda_t) = \sqrt{E^*(\lambda_t)/a}$ where λ_t is the elongation of the touching nuclei, i.e. of the initial DNS. In the calculations we assume that the excitation energy of the initial DNS is $E^*(\lambda_t)$=30 MeV in all reactions considered. In (6.9), $\omega^{B_i^j}$ is the frequency of the inverted harmonic oscillator approximating the potential in the variable j on the top of the fusion or quasifission barriers B_i^j, and ω_j is the frequency of the harmonic oscillator approximating the potential in the variable j for the initial DNS. The frequencies $\omega^{B_i^j}$ and ω_j are calculated using the absolute values of the second derivative of the potential with respect to the variable j (on the top of the barrier B_i^j and for the initial DNS, respectively) as well as the corresponding mass parameter M_{jj} (e.g, $\omega^{B_i^j} = \sqrt{|\partial^2 V/\partial j^2|_{B_j^i}/M_{jj}}$). The method of calculation of the mass parameters $M_{\eta\eta}$ and $M_{\lambda\lambda}$ is presented in chapter 5 [43]. The microscopical values of $M_{\eta\eta}$ and $M_{\lambda\lambda}$ are close to the corresponding hydrodynamical values [84] at the touching configuration of the nuclei (see chapter 5). In our calculations of the fusion probabilities, the following values are used $\hbar\omega^{B_{qf}^{\lambda}} \approx 0.8$–$1.0$ MeV, $\hbar\omega^{B_{fus}^{\eta}} \approx 1.5$–$2.0$ MeV, $\hbar\omega_{\lambda} \approx 1.5$–$2.0$ MeV and $\hbar\omega_{\eta} \approx 0.8$–$1.0$ MeV for the reactions considered. The value of $\hbar\omega^{B_{fus}^{\lambda}}$ at the inner fusion barrier in λ is about 0.5–0.6 MeV and agrees with the one obtained in the calculations of fission [116] at the saddle point. The friction coefficients ((5.9) and (5.23)) in λ and in η obtained with Γ=2 MeV at the touching configuration λ_t have the same order of magnitude as the ones calculated within the one-body dissipation models [34]. The values obtained for $P_{fus}^{\lambda(\eta)}$ depend rather weakly on Γ in (6.9)[34]. The possibility to apply the Kramers expression to relatively small barriers ($B_i^j/T > 0.5$) was demonstrated in [117].

6.1 Results and discussion

The time-dependent diabatic potentials for the reactions ^{110}Pd+^{110}Pd and ^{124}Sn+^{124}Sn are presented in Figs. 6-2a and 6-2b. The time-dependent inner fusion barrier B_{fus}^{λ} in λ appears

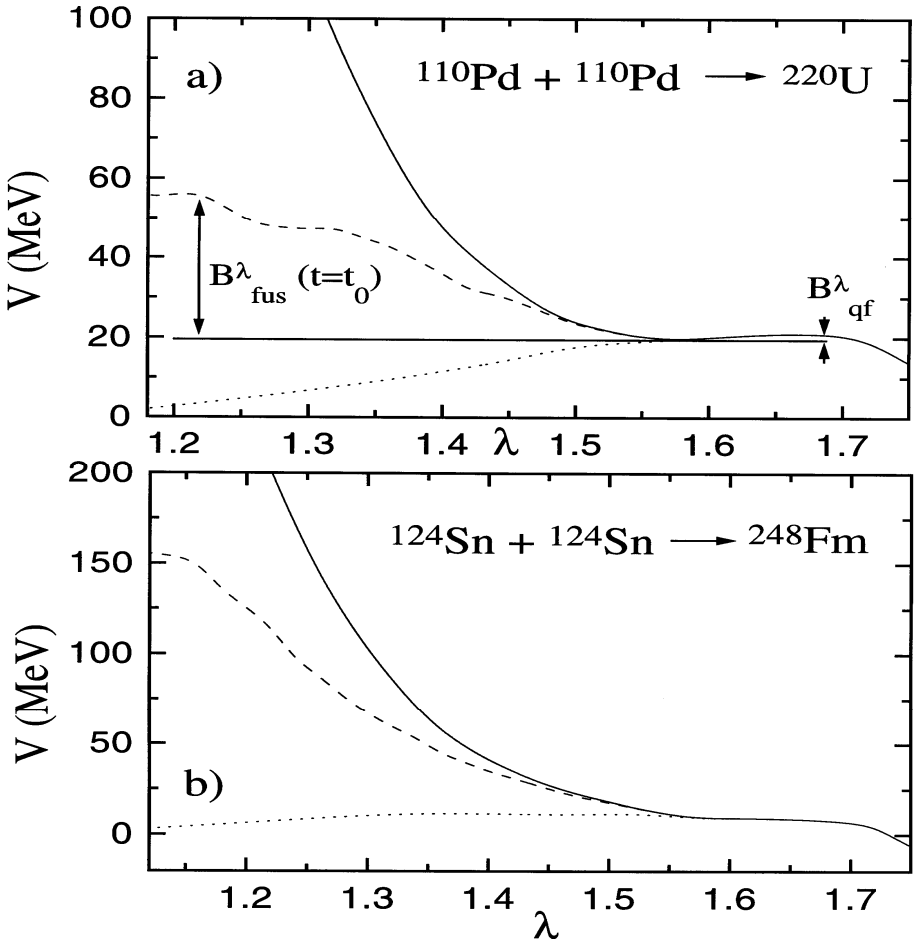

Figure 6-2: a) Time-dependent dynamical potential $V(\lambda, t)$ as a function of elongation λ for the system $^{110}Pd + ^{110}Pd$. The initial diabatic potential $V(\lambda, t = 0) = V_{diab}(\lambda)$ and the adiabatic potential $V_{adiab}(\lambda)$ are shown by solid and dotted curves, respectively. The diabatic potential $V(\lambda, t = t_0)$ at the lifetime t_0 of the DNS is presented by a dashed curve. The nuclei are considered spherical with the neck parameter $\varepsilon = 0.74$. The parameter $\Gamma_0^{-1} = 0.030 MeV^{-1}$ is used in the calculation of the single-particle widths. The fusion $B^{\lambda}_{fus}(t = t_0)$ and quasi-fission B^{λ}_{qf} barriers in λ are indicated. These barriers are measured with respect to the minimum of the potential. b) The same as in a) but for the system $^{124}Sn + ^{124}Sn$.

due to the dependence of the relaxation time of the diabatic potential on the elongation λ as shown in Fig. 6-3 for the ^{110}Pd+^{110}Pd reaction. The decrease of $< \Gamma >$ in time causes a slower transition of the diabatic potential to the adiabatic potential when this potential approaches the asymptotic adiabatic limit. In the calculations, we use two extreme values of the parameter Γ_0^{-1} because we consider how fast the transition of the diabatic to the adiabatic potential occurs. The structures in the vanishing diabatic potential (Fig. 6-2a) are caused by the structures in $< \Gamma >$ as a function of λ (Fig.6-3) which disappear in time more rapidly than the structures of the diabatic potential. Fig. 6-4a shows the dependence of B_{fus}^{λ} on time for the reactions ^{110}Pd+^{110}Pd (η=0) and ^{56}Cr+^{164}Er (η=0.5) which produce the same compound nucleus ^{220}U. The inner fusion barrier in λ for the asymmetric DNS is pronounced smaller than the one for the symmetric DNS and decreases slower in time. The smaller values of B_{fus}^{λ} for the asymmetric DNS can be explained by the initial diabatic hindrance for the motion to smaller values of λ which is smaller than the hindrance in the symmetric case (Fig. 3-10) [35]. The lifetime t_0 of the DNS formed in both reactions is about $8 \cdot 10^{-21}$s and the values of B_{fus}^{λ} at this time are larger than the corresponding fusion barriers B_{fus}^{η} in η (see Fig. 6-4b and Table 6-1). So, the fusion probability P_{fus}^{λ} in λ is smaller than P_{fus}^{η} in η (Table 6-2). This is also demonstrated in Tables 6-1 and 6-2 for the reactions ^{123}Sn+^{123}Sn, ^{110}Pd+^{136}Xe, ^{86}Kr+^{160}Gd and ^{76}Ge+^{170}Er which lead to the same compound nucleus ^{246}Fm. The calculated values of P_{fus}^{η} are in agreement with fusion probabilities extracted from the experimental data [118]. The fusion barrier along mass asymmetry does not depend on time because the diabatic potential energy at the touching configurations with different η is very close to the adiabatic potential energy. From Tables 6-1 and 6-2 one can see that the fusion probability P_{fus}^{λ} increases with increasing mass asymmetry in the entrance channel. It follows from our analysis that in the λ-channel as well as in the η-channel the complete fusion in symmetric reactions yields smaller cross sections in comparison with asymmetric combinations.

Table 6-1: Quasi-fission and inner fusion barriers in η and λ calculated within the TCSM for various symmetric and asymmetric reactions. The inner fusion barriers in λ are given for the lifetimes t_0 of the DNS formed in these reactions. The notations 1) and 2) mean that the values of $B^{\lambda}_{fus}(t_0)$ are calculated with $\Gamma_0^{-1} = 0.030\ MeV^{-1}$ and $0.061\ MeV^{-1}$, respectively.

Reactions	B^{λ}_{qf} $[MeV]$	B^{η}_{fus} $[MeV]$	t_0 $[10^{-21}s]$	$^{1)}B^{\lambda}_{fus}(t_0)$ $[MeV]$	$^{2)}B^{\lambda}_{fus}(t_0)$ $[MeV]$
$^{90}Zr + ^{90}Zr \rightarrow ^{180}Hg$	2.9	6	20	10	4
$^{100}Mo + ^{100}Mo \rightarrow ^{100}Po$	2.2	8	15	12	5
$^{110}Pd + ^{110}Pd \rightarrow ^{220}U$	1.3	12	8	36	14
$^{56}Cr + ^{164}Er \rightarrow ^{246}Fm$	2.6	2	8	14	4
$^{76}Ge + ^{170}Er \rightarrow ^{246}Fm$	0.4	10	5	53	27
$^{86}Kr + ^{160}Gd \rightarrow ^{246}Fm$	0.2	12	4	65	39
$^{110}Pd + ^{136}Xe \rightarrow ^{246}Fm$	0.1	15	3	91	54
$^{123}Sn + ^{123}Sn \rightarrow ^{246}Fm$	0.1	16	3	112	67
$^{136}Xe + ^{136}Xe \rightarrow ^{272}Hs$	0	22	2	237	154

Table 6-2: Fusion probabilities $P^{\lambda,\eta}_{fus}$ in the $\lambda-$ and $\eta-$ channels calculated for the reactions presented in the Table 6-1 are compared with known experimental values $P^{\exp}_{fus}$[34, 42, 78, 118].
The notations 1) and 2) are the same as in Table 6-1.

Reactions	$^{1)}P^{\lambda}_{fus}$	$^{2)}P^{\lambda}_{fus}$	P^{η}_{fus}	$P^{\exp.}_{fus}$
$^{90}Zr + ^{90}Zr \rightarrow ^{180}Hg$	$2{\cdot}10^{-4}$	$2{\cdot}10^{-2}$	$2{\cdot}10^{-1}$	$\sim 10^{-1}$
$^{100}Mo + ^{100}Mo \rightarrow ^{200}Po$	$9{\cdot}10^{-6}$	$3{\cdot}10^{-3}$	$2{\cdot}10^{-2}$	$5{\cdot}10^{-2}$
$^{110}Pd + ^{110}Pd \rightarrow ^{220}U$	$7{\cdot}10^{-15}$	$4{\cdot}10^{-7}$	$3{\cdot}10^{-4}$	$\sim 10^{-4}$
$^{56}Cr + ^{164}Er \rightarrow ^{220}U$	$1{\cdot}10^{-6}$	$2{\cdot}10^{-3}$	$6{\cdot}10^{-1}$	
$^{76}Ge + ^{170}Er \rightarrow ^{246}Fm$	$9{\cdot}10^{-22}$	$3{\cdot}10^{-12}$	$6{\cdot}10^{-4}$	$8{\cdot}10^{-4}$
$^{86}Kr + ^{160}Gd \rightarrow ^{246}Fm$	$4{\cdot}10^{-26}$	$2{\cdot}10^{-16}$	$7{\cdot}10^{-5}$	$5{\cdot}10^{-5}$

As shown in Figs. 6-2a and 6-2b, the value of $B^{\lambda}_{fus}(t_0)$ for the reaction ^{124}Sn+^{124}Sn is larger than the value for ^{110}Pd+^{110}Pd. The increasing mass number A of the system generally causes an increase of the repulsive character of the initial diabatic potential [35] and decreases the value of the quasifission barrier which mainly determines the DNS lifetime t_0. The same behaviour of the fusion probability P^{λ}_{fus} is obtained for the symmetric reactions ^{90}Zr + ^{90}Zr, ^{100}Mo + ^{100}Mo, ^{110}Pd + ^{110}Pd, ^{123,124}Sn + ^{123,124}Sn and ^{136}Xe + ^{136}Xe as well (Table 6-2). Despite of the strong decrease of B^{λ}_{fus} with the change of the parameter Γ_0 from the maximal to the minimal value, the fusion probabilities obtained in the λ–channel remain to be much smaller than the fusion probabilities obtained in the η–channel which are similar to the experimental values [78, 118] (see Table 6-2). In the heavier system the difference between the fusion barriers and probabilities in both channels is larger and the λ–channel is practically closed. This means a dominance of the fusion in the mass asymmetry degree of freedom which is the fundamental assumption in the DNS concept .

The time–dependent transition between diabatic and adiabatic potentials is a slower process than the quasi-fission one and the system has not enough time for destroying "memory" on the diabatic (structural) forbiddenness that is in agreement with conclusions in Ref. [36]. As the result, a large hindrance for the motion to smaller elongations λ of the DNS is obtained. The comparison of the calculated energy thresholds for the complete fusion in the λ– and η–channels shows that the DNS favorably evolves to the compound nucleus in mass asymmetry.

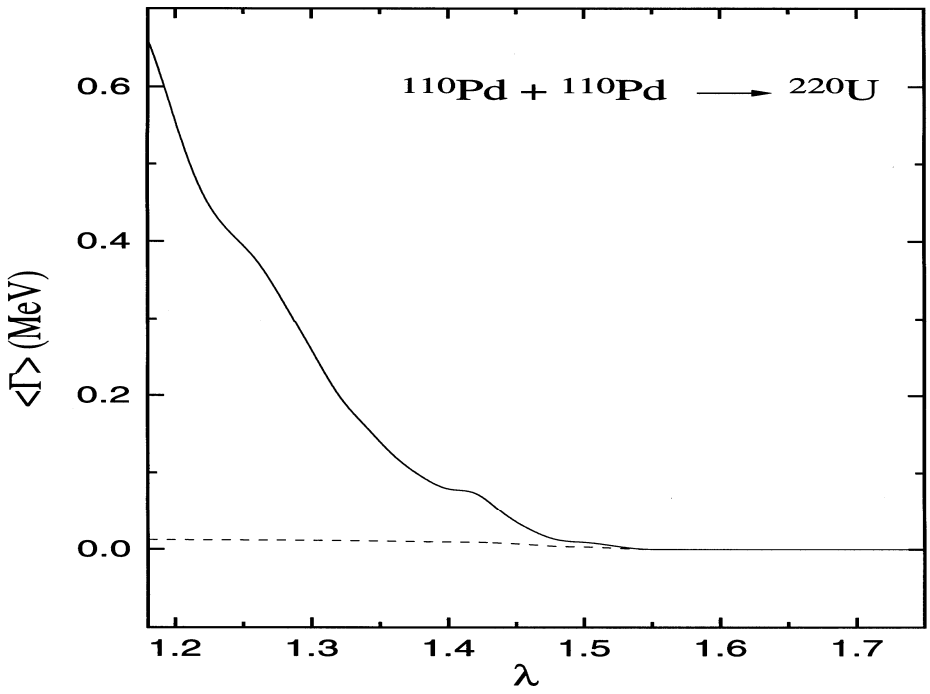

Figure 6-3: Time-dependent average width $< \Gamma(\lambda, t) >$ as a function of elongation λ for the system $^{110}Pd + ^{110}Pd$. The dependences $< \Gamma(\lambda, t = 0) >$ and $< \Gamma(\lambda, t = t_0) >$ are shown by solid and dashed curves, respectively.

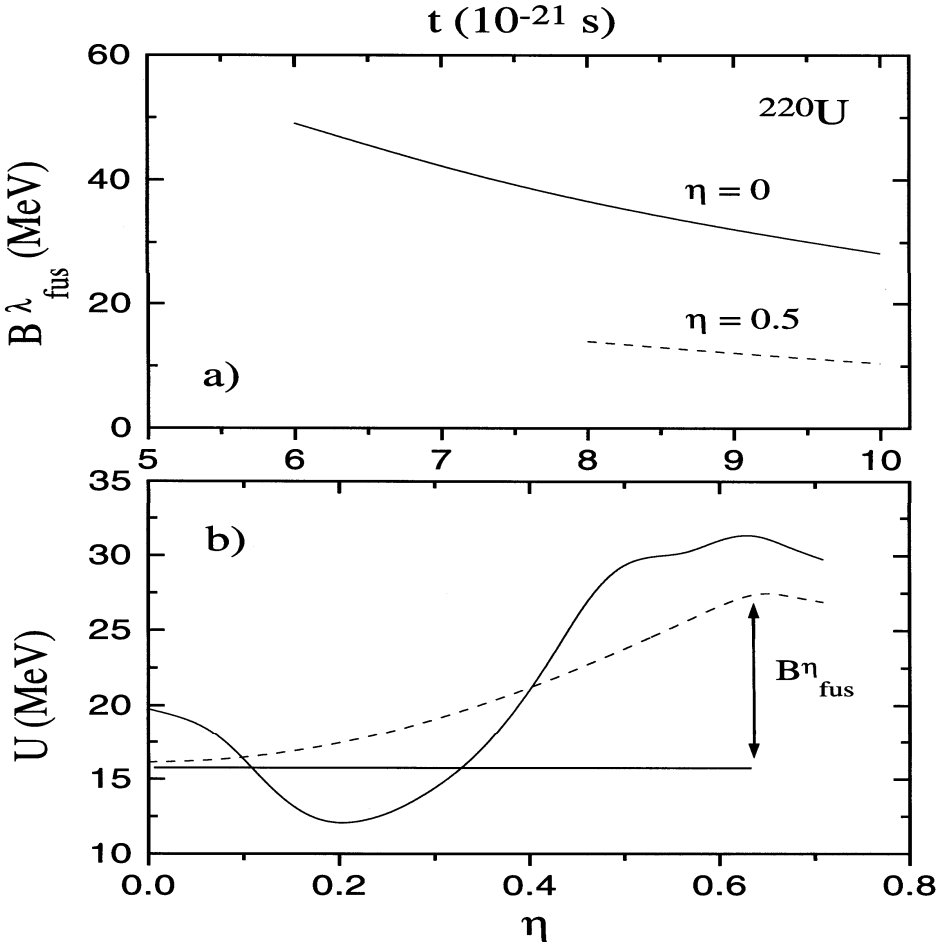

Figure 6-4: a) Inner fusion barriers $B^{\lambda}_{fus}(t)$ in λ as a function of time for the systems $^{110}Pd + ^{110}Pd$ (solid curve) and $^{56}Cr + ^{164}Er$ (dashed curve) which produce the same compound nucleus ^{220}U. The nuclei are considered spherical with $\varepsilon = 0.74$. The parameter $\Gamma_0^{-1} = 0.030 MeV^{-1}$ is used in the calculation of single-particle widths. For times smaller than $6 \times 10^{-21} s$ and $8 \times 10^{-21} s$ for $\eta = 0$ and 0.5, respectively, the potential $V(\lambda, t)$ is only repulsive and has no barrier (see Fig. 6-2). b) Calculated adiabatic potential energy of the DNS in the touching configuration of the nuclei as a function of mass asymmetry η for reactions leading to the same compound nucleus ^{220}U. The potential is calculated within the adiabatic TCSM with (solid curve) and without (dashed curve) shell corrections. The fusion barrier B^{η}_{fus} in η for the system $^{110}Pd + ^{110}Pd$ is shown.

Chapter 7

In the quasi-fission process, the large mass rearrangements between the interacting heavy ions occur at a short time scale [11, 112]. One of the experimental signatures [113] of this process is the large width of mass distributions, incompatible with compound nucleus fission. Conceptually, the quasi-fission bridges the gap [106] between the deep-inelastic collisions, where the reaction partners get into sufficiently close contact to exchange many particles practically without altering their average mass and charge [33], and the complete fusion process, where the reaction partners completely lose their identity by transformation into a compound nucleus [113]. All these types of reaction are organically connected and are derived from the evolution of a dinuclear system (DNS) [18, 34] which is formed in the entrance channel during the capture stage of reaction, after the dissipation of the collision kinetic energy. The decay of the DNS when it evolves in the mass asymmetry coordinate predestines the charge and mass distributions of the reaction products. The competition between the complete fusion and the quasi-fission process occurs in reactions with massive nuclei at low bombarding energies (< 15 MeV/u) [34].

In this chapter, the quasi-fission process is described as the evolution of the DNS in the Z (A) coordinate by nucleons transfer between nuclei taking into account the DNS decay in the internuclear distance R (or elongation λ). Here, Z (A) denotes the charge (mass) number of the light fragment of the DNS. For the sake of simplicity, we will use the variables $Z(A)$ instead of the charge (mass) asymmetry η (η_Z). Since the isotopic composition of the nuclei forming the DNS

is chosen with the condition of the N/Z-equilibrium in the system, mass and charge evolutions are described analogously. A diffusion process leads to the exchange of nucleons between the two touching fragments, thus generating a time-dependent distribution in the $Z(A)$ variables of the DNS. This process can be described by a master-equation [33, 44, 73, 119] for the probability $P_Z(t)$ of finding the system at the time t in the configuration with the charge number of the light fragment Z. The asymmetric DNS evolves to a compound nucleus or to a symmetric DNS. The melting of the DNS nuclei in variable R is strongly hindered [35, 36, 42, 66]. The decay in R affects the motion of the system in Z. In order to take the effect of the DNS decay into consideration, we can rewrite the known master-equation for $P_Z(t)$ [33, 44, 73, 119] as follows

$$\frac{\partial P_Z(t)}{\partial t} = \Delta^{(-)}_{(Z+1)} P_{(Z+1)}(t) + \Delta^{(+)}_{(Z-1)} P_{(Z-1)}(t) - (\Delta^{(+)}_Z + \Delta^{(-)}_Z + \Lambda^{qf}_Z) P_Z(t), \tag{7.1}$$

where the microscopically calculated transport coefficients $\Delta^{(\pm)}_Z$ are given by the expression (4.3) and Λ^{qf}_Z is the rate of decay probability in R. In the right side of Eq. (7.1), only the transitions $Z \rightleftharpoons Z+1$ and $Z \rightleftharpoons Z-1$ are taken into account in the spirit of the independent-particle model.

For decay, the DNS should overcome the potential barrier B_{qf}, which coincides with the depth of the pocket in the double-folding nucleus-nucleus potential as a function of R. The bottom of this pocket corresponds to the distance $R_m = R_1 + R_2 + 0.5fm$ (R_i is the radius of the nuclei). The values of the quasifission barriers B_{qf} which depend on Z are mainly responsible for the lifetime t_0 of the DNS. During this time, the DNS evolves in the variables Z. The decay of the DNS in R is treated using the one-dimensional Kramers rate of probability Λ^{qf}_Z (6.9). In our calculations, the values $\hbar\omega^{B_{qf}} = 1.0\ MeV$ and $\hbar\omega = 2.0\ MeV$ are used for the reactions considered.

The measurable quasi-fission charge (mass) yield is expressed through the formation probability $P_Z(t)$ of the DNS configuration with charge (mass) asymmetry Z and the decay probability in R described by the Kramers rate Λ^{qf}_Z

$$Y_Z(t_0) = \Lambda^{qf}_Z \int_0^{t_0} P_Z(t) dt. \tag{7.2}$$

The value of t_0 is determined in the solution of the Eq. (7.1). The decay of the DNS with $Z > Z_{BG}$ (Z_{BG} corresponds to the barrier of the DNS potential energy as a function of the charge asymmetry) mainly contributes to the quasi-fission yield, and the lifetime t_0 is calculated from the condition $\sum\limits_{Z>Z_{BG}} \Lambda_Z^{qf} \int\limits_0^{t_0} P_Z(t)dt \approx 1$. It is assumed that the DNS with $Z < Z_{BG}$ evolves to a compound nucleus with a great probability. Only for large angular momenta, which are not considered here, there is a certain decay probability of the DNS with $2 < Z < Z_{BG}$ [120]. The factors $P_Z(t)$ and Λ_Z^{qf} are considered separately because the characteristic time for proton transfer from one nucleus to the other is much shorter than the decay time of the DNS. Since we consider reactions with heavy nuclei which occur above and near the Coulomb barrier, the partial waves with angular momentum less than $40\hbar$ contribute to the quasi-fission, and the values of B_{qf} weakly depend on the angular momentum due to the large moment of inertia of the DNS. The earlier calculations [33, 69, 73] of charge (mass) distributions in deep-inelastic collisions were performed without taking into account the influence of the decay probability Λ_Z^{qf} in (7.1) and assuming $Y_Z(t_0) \approx P_Z(t_0)$.

7.1 Results and discussion

Figs. 7-1 to 7-3 show the quasi-fission charge and mass distributions for the hot fusion reactions with the projectile ^{48}Ca on the targets ^{208}Pb, ^{238}U and ^{244}Pu, which lead to the synthesis of the elements ^{256}No, ^{286}112 and ^{292}114, respectively. These reactions were carried out at the FLNR JINR [11]. The bombarding energy of ^{48}Ca ions was 233 MeV, which corresponds to an excitation energy of the compound nuclei of $E^* \approx 33$ MeV. In these Figures, we show the part of the quasifission charge (mass) distributions corresponding to the light fragments. In Figs. 7-1 and 7-2, the distributions reveal large widths and one can observe a notable drift in mass and in charge away from the initial mass (charge) asymmetry. The masses of the products are substantially different from the target–projectile masses. One can see that the symmetric fragments can be formed with quite a large cross section in the quasi-fission process. The main peak of the charge and mass distributions is around the initial configuration of the DNS. The form of mass (charge) distribution changes drastically as one goes from the reaction ^{48}Ca+^{208}Pb$\rightarrow^{256}$No (Fig. 7-3) to the reactions ^{48}Ca+^{238}U,^{244}Pu$\rightarrow^{286}$112,^{292}114 (Figs. 7-1 and

7-2). In the reactions leading to the nuclei $^{286}112$ and $^{292}114$, the decay of the more symmetric DNS configurations becomes more pronounced. The motion of the initial DNS to more asymmetric configurations (mass asymmetry channel of fusion) in the reaction ^{48}Ca+^{208}Pb is more favourable than in the reactions ^{48}Ca+^{238}U and ^{48}Ca+^{244}Pu, where the distributions show similar features for $Z < 20$ and $A < 48$. So, the fusion probability in the mass asymmetry coordinate is significantly larger in the ^{48}Ca+^{208}Pb reaction than in the reactions ^{48}Ca+^{238}U and ^{48}Ca+^{244}Pu.

The structures in the distribution of quasi-fission products reflect the influence of the shell effects on the nucleon-exchange process, and the maxima in the charge (mass) distributions are related to the decay of the DNS consisting of the magic nuclei. In the present microscopical approach, the shell effects mean the influence of peculiarities of the single particle spectra near the Fermi surfaces of the DNS nuclei on the nucleon-exchange process. The absence of local peaks for some magic nuclei is explained by the shell structure of the conjugated nucleus and the influence of the neutron subsystem.

In the reactions ^{48}Ca+^{238}U and ^{48}Ca+^{244}Pu, the maximum yield of the quasi-fission fragments occurs, for $Z > 20$ and $A > 48$, around the nuclei ^{78}Zn and ^{32}Ge, respectively, for the light fragment with the corresponding heavy fragment ^{208}Pb. The height of this peak is 6 (3) times larger than the height of the peak in the symmetric mass region in the reaction ^{48}Ca+^{238}U (^{48}Ca+^{244}Pu). One can see that the results are in good agreement with the available experimental data, which were extracted from Ref.[11]. This experimental mass distribution includes the quasi-fission events in all angles measured. It should be noted that near the initial DNS configuration, the quasi-fission events overlapping with the products of other reaction channels (elastic and quasi-elastic peaks) were not taken into account in the experimental data because they cannot be clearly distinguish. In our calculations we assume that the DNS is formed in all reactions considered. In general, the formation of the DNS also depends on the capture probability, which is determined by the dynamical aspects of the approach stage of the reaction and by the depth of the pocket in the nucleus-nucleus interaction potential in the entrance channel [38].

The excitation energy of the initial DNS in all reactions considered is E^*=10 MeV and the lifetime t_0 of the DNS is about $(3-4)\times 10^{-20}$s. The initial excitation energy E^* can be

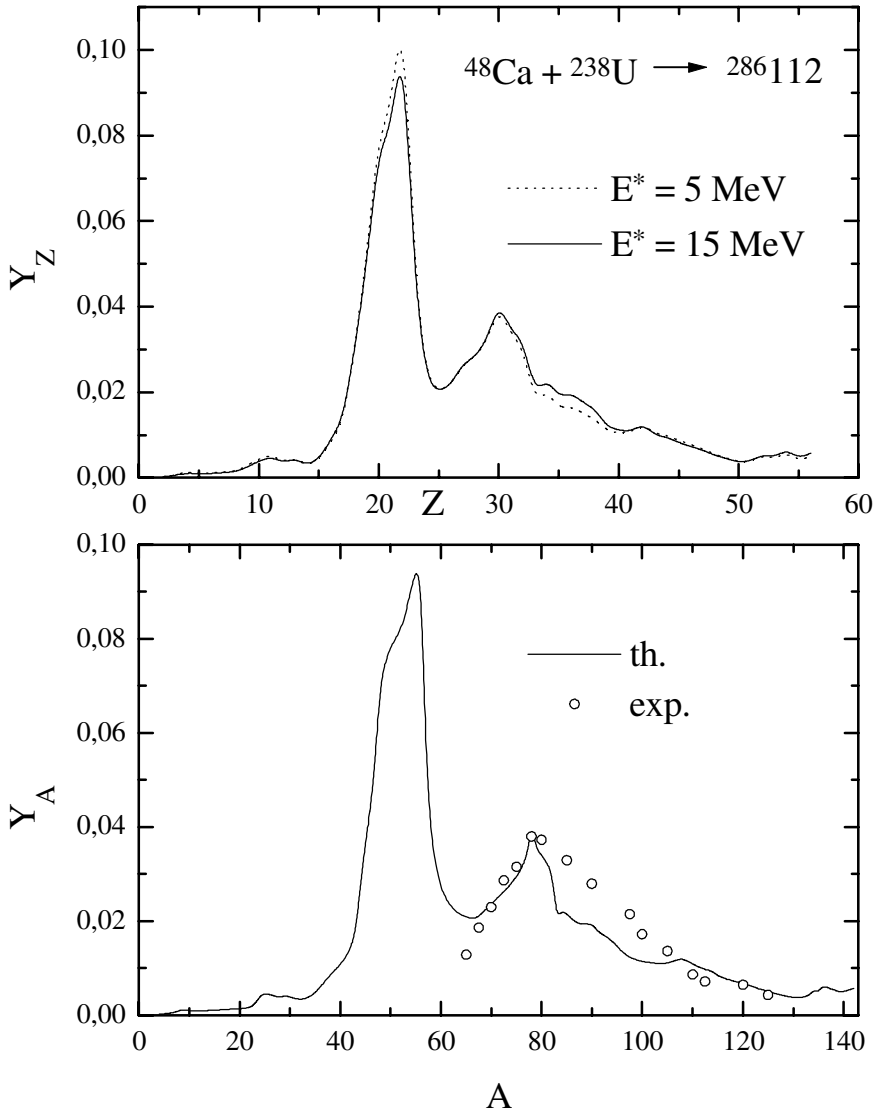

Figure 7-1: Charge (upper part) and mass (lower part) distributions of the quasi-fission products as a function of the charge Z and mass A numbers of the light fragments, respectively, for the hot fusion reaction $^{48}Ca +^{238} U \rightarrow^{286}$ 112. The charge distribution is calculated for two values of the excitation energy of the initial DNS: $E^* = 5MeV$ (dotted line) and $E^* = 15MeV$ (solid line). The mass distribution is compared with the experimental data [11] (open points) for $E^* = 10MeV$.

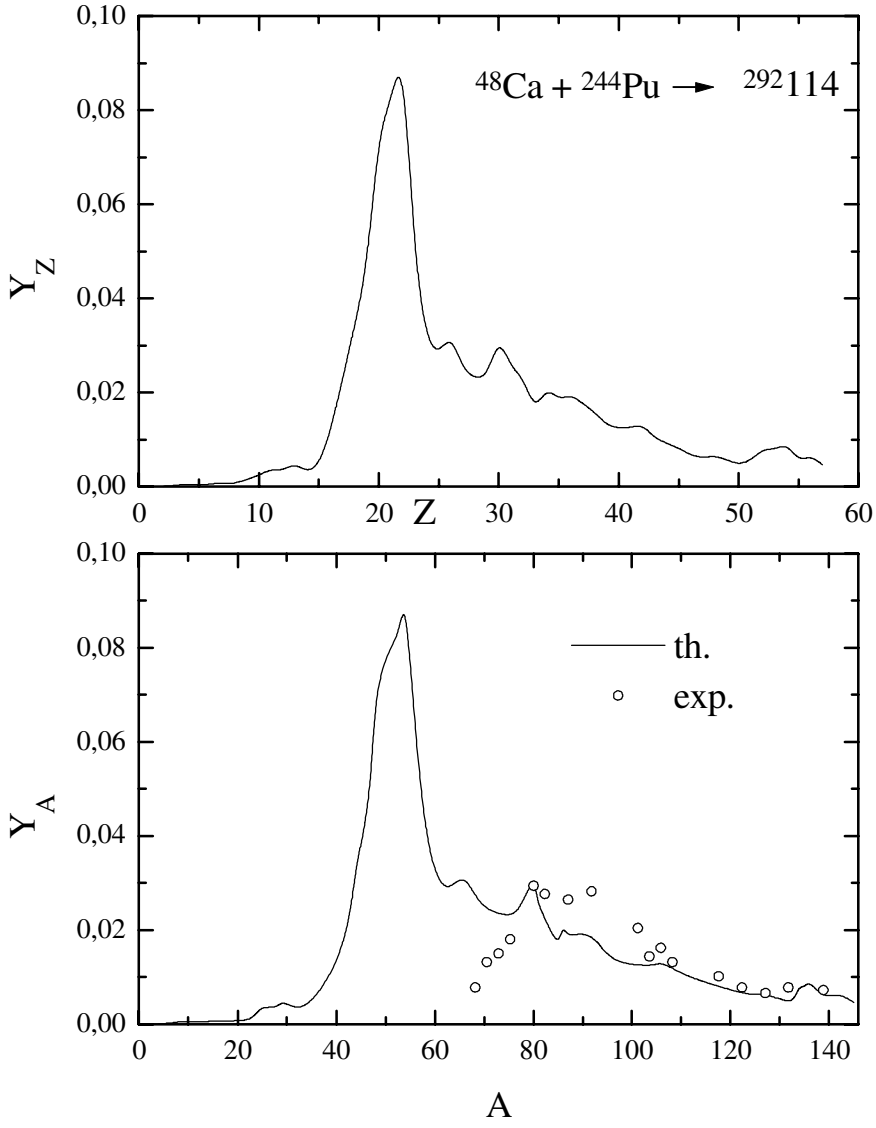

Figure 7-2: The same as in Fig. 7-1 for the hot fusion reaction $^{48}Ca +^{244} Pu \rightarrow^{292}$ 114. The experimental mass distribution (open points) is taken from the Ref. [11]. The excitation energy of the initial DNS is $E^* = 10\ MeV$ (upper and lower parts).

estimated from the difference between the bombarding energy $E_{c.m.}$ in the system of the center of mass and the value of the nucleus-nucleus potential for R corresponding to the bottom of the pocket for the initial configuration of the DNS. The charge (mass) quasi-fission distributions depend slightly on the excitation energy E^* of the initial DNS (Fig. 7-1). This is due to the weak dependence of the transport coefficients $\Delta_Z^{(\pm)}$ on the temperature [33]. With an increasing temperature of the system, the influence of the shell effects on the process of nucleon transfer decreases more slowly than the exponential decrease of the shell correction in the potential energy [33]. It was experimentally found [113] in the quasifission reactions ^{238}U+^{16}O, ^{26}Mg, ^{27}Al, ^{32}S, ^{35}Cl, ^{40,48}Ca and ^{nat}Zn at several bombarding energies, that the mass asymmetry motion is dominated by the one-body dissipation which is independent of temperature. The observed relaxation times for the mass asymmetry mode of all the systems considered were in agreement with the wall dissipation picture [113].

Fig. 7-3 shows the quasi-fission charge and mass distributions for the cold fusion reactions with the projectiles ^{50}Ti, ^{64}Ni and ^{76}Ge on the target ^{208}Pb, which lead to the synthesis of the elements ^{258}104, ^{272}110 and ^{284}114, respectively, with an excitation energy about 11-16 MeV [7, 8]. The ratio between the drifts of mass and charge toward symmetric configurations of the DNS and toward more asymmetric ones becomes considerably larger with the increase of the charge number of the superheavy element. Due to this fact, the complete fusion probability in the mass asymmetry degree of freedom decreases from the nucleus ^{258}104 to ^{272}110. For the reaction ^{76}Ge+^{208}Pb$\rightarrow$^{284}114, we found that the quasi-fission products are practically associated with fragmentations near the initial DNS due to small values of quasi-fission barriers B_{qf}. Comparing Fig. 7-3 with Fig.7-2, we see that the mass and charge yields of the quasi-fission products for nearly symmetric configurations of the DNS are larger for the hot fusion reaction ^{48}Ca+^{244}Pu than for the cold fusion reaction ^{76}Ge+^{208}Pb. The quasi-fission barrier B_{qf} of the initial DNS becomes larger with decreasing Z, and the nucleon transfer plays a larger role in the evolution of this DNS than the decay process. This is consistent with the conclusion that the hot fusion reaction ^{48}Ca+^{244}Pu$\rightarrow$^{292}114 is preferable for the synthesis of the element 114, although the survival probability of the compound nucleus decreases with increasing excitation energy [20, 22]. In the cold fusion reactions, the quasi-fission is an important factor decreasing the complete fusion cross sections with increasing atomic number of the superheavy element. Producing the

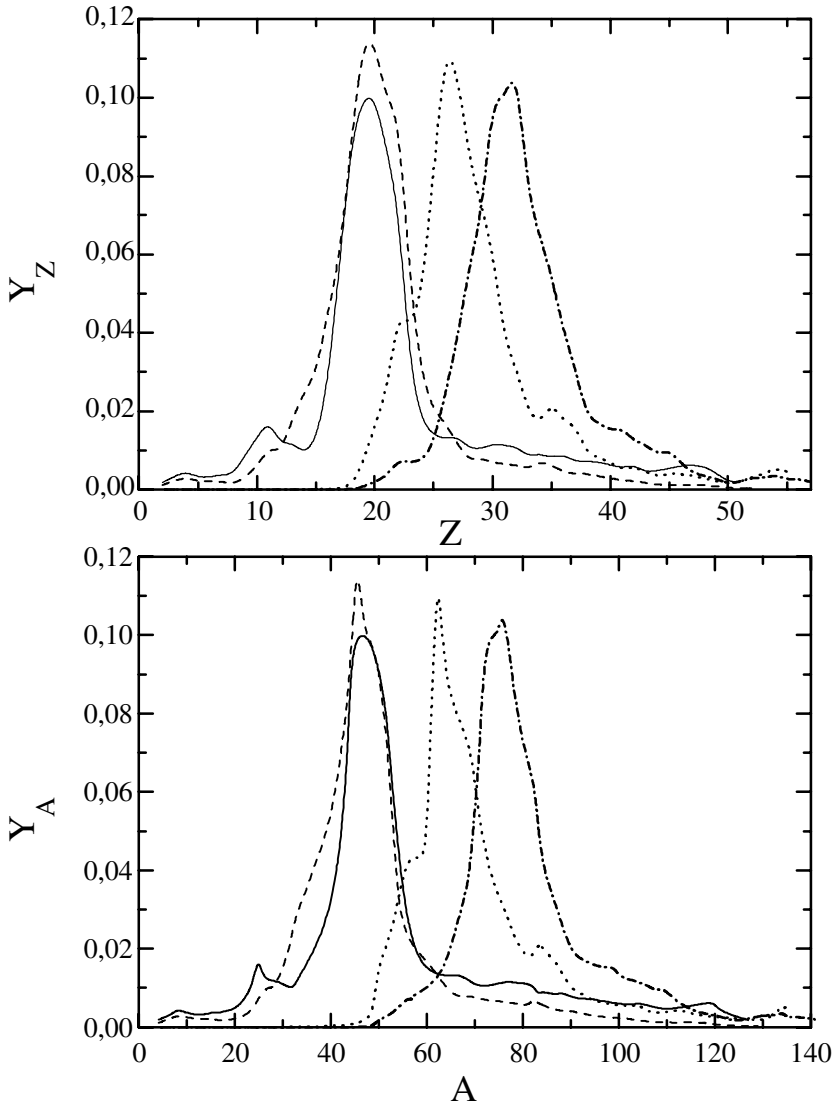

Figure 7-3: The same as in Fig. 7-2 for the fusion reaction $^{48}Ca +^{208} Pb \rightarrow^{256}$ 102 (solid line) and for the cold fusion reactions $^{50}Ti +^{208} Pb \rightarrow^{258}$ 104 (dashed line), $^{64}Ni +^{208} Pb \rightarrow^{272}$ 110 (dotted line) and $^{76}Ge +^{208} Pb \rightarrow^{284}$ 114 (dashed-dotted line).

elements from Z=104 to Z=112 in the cold fusion reactions, the experimentalists observed a rapid fall-off of the evaporation residue cross sections (about four orders of magnitude) with increasing charge number of the compound nucleus [7, 8]. In the model of fusion based on the DNS-concept, the fusion cross sections and excitation functions for the cold fusion reactions leading to the formation of superheavy elements are obtained in good agreement with the experimental data [20].

The structure of the mass (charge) distribution of the quasi-fission products well corresponds to the peculiarities of the driving potential (the DNS potential energy as a function of mass (charge) asymmetry) shown in chapter 4. In order to illustrate the connection between the quasi-fission product yield and the driving potential, Fig. 7-4 shows the quasi-fission charge distribution for the reactions ^{110}Pd+^{136}Xe (η=0.1),^{86}Kr+^{160}Gd (η=0.3) and ^{76}Ge+^{170}Er (η=0.4), which lead to the formation of the same compound nucleus ^{246}Fm. The distributions reveal large widths and one can observe a notable drift in charge (mass) away from the initial charge (mass) asymmetry of the interacting nuclei. The product masses are substantially different from the target–projectile masses. It is seen that the symmetric fragments can be formed in the quasi-fission process if the entrance DNS is an asymmetric one. We can observe that the main peak of the distributions is around the initial configuration of the DNS. Comparing Fig. 7-4 with Fig. 4-7a), we observe that there is a correlation between the peaks of the quasi-fission distribution and the minima of the driving potential. The inner fusion barrier B_η increases with decreasing mass asymmetry η (Figs. 4-1 to 4-7b)), while the quasi-fission barrier B_{qf} becomes smaller because the Coulomb repulsion increases with decreasing η and leads to very shallow pockets in the nucleus-nucleus potential for nearly symmetric configurations. Therefore, the decay of the initial DNS dominates in symmetric or nearly symmetric collisions. The experimental fusion probability becomes larger with the increase of the mass asymmetry η in the entrance channel [118]. This experimental evidence for a hindrance of fusion has been mainly concluded from the impossibility to produce fermium evaporation residues with nearly symmetric projectile-target combinations [118].

The main conclusions are: 1) The quasi-fission products of fusion reactions are correctly described within the DNS model: diffusion in charge (mass) asymmetry and in relative distance (the DNS decay) coordinates contributes to the yield of quasi-fission products. 2) The quasi-

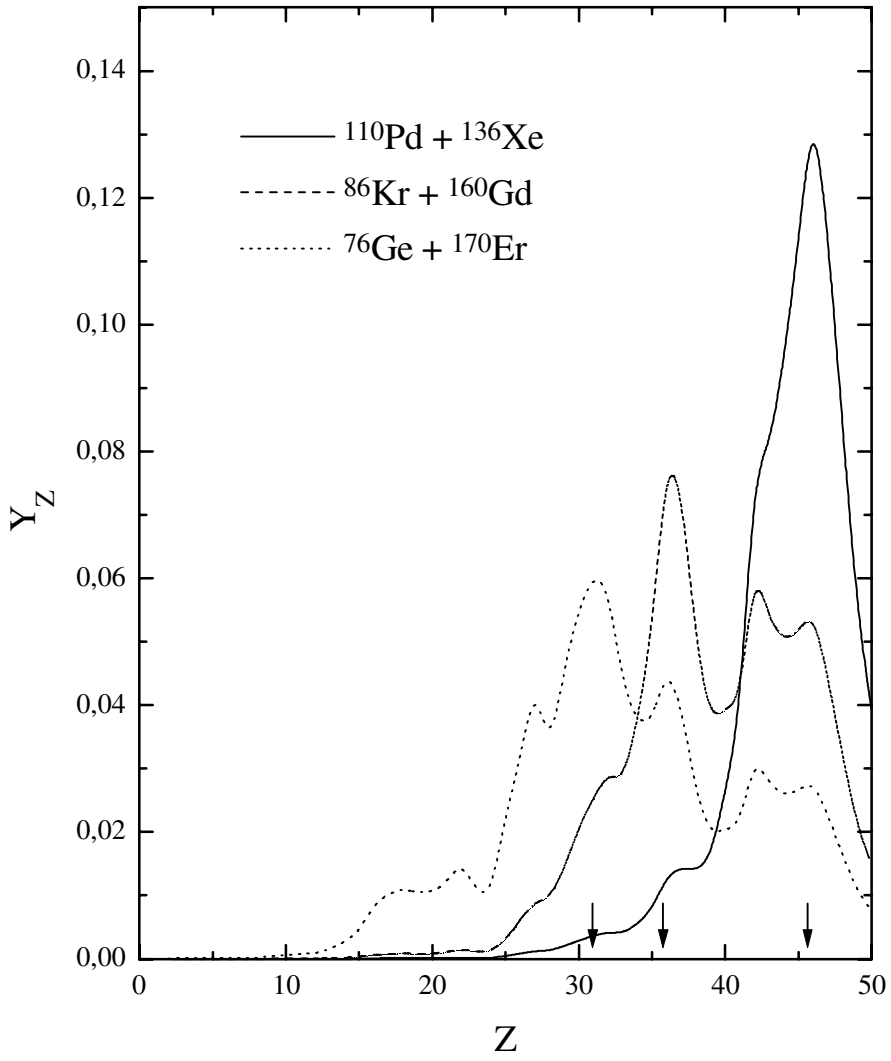

Figure 7-4: Charge distributions of the quasi-fission products for the reactions $^{110}Pd + ^{136}Xe$ ($\eta = 0.1$, solid line), $^{86}Kr + ^{160}Gd$ ($\eta = 0.3$, dashed line) and $^{76}Ge + ^{170}Er$ ($\eta = 0.4$, dotted line) which lead to the same compound nucleus ^{246}Fm. The arrows denote the initial DNS. The excitation energy of the initial DNS formed in these reactions is $E^* = 20$ MeV.

fission process is an important factor which reduces the probability of complete fusion of heavy nuclei. Since the quasi-fission dominates in the cold and hot fusion reactions, the comparison of the theoretical and experimental data is a critical test for the existing fusion models.

Chapter 8

8.1 Summary

Depending on the main degree of freedom used for the description of fusion, two different types of models for fusion can be distinguished. The first type of models assumes a melting of nuclei along the internuclear distance (or elongation λ) [15, 16]. The second type is the dinuclear system model [17, 34]. Models describing the fusion process as an internuclear melting of nuclei often use adiabatic potential energy surfaces. These potentials are calculated with the macroscopic-microscopic method of the Strutinsky formalism. Without regarding the competition between complete fusion and quasi-fission, the first type of models overestimates the fusion cross section of heavy nuclei [18]. However, the dinuclear system model describes the experimental fusion data quite well. In this model, the fusion process is considered as the evolution of a dinuclear system caused by the transfer of nucleons from the light nucleus to the heavy one. The dinuclear system consists of two touching nuclei, which conserve their individuality, and evolves in the mass asymmetry η to a compound nucleus or decays in the elongation λ. The model assumes that the motion of the dinuclear system to smaller elongations λ is strongly hindered. This is phenomenologically described with a double folding potential in frozen density approximation which shows a minimum near the touching configuration of the nuclei.

We have investigated the fusion and quasi-fission process of heavy nuclei using the two-center shell model (TCSM). The diabatic potential energy surfaces as a function of the elongation λ,

the neck coordinate ε and of the mass asymmetry η were calculated for the entrance phase of collisions between spherical heavy nuclei. The effect of the deformation of the nuclei and of the temperature on the diabatic potential energy as a function of the elongation λ was analysed. In a diabatic description the nucleons do not occupy the lowest free single-particle levels as in the adiabatic case, but remain in the diabatic levels during the collective motion of the nuclear system. As a result, the diabatic potential energy surface is raised with respect to the adiabatic potential energy surface and new potential barriers for collective variables may appear. From the study of the diabatic single-particle spectrum, we obtained that the diabatic effects for the motion of the system in λ and in ε are already important for relatively small excitation energies of 6–14 MeV. Diabatic TCSM levels do not show avoided level crossings. Avoided level crossings can be removed from the adiabatic TCSM by eliminating the symmetry-violating parts from the adiabatic Hamiltonian of the TCSM. Since the diabatic effects are small near the touching of the nuclei, they are not important for the potential of the dinuclear system as a function of the mass asymmetry η at the touching configuration of the nuclei. The isotopic dependence of the potential as a function of the mass asymmetry coordinate η at the touching configuration of the nuclei calculated within the adiabatic TCSM using the Strutinsky method was studied for various heavy dinuclear systems. Moreover, this potential was compared with the potentials calculated with a phenomenological method and with another alternative microscopical method. The phenomenological method uses the binding energy of the nuclei and the nucleus-nucleus potential which includes the Coulomb and nuclear terms. The nuclear part of the nucleus-nucleus potential is calculated using a double-folding procedure. With the alternative microscopical method, the potential energy is calculated using the rate of probability of nucleon transfer between the nuclei of the dinuclear system.

Mass parameters as a function of the elongation λ, the neck coordinate ε, the mass asymmetry η and of the deformation β_i for heavy dinuclear systems were evaluated in the TCSM. Formulas for the masses are derived within the linear response theory by taking into account the fluctuation-dissipation theorem and the width of single particle states, and by other methods as Fermi's golden rule and a spectral smoothing in the mean–field cranking formula.

In order to study whether the fusion is possible in the elongation coordinate λ, we considered the transition from the diabatic potential to the adiabatic one in the motion of the system in

λ during the lifetime t_0 of the dinuclear system. The competition between two possible fusion channels was studied. The λ–channel describes the transition of two nuclei into the compound nucleus with the elongation coordinate λ for a fixed mass asymmetry η during the fusion. The second channel, named η–channel, describes the evolution of the dinuclear system to the compound nucleus as a change of the mass asymmetry η by nucleon transfer from the light nucleus to the heavy one.

The quasi-fission process of the dinuclear system was studied solving a transport master-equation for the exchange of nucleons between the parts of the dinuclear system, which also takes the decay of the dinuclear system in the elongation λ into account.

In this work, we have obtained the following results:

• The diabatic effects in the entrance phase of the reaction give rise to hindrances for the growth of the neck and for the motion to smaller relative distances.

• The diabatic potentials as a function of the elongation λ are similar to the phenomenological double folding potentials used in the dinuclear system model of fusion.

• For the asymmetric dinuclear system, the diabatic hindrance for the motion to smaller elongations λ is smaller than for the symmetric dinuclear system. Therefore, its evolution to the compound nucleus in λ is more favored.

• The potentials as a function of the mass asymmetry η at the touching configuration of the nuclei calculated within the TCSM are similar to the ones calculated using other methods.

• The isotopic dependence of the fusion barrier in η, calculated within the TCSM, agrees with the isotopic behaviour of the experimental surplus of energy $\Delta B^{\exp} = B^{\exp} - B_{Bass}$ above the Bass barrier B_{Bass}.The value of $B^{\exp}$ is defined as the value of the bombarding energy for a fusion probability 0.5.

• The adiabatic and diabatic microscopical mass parameters for the neck degree of freedom ε are much larger than the one obtained in the hydrodynamical model with the Werner-Wheeler approximation. By applying the microscopical mass parameters, we find a relatively stable neck during the time of reaction.

• The dinuclear system is stable against a melting in λ and ε. The diabatic effects and the microscopic mass parameters give a justification for the use of the dinuclear system in heavy ion collisions at low energies.

• The time-dependent transition between the diabatic and adiabatic potentials is a slower process than the quasi-fission process and the system has no time for destroying the "nuclear memory" about the diabatic (structural) forbiddeness for the motion to smaller elongations λ.

• The fusion probabilities obtained in the λ-channel are much smaller than the probabilities obtained in the η-channel of fusion, which are similar to the experimental values. The heavier the system, the greater is the difference between the fusion barriers and probabilities in both channels of fusion. The λ-channel is practically closed.

• The fusion in the mass asymmetry degree of freedom considered in the dinuclear system concept dominates the complete fusion process for heavy systems.

• Using a transport master-equation to describe the nucleon transfer between the nuclei forming a dinuclear system, which takes the decay of the dinuclear system in the elongation λ into account, the quasi-fission products of fusion reactions are correctly described and are in agreement with the experimental data.

• The quasi-fission process is an important factor which reduces the probability of complete fusion of heavy nuclei.

8.2 Outlook

The search of the fission path in the multi-dimensional space of collective variables is still an open problem. The fission process is usually considered as an adiabatic process where the relevant collective variables are the elongation, the mass asymmetry, the neck coordinate and the deformation of the fragments [94]. In addition to the potential energy, the friction and the mass tensor play an important role in the dynamics of the fissioning system. There is not yet a fission model in which it is possible to explain all experimental observables of the fission process, e.g., mass and charge distributions, total kinetic energy distribution, two-dimensional mass-total kinetic energy distribution, angular distribution of the fragments, etc. The most promising model is the Brosa model of the multi-modal fission ([121], [122]).

It will be interesting to study as a possible fission path the inverse path used by the dinuclear system model of fusion. The fission phenomenon could be treated as a two-step process: a light nucleus (α-particle) is created within the diffuse edge of the fissioning nucleus; then this

nucleus grows, gaining nucleons from its partner nucleus till the dinuclear system dissociates. Preliminary estimations show that the heights of the barriers for the asymmetric and symmetric fissions as well as the competition between asymmetric and symmetric fission channels and the properties of charge, mass, energetic distributions of the fission products are reproduced in this approach. The spontaneous fission process could be considered as a tunneling process in the mass asymmetry degree of freedom η. The role of diffusion and friction in the tunneling in η for the dinuclear system could be considered using the Lindblad axiomatic approach for open quantum systems [123, 124]. Changes in the deformation of the nuclei during the tunneling process could also be taken into account. The nuclei Fm and Cf are especially attractive for this study.

Using the structural forbiddenness concept [63], we could study the hindrances for the fragmentation process in λ and η degrees of freedom. The comparison of the calculated energy thresholds (fission barriers) for the fission in λ and η variables could provide the answer about the favorable fission path.

Appendix A

For describing nucleus-nucleus collisions, we use the TCSM [40] as a single-particle model. The Hamiltonian of the model is

$$H = -\frac{\hbar^2\nabla^2}{2m_0} + V(\rho, z) + V_{LS}(\mathbf{r}, \mathbf{p}, \mathbf{s}) + V_{L^2}(\mathbf{r}, \mathbf{l}), \tag{A.1}$$

in cylinder coordinates z, ρ and φ. The momentum-independent part of the potential may be expressed as

$$V(\rho, z) = \frac{f_0}{2} m_0 \omega^2 z'^2 (1 + cz' + dz'^2) + \frac{1}{2} m_0 \alpha^2 (1 + gz'^2)\rho^2. \tag{A.2}$$

The momentum-dependent parts are

$$V_{LS} = -\left\{ \frac{\hbar\kappa}{m_0\omega_0}, (\nabla V \times \mathbf{p}) \cdot \mathbf{s} \right\}, \tag{A.3}$$

$$V_{L^2} = -\frac{1}{2}\left\{ \frac{\hbar\kappa\mu}{m_0\omega_0^3}, \mathbf{l} \right\} + \hbar\kappa\mu\omega_0 \frac{N(N+3)}{2}\delta_{if}, \tag{A.4}$$

with the abbreviation $z' = z - z_i$. The positions of the centers are denoted by z_1 and z_2, $z_1 \leq 0 \leq z_2$. The behaviour of $V(\rho, z)$ along the z-axis can be seen from Fig. A-1, where the potential is plotted below the associated nuclear surface. To the left of z_1 and to the right of z_2 the potential (A.2) is simply that of a deformed oscillator. Between the centers, however, there are considerable deviations caused by a variable barrier and by the need of joining the

fragments continuously.

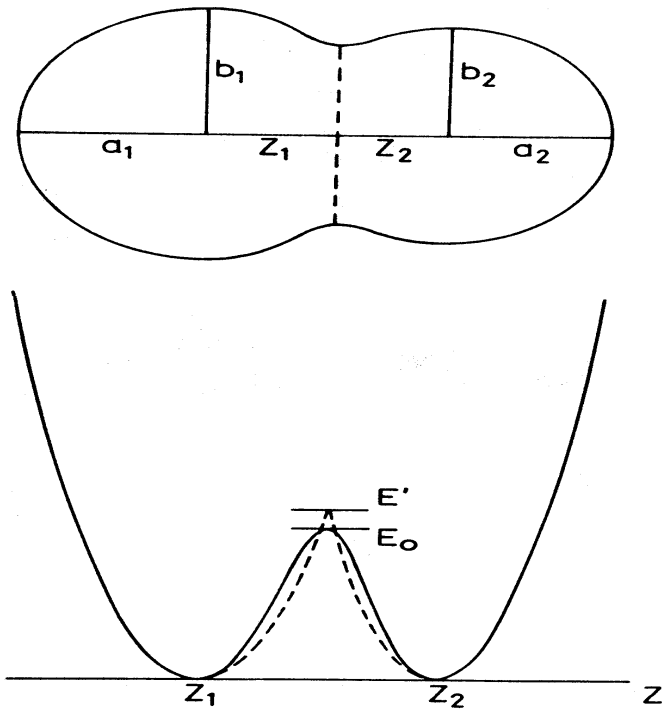

Figure A-1: The potential along the z-axis and the associated nuclear shape. The designations of the geometrical quantities have been indicated and the quantities for the definition of the parameter $\varepsilon = E_0/E'$ are shown.

The constants are listed in Table A and $\mathbf{l} = (\nabla V \times \mathbf{p})/m_0\omega_0^2$. In these formulas, $\{A, B\} = AB + BA$ denotes the anticommutator of A and B and δ_{if} is the Kronecker symbol. The quantity N should be chosen such that it approaches the usual principal quantum number of the spherical oscillator in the limiting cases of a single sphere and that of two separate fragments with a large separation.

The coefficients g, c and d are determined by requiring that the potential and its derivative with respect to z is continuous at $z = 0$.

The oscillator frequencies, ω and α, must be determined numerically from the assumption of volume-conservation inside the equipotential surface $V(\rho, z) = V_0$ with

$$V_0 = \frac{1}{2} m_0 \varpi^2 R_0^2. \tag{A.5}$$

The volume is

$$W_0 = \frac{4\pi}{3} R_0^2, \tag{A.6}$$

where

$$\begin{aligned} R_0 &= 1.2249 fm \cdot A^{1/3} \\ \hbar\varpi &= 41 MeV \cdot A^{-1/3} \end{aligned}$$

The coordinates of the centers, z_1 and z_2, are calculated with the condition that the barrier must have the same position on the z-axis as in the two-center oscillator [125]

$$E' = \frac{1}{2} m_0 \omega^2 z_0^2 = \frac{1}{2} m_0 \omega_{z_1}^2 z_1^2 = \frac{1}{2} m_0 \omega_{z_2}^2 z_2^2. \tag{A.7}$$

The constants g, c, d, ω, α, z_1 and z_2 depend on the nuclear shapes, which are defined by the collective coordinates: elongation λ, mass asymmetry η, neck parameter ε and deformations β_i of the axial symmetric fragments.

The parameters κ, μ and ω_0 are determined by a convenient interpolation method regarding these parameters as functions of extrapolated masses of the fragments in order to achieve the correct transition from the system of two separate nuclei to the compound-system configuration. The additional undefined quantity f_0 has little influence on the total energy for a wider range of values, and from liquid drop model calculations it was found that $f_0 = 4\varepsilon$ is a good approximation to the value giving minimal energy.

Table A

Symbol	$z < z_1$	$z_1 < z < 0$	$0 < z < z_2$	$z_2 < z$
ω	ω_{z_1}	ω_{z_1}	ω_{z_2}	ω_{z_2}
α	ω_{ρ_1}	ω_{ρ_1}	ω_{ρ_2}	ω_{ρ_2}
c	0	c_1	c_2	0
d	0	d_1	d_2	0
g	0	g_1	g_2	0
z'	$z - z_1$	$z - z_1$	$z - z_2$	$z - z_2$
κ	κ_1	κ_1	κ_2	κ_2
μ	μ_1	μ_1	μ_2	μ_2
ω_0	ω_{01}	ω_{01}	ω_{02}	ω_{02}
$\mathbf{l}$	$\mathbf{l}_1$	$\mathbf{l}_1$	$\mathbf{l}_2$	$\mathbf{l}_2$
f_0	1	f_0	f_0	1

The single-particle-energies are obtained through a diagonalization of the Hamiltonian (A.1) in the basic functions $< \rho\varphi z \mid n_z n_\rho l_z >$ given by Holzer et al. [125] for the symmetric two-center oscillator, multiplied by spin wave functions $\mid s_z >$. The wave functions $< \rho\varphi z \mid n_z n_\rho l_z >$ can be written as

$$< \rho\varphi z \mid n_z n_\rho l_z >= \varphi_{n_z}(z) \cdot \chi_{n_\rho}^{|l_z|}(\rho) \cdot \nu_{l_z}(\varphi), \tag{A.8}$$

where

$$\nu_{l_z}(\varphi) = \frac{1}{\sqrt{2\pi}} \exp(il_z\varphi), \tag{A.9}$$

for arbitrary integers l_z.

$$\chi_{n_\rho}^{|l_z|}(\rho) = C^{-1} k_\rho^{\frac{|l_z|+1}{2}} \exp(-\frac{1}{2}k_\rho\rho^2) \cdot \rho^{|l_z|} \cdot L_{n_\rho}^{|l_z|}(k_\rho\rho^2), \tag{A.10}$$

with a normalization constant C and $k_\rho = \frac{m_0\omega_\rho}{\hbar}$. n_ρ is a non-negative integer, and $L_n^\alpha(x)$ is a Laguerre polynomial.

$$\varphi_{n_z}(z) = \left\{ \begin{array}{c} C_{z_1}^{-1} U(-n_{z_1} - \frac{1}{2}, -\sqrt{2k_{z_1}}(z - z_1)) \text{ if } z < 0 \\ C_{z_2}^{-1} U(-n_{z_2} - \frac{1}{2}, \sqrt{2k_{z_2}}(z - z_2)) \text{ if } z > 0 \end{array} \right\}, \tag{A.11}$$

with normalization factors C_{z_1} and C_{z_2}. The quantum number n_z assumes different values on both sides of the origin, too. As the energy

$$E = \hbar\omega(n_z + \frac{1}{2}) + \hbar\omega_\rho(2n_\rho + \mid l_z \mid +1) \tag{A.12}$$

should not depend on z, the values n_{z_1} and n_{z_2} are related by

$$\omega_{z_1}(n_{z_1} + \frac{1}{2}) = \omega_{z_2}(n_{z_2} + \frac{1}{2}). \tag{A.13}$$

$U(a, x)$ denotes a parabolic cylinder function [40]. The values of n_z must be determined numerically from assuring the continuity of the logarithmic derivative of (A.11) in $z = 0$.

The Hamiltonian (A.1) can be split into several parts which are treated separately

$$H = H_0 + H_1 + V_{LS} + V_{L^2}. \tag{A.14}$$

H_0 is the Hamiltonian of a two-center oscillator

$$H_0 = -\frac{\hbar^2\nabla^2}{2m_0} + \frac{1}{2}m_0\omega^2 z'^2 + \frac{1}{2}m_0\omega_\rho^2\rho^2, \tag{A.15}$$

and H_1 is given by

$$H_1 = \frac{f_0}{2}m_0\omega^2 z'^2(cz' + dz'^2) + \frac{(f_0 - 1)}{2}m_0\omega^2 z'^2 + \frac{1}{2}m_0\left[\alpha^2(1 + gz'^2) - \omega_\rho^2\right]\rho^2, \tag{A.16}$$

where ω_ρ is an optimal value between $\omega_\rho = \min(\omega_{\rho_1}, \omega_{\rho_2})$ and $\omega_\rho = \frac{1}{2}(\omega_{\rho_1} + \omega_{\rho_2})$.

During the calculation of matrix elements it turns out to be advantageous to introduce another quantum number

$$N_\rho = 2n_\rho + \mid l_z \mid \tag{A.17}$$

instead of n_ρ, and to multiply the basic functions with a phase factor . So the functions actually used are

$$\mid n_z N_\rho l_z s_z >= (-1)^{\frac{1}{2}(l_z+|l_z|)} \mid n_z, \frac{N_\rho - \mid l_z \mid}{2}, l_z > \cdot \mid s_z > . \tag{A.18}$$

The matrix elements are presented in [40].

Appendix B

The collective response function [86] can be derived by introducing a (hypothetical) external force $\hat{F}\ \widetilde{f}_{ext}(t)$ and by evaluating how the deviation of $< \hat{F} >_\omega$ from some properly chosen static value reacts to this external field in linear order

$$\delta < \hat{F} >_\omega = -\chi_{coll}(\omega) \cdot f_{ext}(\omega). \tag{B.1}$$

The collective response function can be brought to the form [86]

$$\chi_{coll}(\omega) = \frac{\chi(\omega)}{1 + k\chi(\omega)}. \tag{B.2}$$

Here, $\chi(\omega)$ is the Fourier transform of the response function for intrinsic motion. Its time-dependent version reads

$$\tilde{\chi}\ (t-s) = \vartheta(t-s)\frac{i}{\hbar} tr\left\{\widehat{\rho}_{qs}(Q_0, T_0)\left[\hat{F}(t), \hat{F}(s)\right]\right\}, \tag{B.3}$$

where $\vartheta(x)$ is the Heavyside's function. In the expression (B.3) the time development of the field operators is defined by the same Hamiltonian $\hat{H}(x_i, p_i, Q)$ which appears in the density $\widehat{\rho}_{qs}$.

The coupling constant k is written in the form

$$-k^{-1} = < \frac{\partial^2 \hat{H}(x_i, p_i, Q)}{\partial Q^2} >_{Q_0, T_0} = \frac{\partial^2 E(Q, S_0)}{\partial Q^2}|_{Q_0} + \chi(\omega = 0) = C(0) + \chi(0) \tag{B.4}$$

with $\chi(0)$ and $C(0)$ being the static intrinsic response and stiffness, respectively. Since the constant k is entirely determined by quasi-static properties, it is no surprise that E is the internal energy at a given entropy S_0 or the free energy at a given temperature T_0. The structure of Eq.(B.2) reflects self–consistency between the treatment of collective and microscopic dynamics. It expresses the response of the system of interacting nucleons in terms of the response of the individual nucleons.

In the local harmonic approximation [86], the inverse of the collective response function $\chi^{-1}_{coll}(\omega)$ is considered as the inverse of the damped oscillator response function $\chi^{-1}_{osc}(\omega)$ which is expressed as

$$\chi^{-1}_{osc}(\omega) = C^F - i\gamma^F\omega - M^F\omega^2, \tag{B.5}$$

where C^F, γ^F and M^F are related to the derivative of the effective collective potential, calculated in linearized form, to a friction force and to an inertial one, respectively. The associated "transport coefficients" have been marked by a superscript F to indicate that they are associated with the quantity $\delta < \hat{F} >$. The transport coefficients $\Upsilon = M, \gamma, C$ of the Q-mode are related to the transport coefficients $\Upsilon^F = M^F, \gamma^F, C^F$ of the $\delta < \hat{F} >$-mode by the relation $\Upsilon^F = k^2\Upsilon$ [86]. An expression like (B.5) may be obtained by expanding $\chi^{-1}_{coll}(\omega)$ (B.2) to second order in ω. In this way one gets

$$\begin{aligned} C &\approx \frac{1}{k^2\chi_{coll}(\omega)} \mid_{\omega=0}, \\ \gamma &\approx \frac{1}{k^2}\frac{\partial\chi^{-1}_{coll}(\omega)}{\partial\omega} \mid_{\omega=0}, \\ M &\approx \frac{1}{2k^2}\frac{\partial^2\chi^{-1}_{coll}(\omega)}{\partial\omega^2} \mid_{\omega=0}. \end{aligned} \tag{B.6}$$

[1] S.G.Nilsson et al., Phys. Lett. B28 (1969) 458; Nucl. Phys. A 131 (1969) 1.

[2] U.Mosel and W. Greiner, Z. Phys. 217 (1968) 256; 222 (1968) 261.

[3] K.Rutz et al., Phys. Rev. C 56 (1997) 238.

[4] P.Armbruster, Ann. Rev. Nucl. Part. Sci. 35 (1985) 135; IL Nuovo Cim. A110 (1997) 1111.

[5] Yu.Ts.Oganessian et al., Nucl. Phys. A 239 (1975) 353.

[6] R.K.Gupta, C.Parvulescu and A.Sandulescu, Z. Phys. A 283 (1977) 217; Z. Naturforsch. 32a (1977) 704.

[7] S.Hofmann et al., Z. Phys. A 350 (1995) 277; A 350 (1995) 281; A 354 (1996) 229; S.Hofmann, Rep. Prog. Phys. 61 (1998) 639.

[8] G.Münzenberg, Rep. Prog. Phys. 51 (1988) 57.

[9] S.Hofmann and G.Münzenberg, Rev. Mod. Phys. (to be published).

[10] V.Ninov et al, Phys. Rev. Lett. 83 (1999) 1104.

[11] M.G.Itkis et al, *in* Second Int. Conf. on Fission, St. Andrews, June 28-July 2, 1999.

[12] Yu.Ts.Oganessian et al., Eur. Phys. J. A 5 (1999) 63; Nature 400 (1999) 242; A.V.Yeremin, V.K.Utyonkov and Yu.Ts.Oganessian, *in* Proc.Tours Symposium on Nuclear Physics III, Tours, 1997, eds. M. Arnould et al. (AIP,New York, 1998) p.16.

[13] G.Münzenberg et al, *in* MAFF Collaboration-Meeting, München-November 27, 1998.

[14] A.S.Iljinov, Yu.Ts.Oganessian and E.A.Cherepanov, Sov. J. Nucl. Phys. 36 (1982) 118.

[15] P.Fröbrich, Phys. Rep. 116 (1984) 337.

[16] W.J. Swiatecki, Progr. Part. Nucl. Phys. 4 (1980) 383; Phys.Scripta 24 (1981) 113; S. Bjornholm and W.J.Swiatecki, Nucl. Phys. A 391 (1982) 471.

[17] N.V.Antonenko, G.G.Adamian, A.Diaz-Torres, V.V.Volkov and W.Scheid, *in* Proc. of the Predeal Int. Summer School "Structure and Stability of Nucleon and Nuclear Systems", Predeal, August 24-September 5, 1998, eds. A.A.Raduta, S.Stoica and I.I.Ursu (Word Scientific,1999) p. 209.

[18] N.V.Antonenko, E.A.Cherepanov, A.K.Nasirov, V.B.Permjakov and V.V.Volkov, Phys. Lett. B 319 (1993) 425; Phys. Rev. C 51 (1995) 2635.

[19] V.V. Volkov, *in* Proc. Int. School-Seminar on Heavy Ion Physics, Dubna, 1986 (JINR, Dubna, 1987) p.528; Izv. AN SSSR ser. fiz. 50 (1986) 1879; *in* Proc. Int. Conf. on Nuclear reaction Mechanisms, Varenna, 1991, ed. E. Gadioli (Ricerca Scientifica,1991) p.39.

[20] G.G.Adamian, N.V.Antonenko, W.Scheid and V.V.Volkov, Nucl. Phys. A 633 (1998) 409.

[21] N.V.Antonenko, G.G.Adamian, W.Scheid and V.V.Volkov, IL Nuovo Cim. A110 (1997) 1143.

[22] E.A.Cherepanov, Pramana J. of Phys. 23 (1999) 1.

[23] V.V.Volkov, G.G.Adamian, N.V.Antonenko, E.A.Cherepanov and A.K.Nasirov, IL Nuovo Cim. A110 (1997) 1127.

[24] Y.Abe, Y.Aritomo, T.Wada and M.Ohta, J. Phys. G 23 (1997) 1275; Phys. Rev. C 59 (1999) 796.

[25] B.I.Pustylnik, *in* Book VI Int. School-Seminar Heavy Ion Physics 22-27 September 1998, Dubna, Russia, Word Scientific, p.431.

[26] R.Smolańczuk, Phys. Rev. C 59 (1999) 2634.

[27] N.V.Antonenko et al., *in* 1^{st} Int. Conf. on the Chem. and Phys. of the Transactinide Elements, September 26-30, 1999, Seeheim, Germany.

[28] V.V.Volkov, Phys. Rep. 44 (1978) 93.

[29] H.H.Freiesleben and J.V.Kratz, Phys. Rep. 106 (1984) 1.

[30] R.T.Souza et al., Phys. Rev. C 39 (1989) 114.

[31] R.V.Jolos et al., Sov. J. Nucl. Phys. 50 (1989) 239.

[32] V.V.Volkov, Izv. Akad. Nauk SSSR, Ser. Fiz. 50 (1986) 1879.

[33] G.G.Adamian, A.K.Nasirov, N.V.Antonenko and R.V.Jolos, Phys. Part. Nucl. 25 (1994) 583.

[34] G.G.Adamian, N.V.Antonenko and W. Scheid, Nucl. Phys. A 618 (1997) 176; A 627 (1997) 361.

[35] A.Diaz-Torres, N.V.Antonenko and W.Scheid, Nucl. Phys. A 652 (1999) 61.

[36] G.G.Adamian, N.V.Antonenko and Yu.M.Tchuvil'sky, Phys. Lett. B451 (1999) 289.

[37] G.G.Adamian, N.V.Antonenko, R.V.Jolos and W.Scheid, Nucl. Phys. A 619 (1997) 241.

[38] R.V.Jolos, A.I.Muminov and A.K.Nasirov, Eur. Phys. J. A 4 (1999) 245.

[39] E.A.Cherepanov, *in* Proc. of Int. Symposium on Ion-Beam Nucl. Spectroscopy, Debrecen, Hungary, 1984, Budapest, 1984, p. 499.

[40] J.Maruhn and W. Greiner, Z. Phys. 251 (1972) 431.

[41] V.M.Strutinsky, Nucl. Phys. A 95 (1967) 420; A 112 (1968) 1.

[42] G.G.Adamian, N.V.Antonenko, S.P.Ivanova and W.Scheid, Nucl. Phys. A 646 (1999) 29.

[43] G.G.Adamian, N.V.Antonenko, A.Diaz-Torres and W.Scheid, Nucl. Phys. A (in press)

[44] W.Nörenberg and H.A.Weidenmüller, *in* Introduction to the theory of heavy-ion collisions (Springer, Heidelberg, 1980)

[45] W.Nörenberg, Z. Phys. A 274 (1975) 241; 276 (1976) 84.

[46] D.H.Gross, Nucl. Phys. A 240 (1975) 472.

[47] J.Blocki et al, Ann. of Phys. 113 (1978) 330.

[48] H.Hofmann and P.J.Siemens, Nucl. Phys. A 257 (1976) 165; A 275 (1977) 464.

[49] J.W.Negele, Rev. Mod. Phys. 54 (1982) 913.

[50] S.Ayik, Z. Phys. A 298 (1980) 83; Nucl. Phys. A 370 (1981) 317.

[51] W.Nörenberg, Phys. Lett. B 104 (1981) 107; S.Ayik and W.Nörenberg, Z. Phys. A 309 (1982) 121; W.Cassing and W.Nörenberg, Nucl. Phys. A 401 (1983) 467; W.Nörenberg, Nucl. Phys. A 409 (1983) 191c.

[52] W.Cassing and W.Nörenberg, Nucl. Phys. A 433 (1985) 467.

[53] L.Landau, Phys. Z. Sowjetunion 1 (1932) 88; 2 (1932) 46; E.C.G.Stueckelberg, Helv. Phys. Acta 5 (1932) 369; C.Zener, Proc. Roy. Soc. A 137 (1932) 696.

[54] W.Lichten, Phys. Rev. 131 (1963) 229; 164 (1967) 131.

[55] E.E.Nikitin and S. Ya. Umanskii, *in* Theory of Slow Atomic Collisions, (Springer, Heidelberg, 1984).

[56] J.v.Neumann and E.Wigner, Z. Phys. 30 (1929) 467.

[57] A.Lukasiak, W.Cassing and W.Nörenberg, Nucl. Phys. A 426 (1984)181.

[58] D.L.Hill and J.A.Wheeler, Phys. Rev. 89 (1953) 1102.

[59] H.C.Pauli and L.Wilets, Z. Phys. A 277 (1976) 83.

[60] G.Schütte, Phys. Rep. 80 (1981) 113.

[61] J.B.Delos, Rev. Mod. Phys. 53 (1981) 287.

[62] C.E. Aguiar, V.C. Barbosa and R. Donangelo, Nucl. Phys. A 517 (1990) 205;T. Tokuda, K. Okazaki,T. Wada,M. Ohta and Y. Abe, *in* Proc.Tours Symposium on Nuclear Physics III, Tours, 1997, eds. M. Arnould et al. (AIP,New York, 1998) p.171.

[63] Yu.F.Smirnov and Yu.M.Tchuvil'sky, Phys. Lett. B 134 (1984) 25; O.F. Nemec, V.G.Neudachin, A.T.Rudchik, Yu.F.Smirnov and Yu.M.Tchuvil'sky, Nucleon associations in the atomic nuclei and nuclear reactions of multinucleon transfers, Naukova Dumka, Kiev (1988).

[64] A.Lukasiak and W.Nörenberg, *in* Int. Conf. on Heavy-Ion Physics and Nuclear Physics, Catania, March 21-26, 1983, p.128.

[65] G.G.Adamian, N.V.Antonenko, R.V.Jolos, S.P.Ivanova and O.I.Melnikova, Int. J. Mod. Phys. E 5 (1996) 191.

[66] A. Diaz-Torres, G.G. Adamian, N.V. Antonenko and W. Scheid, Phys. Lett. B (submitted for publication).

[67] G.G.Adamian, N.V.Antonenko and W.Scheid, Nucl. Phys. A (submitted for publication)

[68] A.M.Wapstra and G. Audi, Nucl. Phys. A 440 (1985) 327.

[69] P.Gippner et al, Phys. Lett. B 252 (1990) 198.

[70] S.Raman et al, At. Data and Nucl. Tables 36 (1987) 18.

[71] P.Möller, J.R.Nix,W.D.Myers and W.J.Swiatecki, At. Data and Nucl. Tables 59 (1995) 185.

[72] W.Reisdorf, J. Phys. G 20 (1994) 1297.

[73] G.G.Adamian, N.V.Antonenko, R.V.Jolos and A.K.Nasirov, Nucl. Phys. A 551 (1993) 321.

[74] N.V.Antonenko and R.V.Jolos, Phys. Scr. T32 (1990) 27.

[75] G.G.Adamian, R.V.Jolos and A.K.Nasirov, Sov. J. Nucl. Phys. 55 (1992) 660.

[76] D.Berdichevsky, A.Lukasiak, W.Nörenberg and P.Rozmej, Nucl. Phys. A 499 (1989) 609.

[77] R.Bass, Phys. Rev. Lett. 39 (1977) 265; *in* Lecture Notes in Physics 117 (Berlin: Springer, 1980) p. 281.

[78] K.H.Schmidt and W.Morawek, Rep. Prog. Phys. 54 (1991) 919.

[79] A.B.Quint et al., Z. Phys. A 346 (1993) 119.

[80] C.C.Sahm et al., Z. Phys. A 319 (1984) 113; Nucl. Phys. A 441 (1985) 316.

[81] G.Nuhn, W.Scheid and J.Y.Park, Phys. Rev. C 35 (1987) 2146.

[82] G. Bertsch, *in* Frontiers and borderlines in many–particles physics, Enrico Fermi School (CIV, Corso, 1988) p.41.

[83] W.U. Schröder and J.R. Huizenga, *in* Treatise on heavy-ion science. Ed. D.A. Bromley (Plenum, New York, 1984) vol. 2., p. 115.

[84] G.G.Adamian, N.V.Antonenko and R.V.Jolos, Nucl. Phys. A 584 (1995) 205.

[85] J. Richert, T. Sami and H.A. Weidenmüller, Phys. Rev. C 26 (1982) 1018.

[86] H. Hofmann, Phys. Rep. 284 (1997) 139.

[87] F.A. Ivanyuk et al., Phys. Rev. C 55 (1997) 1730.

[88] V. Schneider, J.Maruhn and W.Greiner, Z. Phys. A 323 (1986) 111.

[89] J.R. Primack, Phys. Rev. Lett. 17 (1966) 539.

[90] J.J. Griffin, Nucl. Phys. A 170 (1971) 395.

[91] T. Lederberger and H.C. Pauli, Nucl. Phys. A 207 (1973) 1.

[92] V.M. Kolomietz and P.J. Siemens, Nucl. Phys. A 314 (1979) 141.

[93] S. Yamaji, F.A. Ivanyuk and H. Hofmann, Nucl.Phys. A 612 (1997) 1.

[94] W. Greiner and J.A. Maruhn, Nuclear Models (Springer-Verlag, Berlin/Heidelberg, 1996).

[95] M. Brack, J. Damgaard, A.S. Jensen, H.C. Pauli, V.M. Strutinsky and C.Y. Wong, Rev. Mod. Phys. 44 (1972) 320.

[96] F.A. Ivanyuk, Z. Phys. A 334 (1989) 69.

[97] H. Hofmann et al, Nucl. Phys. A 598 (1996) 187.

[98] X. Wu et al., Phys. Rev. Lett. 79 (1997) 4542.

[99] K. Fujikawa and H. Terashima, Phys. Rev. E 58 (1998) 7063.

[100] J. Schirmer, S. Knaak and G. Güssmann, Nucl. Phys. A 199 (1973) 31.

[101] A.Bohr and B.R.Mottelson, Nuclear Structure, vol. 1 (W.A. Benjamin, INC., Massachusetts, 1975).

[102] A.S.Jensen, P.J.Siemens and H.Hofmann, *in* Nucleon-nucleon interaction and the many-body problem, Eds.: S.S.Wu and T.T.S.Kuo, World Scientific (1984).

[103] D.Pines, P. Nozieres, *in* The Theory of Quantum Liquids, vol. 1, (W.A. Benjamin, New York, 1966).

[104] W.Nörenberg, Nucl. Phys. A 459 (1986) 77.

[105] W.Nörenberg and C.Riedel, Z. Phys. A 290 (1979) 335; H. L. Yadav and W.Nörenberg, Phys. Lett. B 115 (1982) 179.

[106] C.Gregoire, C.Ngo, B.Remaud, Phys. Lett. B 99 (1981) 17; Nucl. Phys. A 383 (1982) 392.

[107] A.B.Larionov et al., Nucl. Phys. A 648 (1999) 157.

[108] G.F.Bertsch, P.F.Bortignon and R.A.Broglia, Rev. Mod. Phys. 55 (1983) 287.

[109] H.S.Köhler, Nucl. Phys. A 378 (1982) 159; Nucl. Phys. A 378 (1982) 181.

[110] A.Ignatyuk et al., Sov. J. Nucl. Phys. 21 (1975) 612.

[111] P.Reiter et al., Phys. Rev. Lett. 82 (1999) 509.

[112] B. Heusch et al., Z. Phys. A 288 (1978) 391; C. Lebrun et al., Nucl. Phys. A 321 (1979) 207; B. Borderie et al., Z. Phys. A 299 (1981) 263; B. B. Back et al., Phys. Rev. Lett. 46 (1981) 1063; 50 (1983) 818; R. Bock et al., Nucl. Phys. A 388 (1982) 334; M. B. Tsang et al., Phys. Lett. B 129 (1983) 18; Z. Zheng et al., Nucl. Phys. A 422 (1984) 447; J. Töke et al., Nucl. Phys. A 440 (1985) 327.

[113] W.Q.Shen et al., Phys. Rev. C 36 (1987) 115.

[114] M.Thoennessen et al., Phys. Rev. Lett. 70 (1993) 4055; P.Paul and M.Thoennessen, Ann. Rev. Nucl. Part. Sci. 44 (1994) 65.

[115] H.A.Kramers, Physica VII 4 (1940) 284; V.M.Strutinsky, Phys. Lett. B 47 (1973) 121; P.Grangé, Li Jun-Qing and H.A.Weidenmüller, Phys. Rev. C 27 (1983) 2063; H. A. Weidenmüller and Jing-Shang Zhang, J. Stat. Phys. 34 (1984) 191; P.Grangé,Nucl. Phys. A 428 (1984) 37c; P.Fröbrich and G.R.Tillack, Nucl. Phys. A 540 (1992) 353.

[116] S.Yamaji, F.A.Ivanyuk and H.Hofmann, Nucl.Phys. A 612 (1997) 1.

[117] I.I.Gonchar and G.I.Kosenko, Sov. J. Nucl. Phys. 53 (1991) 133.

[118] H.Gäggeler et al., Z. Phys. A 316 (1984) 291.

[119] L.G.Moretto and J.S.Sventek, Phys. Lett. B58 (1975) 26.

[120] N.V.Antonenko, S.P.Ivanova, R.V.Jolos and W.Scheid, Phys. Rev. C 50 (1994) 2063; N.V.Antonenko and R.V.Jolos, Z. Phys. A 341 (1992) 459.

[121] U.Brosa, S. Großman and A. Müller, Phys. Rep. 197 (1990) 167.

[122] S.Oberstedt, F.-J. Hambsch and F. Vives, Nucl. Phys. A 644 (1998) 289.

[123] G.Lindblad, Comm. Math. Phys. 48 (1976) 119; Rep. on Math. Phys. 10 (1976) 393.

[124] G.G.Adamian, N.V.Antonenko and W.Scheid, Phys. Lett. A 244 (1998) 482.; Nucl. Phys. A 645 (1999) 376.; Phys. Lett. A 260 (1999) 39.

[125] P.Holzer, U.Mosel and W.Greiner, Nucl. Phys. A 138 (1969) 241.